Miniaturized Dielectric Elastomer Actuator for Mechanical Stimulation of Monolayer Cell Cultures

THÈSE N^{O} 7406 (2016)

PRÉSENTÉE LE 7 DÉCEMBRE 2016
À LA FACULTÉ DES SCIENCES ET TECHNIQUES DE L'INGÉNIEUR
LABORATOIRE DES MICROSYSTÈMES POUR LES TECHNOLOGIES SPATIALES
PROGRAMME DOCTORAL EN MICROSYSTÈMES ET MICROÉLECTRONIQUE

ÉCOLE POLYTECHNIQUE FÉDÉRALE DE LAUSANNE

POUR L'OBTENTION DU GRADE DE DOCTEUR ÈS SCIENCES

PAR

Alexandre POULIN

acceptée sur proposition du jury:

Prof. S. N. Henein, président du jury
Prof. H. Shea, Dr S. Rosset, directeurs de thèse
Prof. B. Müller, rapporteur
Prof. S. Seelecke, rapporteur
Prof. Ph. Renaud, rapporteur

ÉCOLE POLYTECHNIQUE
FÉDÉRALE DE LAUSANNE

Suisse
2016

La persévérance est la noblesse de l'obstination.
— A. Decourcelle

Acknowledgements

I am deeply grateful to Prof. Herbert Shea, who gave me the opportunity to join his laboratory, and work on this highly motivating project. I feel fortunate to have had a thesis advisor with such dedication to being a good mentor for his students. Thank you for your availability and support when I needed it, for your enthusiasm and encouragement in all my projects, and for your precious advices.

I am deeply thankful to Samuel Rosset, who co-supervised my thesis with great dedication, and patiently shared with me his extensive scientific knowledge and practical experience. Thank you for your availability and for your precious scientific inputs.

I am very thankful to Prof. Simon Nessim Henein, Prof. Phillippe Renaud, Prof. Bert Müller, and Prof. Stefan Seelecke, who graciously accepted to review and evaluate this thesis.

The support and collaboration of the LMTS members was essential to this thesis. I would like to thank Samin Akbari, Matthias Imboden, and Francesca Sorba for their help with the cell stretcher. I would also like to thank Alexis Marette for our collaboration on low-voltage DEAs. I would like to thank Danick Briand, Çağlar Ataman, Vinu Venkatraman, Simon Dandavino, Subha Chakraborty, Daniel Courtney, Seun Araromi, Jun Shintake, Nadine Besse, Juan Zarate, Samuel Schlatter, Xiaobin Ji, Marianna Fighera, Joanna Bitterli, Rubaiyet Haque, and David McCoul, for their support, and for the great working environment. A special mention to Myriam Poliero, Luc Maffli, Anna Kamowat, and Christine de Saint-Aubin for the good times we had as office mates.

An important part of this thesis relied on collaborations with external partners, without whom the biological experiments would not have been possible. I would like to thank Cansaran Saygılı Demir and Tatiana Petrova from UNIL for our successful collaboration, and for its continuation. I would also like to express my gratitude toward Cristina Martin Olmos, Marta Liley and Marta Giazzon from CSEM, as well as Etienne de Coulon and Stephan Rohr from Bern University, for their precious help with the biological experiments.

Lastly, I would like to thank my family and friends for their unconditional support and continuous encouragements, and Gizem, for always being there for me and brightening my life.

Neuchâtel, September 27, 2016 A. P.

Abstract

This thesis advances the field of dielectric elastomer actuators (DEAs) through the development of DEA designs, fabrication processes, strain characterization technique and modelling tool. It provides the first demonstration that DEAs can be interfaced with living cells, opening the door to real-world applications in mechanobiology, an important step for the development of this emerging soft-actuator technology. It also provides a practical approach towards low voltage DEAs, demonstrating a fully-printed actuator that works below 300 V, a range compatible with commercially available CMOS circuitry, hence enabling a variety of new applications for DEA-based technologies.

The mechanisms by which cells can sense and react to their mechanical environment are still partly unknown, and advances in this field will contribute to better diagnosis and treatment of serious diseases like cancer. Research heavily relies on *in vitro* models, and there is therefore great interests in systems capable of applying precise mechanical strain on cell cultures. This thesis overcomes the many challenges of interfacing DEAs with living cells, and presents a biocompatible device which can sustain standard cell culture protocols like sterilization, incubation, and immersion in growth medium. The device can apply from -10 % to 35 % uniaxial strain on a small cell population (~100 cells), located in a transparent area (0.5 mm x 1.5 mm) of a larger biocompatible membrane. It can be mounted on an inverted microscope, where its design enables real-time high-resolution optical imaging of cells during stretching. With strain rates in the excess of 700 s^{-1}, the *in vivo* environment can be reproduced with unprecedented accuracy. As a demonstration of the technology, in collaboration with the Vascular and Tumor Biology Laboratory at UNIL in Switzerland, a population of lymphatic endothelial cells (LECs) was cycled from 0 % to 10 % strain at 1 Hz for 24 h. The results show stretch-induced alignment of cells perpendicular to strain, and confirm that the device fringing electric field has no effect on LECs morphology. This is the first demonstration that DEAs can be interfaced with living cells, and the first time they are used to observe cell mechanosensitivity.

The driving voltage of DEAs is typically in the kV range, which limits their possible applications. One approach to reduce the actuation voltage is to decrease the membrane thickness, which is typically in the 20-100µm range, as reliable fabrication becomes challenging below this thickness. This thesis presents a pad-printed 3 µm thick DEA, and demonstrates that decreasing the membrane thickness to only a few microns significantly reduces the driving voltage, while maintaining good actuation performance. A radial strain of 7.5 % was achieved at only 245 V, which corresponds to a strain-to-voltage-squared ratio of 125 % kV^{-2}, the highest reported value to date. This thesis also investigates the electrodes stiffening impact, often overlooked in the design and development DEAs. It presents an analytical model which accounts for the electrodes stiffness, and presents a strain-mapping algorithm to compares the strain uniformity of 3 µm- and 30 µm-thick DEAs. The simulation results and the strain-mapping measurements identify the electrodes as an important parameter that should not be neglected in the design and optimization of thin-DEAs.

Key words: dielectric elastomer actuator, biocompatible, high strain rate, cell stretcher, mechanobiology, pad-printing, low voltage, strain mapping

Résumé

Cette thèse contribue à l'avancement du domaine des actionneurs en polymère électroactif (DEA) par le développement de nouvelles configurations d'actionneurs, de nouvelles méthodes de fabrication et de nouveaux outils de modélisation. Elle présente la première démonstration d'intégration de DEA avec des cellules biologiques, ouvrant ainsi la porte à de nombreuses applications pratiques, une étape importante dans le développement de cette nouvelle technologie d'actionneur. Cette thèse présente également une nouvelle technique pour la fabrication de DEA fonctionnant sous les 300 V, et donc maintenant compatible avec des technologies CMOS disponibles commercialement, permettant ainsi des applications auparavant impossibles.

Il est maintenant reconnu que les cellules interagissent avec leur environnement mécanique, et qu'une détérioration de leur mécanosensitivité contribue à plusieurs maladies graves telles le cancer. La recherche dans ce domaine repose principalement sur des modèles *in vitro*, et il y a donc un grand intérêt envers les technologies permettant de déformer mécaniquement des cultures cellulaires. Un milieu de culture déformable utilisant un DEA afin de générer une stimulation mécanique est présenté dans cette thèse. Le système peut déformer une petite population de cellules (~100 cellules), située dans une région (0.5 mm x 1.5 mm) transparente d'une plus grande membrane biocompatible, et leur appliquer jusqu'à 10% de compression uniaxiale, ou 35% de tension uniaxiale. Des taux de déformation supérieurs à 700 s^{-1} sont possibles, permettant ainsi de reproduire l'environnement *in vivo* avec une fidélité inégalée. De plus, le système permet aux cellules d'être imagées en haute-résolution durant leur déformation. Comme preuve de concept, en collaboration avec le Vascular and Tumor Biology Laboratory de l'UNIL en Suisse, une population de cellules endothéliales lymphatiques a été soumise à 10% d'élongation périodique (1 Hz) durant 24 h. Les résultats obtenus montrent que les cellules s'alignement perpendiculairement à l'axe de déformation, alors que les cellules de control (environnement statique) gardent leur orientation arbitraire, et que le champ électrique de dispersion de l'actionner ne démontre aucun effet sur les cellules. Il s'agit de la première démonstration que les DEA peuvent être utilisés pour des applications biologiques, et de la première fois que cette technologie est utilisée pour démontrer la mécanosensitivité cellulaire.

La tension d'actionnement des DEA est typiquement de quelques kV, ce qui limite leurs applications. Une des approches permettant de réduire la tension est de diminuer l'épaisseur de sa membrane diélectrique, qui fait normalement de 20 µm à 100 µm d'épaisseur. Cette thèse présente la fabrication d'un DEA de 3 µm d'épaisseur fabriqué par tampographie. L'actionneur circulaire démontre un déformation radiale de 7.5% à seulement 245 V, ce qui correspond à 125% de déformation par kV^2, de loin la plus haute valeur rapportée à ce jour pour un DEA. L'effet mécanique des électrodes sur la performance des DEA minces est également étudiée. Un modèle analytique prenant en compte la contribution mécanique des électrodes, ainsi qu'un algorithme permettant la mesure de champ de déformation des DEA sont présentés. Les prédictions de ce modèle, ainsi que les mesures de champ de déformation sur des DEA de 3 µm et 30 µm d'épaisseur démontrent que la contribution mécanique des électrodes ne peut être négligée pour les DEA minces.

Mots clefs : Actionneur en polymère électroactif, basse tension, biocompatible, milieu de culture déformable, mécanobiologie, tampographie, mesure de champs de déformation

Contents

Acknowledgements **i**

Abstract **iii**

Résumé **v**

List of figures **xi**

List of tables **xiii**

1 Introduction **1**

- 1.1 Background and motivation 1
- 1.2 Research objectives 2
- 1.3 Thesis outline and contributions 3

2 Fundamentals of dielectric elastomer actuators **5**

- 2.1 Summary 5
- 2.2 Introduction 5
- 2.3 Selected examples 6
  - 2.3.1 Highly compliant systems 6
  - 2.3.2 Large actuation strain 7
  - 2.3.3 Fast response time 8
  - 2.3.4 Optical transparency 9
- 2.4 Working principle 10
  - 2.4.1 Deformation response of dielectric elastomers 10
  - 2.4.2 DEA actuation 10
- 2.5 Materials 14
  - 2.5.1 Dielectric elastomers 14
  - 2.5.2 Stretchable electrodes 15
- 2.6 Conclusion 18

3 Introduction to cell mechanobiology **19**

- 3.1 Summary 19
- 3.2 Introduction to cell mechanobiology 19
- 3.3 Techniques for mechanical stimulation of cells *in vitro* 21

3.4 Deformable bioreactors 23
  3.4.1 Types of strain applied to cells 23
  3.4.2 Commercially available systems 24
  3.4.3 Miniaturized systems 26
3.5 Conclusion 30

4 DEA-based deformable bioreactor - Design and fabrication 31
4.1 Summary 31
4.2 Requirements and design considerations 32
  4.2.1 Key requirements 32
  4.2.2 Membrane material 32
  4.2.3 Electrode material 33
  4.2.4 DEA immersion in a conductive liquid 33
4.3 Design for uniaxial tensile and compressive strain 34
  4.3.1 Role of prestretch 34
  4.3.2 Uniaxial tensile strain 34
  4.3.3 Uniaxial compressive strain 36
4.4 Fabrication process 36
4.5 Conclusion 40

5 DEA-based deformable bioreactor - Actuation performance 43
5.1 Summary 43
5.2 Actuation strain 43
5.3 Stability and lifetime 50
5.4 Dynamic response 51
5.5 Conclusion 54

6 DEA-based deformable bioreactor - Technology validation 57
6.1 Summary 57
6.2 Lymphatic endothelial cells (LECs) 57
6.3 Materials and methods 58
  6.3.1 Cell culture protocol 58
  6.3.2 Mechanical stimulation of LECs 59
  6.3.3 Effects of fringing electric field on LECs 59
  6.3.4 Staining and microscopy 59
  6.3.5 Characterization of cells morphology 60
6.4 Results and discussion 61
  6.4.1 Characterization of the deformable bioreactor 61
  6.4.2 Stretch-induced alignment of lymphatic endothelial cells 62
  6.4.3 Effect of fringing electric field on LECs 64
6.5 Conclusion 66

7 Printing low-voltage DEAs **67**
7.1 Summary . . . 67
7.2 Decreasing the driving voltage of DEAs . . . 68
7.3 Fabrication process of printed DEAs . . . 69
7.4 Actuation performance of printed DEAs . . . 71
7.5 Strain field uniformity of printed DEAs . . . 73
7.6 Modelling the electrodes stiffening impact . . . 76
7.7 Conclusion . . . 80

8 Conclusion **81**
8.1 Summary . . . 81
8.1.1 DEA-based deformable bioreactor . . . 81
8.1.2 Printing low-voltage DEAs . . . 82
8.2 Future work . . . 83
8.2.1 DEA-based deformable bioreactor . . . 83
8.2.2 Pad-printing dielectric elastomer transducers . . . 86
8.3 Concluding remark . . . 87

Bibliography **101**

List of Abbreviations **103**

List of publications **105**

Curriculum Vitae **107**

List of Figures

1.1 Simplifying the *in vivo* environment with *in vitro* models 1

2.1 Working principle of dielectric elastomer actuators 5
2.2 Selected examples of highly compliant dielectric elastomer actuators (DEA) grippers 6
2.3 Selected examples of DEAs which exhibit large actuation strain 7
2.4 Selected examples of DEAs which demonstrate fast actuation 8
2.5 Selected examples of DEAs which demonstrate optical transparency 9
2.6 Stress-stretch relationship a dielectric elastomer membrane 10
2.7 Voltage-stretch response of DEAs 12
2.8 Voltage-stretch response of DEAs under external load 13
2.9 Example of loss of mechanical tension in DEAs 13
2.10 Common types of dielectric elastomer used in the fabrication of DEAs 14
2.11 Common types of carbon-based electrodes 15
2.12 Pad-printing process for the patterning of carbon-based electrodes 16
2.13 Thin-film metal electrodes and their possible configurations 17

3.1 Mechanical environment in the human body 20
3.2 Main techniques for mechanical stimulation of cells *in vitro* 22
3.3 Different types of strain applied to cells by deformable bioreactors 24
3.4 Commercially available deformable bioreactors 25
3.5 Selection of miniaturized pneumatic deformable bioreactors 27
3.6 Selection of miniaturized non-pneumatic deformable bioreactors 29

4.1 Concept of the DEA-based deformable bioreactor 31
4.2 DEA design for tensile and compressive uniaxial strain. 35
4.3 Detailed fabrication process of the DEA-based deformable bioreactor 37
4.4 Dimensions of the fabricated DEA-based deformable bioreactor 39
4.5 Effect of oil immersion on membrane ageing during cyclic actuation 39
4.6 Picture of the fabricated DEA-based deformable bioreactor 40

5.1 Voltage-strain response of the DEA-based deformable bioreactor. 44
5.2 Strain profile of the tensile design 46
5.3 Cross-section of the strain profile of the tensile design 47

5.4 Strain profile of the compressive design 48
5.5 Cross-section of the strain profile of the compressive design 49
5.6 Actuation stability of the DEA-based deformable bioreactor 50
5.7 Static response of the DEA-based deformable bioreactor 52
5.8 Dynamic response of the DEA-based deformable bioreactor. 53
5.9 Complex strain profiles generated by the DEA-based deformable bioreactor . . 54

6.1 Stretching cells with the DEA-based deformable bioreactor 58
6.2 Experimental setup for the biological experiment 60
6.3 Strain-voltage curve of the DEA-based deformable bioreactor 61
6.4 Stretch-induced alignment of LECs perpendicular to stretch 63
6.5 Strain-voltage curve the immobilized DEA-based deformable bioreactor 64
6.6 The fringing electric field shows no effect on LECs morphology 65

7.1 Fabrication process for fully printed 3 µm-thick DEAs 71
7.2 Voltage-strain response of 3 µm- and 30 µm-thick DEAs 72
7.3 Strain mapping by digital image correlation 75
7.4 Strain uniformity of 3 µm- and 30 µm-thick DEAs 76
7.5 Analytical model of DEA that accounts for electrodes stiffness 77
7.6 Strain-voltage curves calculated for decreasing membrane thicknesses 79
7.7 Effect of electrodes stiffening on driving voltage of thin DEAs 80

8.1 Design to generate tensile and compressive strain on a single device 83
8.2 Three-electrodes design to provide integrated capacitive strain sensing 84
8.3 Array configuration for high-throughput experiments 85
8.4 Possible applicatiosn for pad-printed dielectric elastomer membranes 86

List of Tables

4.1 DEA-based deformable bioreactor key requirements 32
4.2 Electrode geometry of the tensile and compressive designs 38
4.3 DEA-based deformable bioreactor key requirements 41

5.1 DEA-based deformable bioreactor key requirements 55

1 Introduction

1.1 Background and motivation

The mechanical environment of cells in the human body can be described as a complex combination of shear, tensile and compressive stress as presented in Fig. 1.1(a). The origin of stress can be internal, like tissue growth and muscle contraction, or it can be external, like gravity or mechanical shocks. Long overlooked, the role of mechanics in cell regulation has become a very active field of research [2]. Advances in mechanobiology have shown that mechanical stimuli can influence fundamental cellular functions such as migration, proliferation, and gene expression, which can contribute to the causes of many diseases and pathological conditions [3]. While mechanosensitivity has been observed for various types of cells [4], the underlying mechanotransduction mechanisms (i.e. the mechanisms by which cells can sense their mechanical environment and translate this information into a biochemical response) remain partly unknown, and progress in this field could lead to better diagnosis and treatment of various conditions ranging from cardiovascular diseases to cancer.

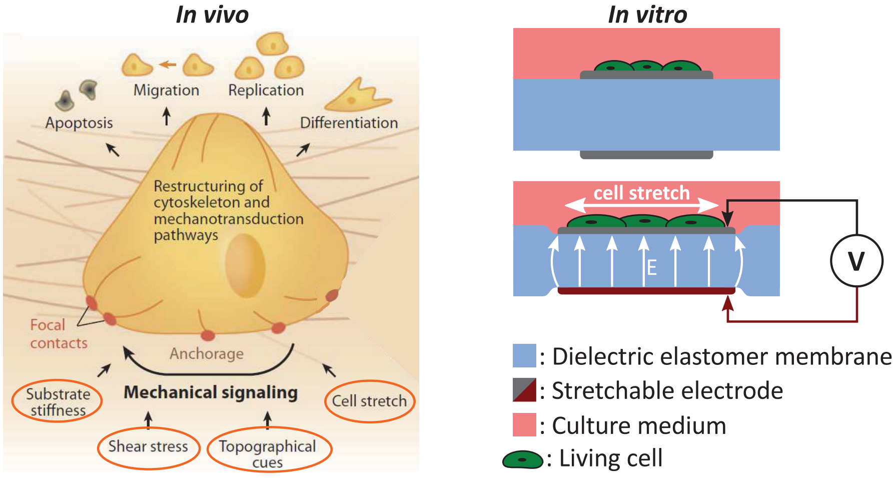
In vivo
Migration
Replication
Apoptosis
Differentiation
Restructuring of cytoskeleton and mechanotransduction pathways
Focal contacts
Anchorage
Mechanical signaling
Substrate stiffness
Cell stretch
Shear stress
Topographical cues
In vitro
cell stretch
E
V
: Dielectric elastomer membrane
: Stretchable electrode
: Culture medium
: Living cell

(a) (b)

Figure 1.1 – (a)Cells are exposed to a complex mechanical environment *in vivo* (Adapted from [1]). (b)In this work, a DEA-based deformable bioreactors is developed for the systematic study of cell mechanotransduction *in vitro*.

Due to the high complexity of the *in vivo* environment, mechanotransduction research often relies on *in vitro* studies, where cells are cultured on soft deformable substrate, and exposed to controlled periodic mechanical strain. Commercially available systems [5–7] provide a reliable solution to mechanical stimulation of cells *in vitro*. They can generate up to 20 % strain, and operate at frequencies below 5 Hz, but are limited by their large size. Bulky systems are indeed difficult to combine with standard equipments such as incubators and microscopes, they make parallelization for high-throughput studies impractical, and waste precious reagents and cells. There is therefore great interests in miniaturized deformable bioreactors i.e. systems designed to culture and stretch cells via the deformation of a soft culture interface [8, 9].

A promising approach is to use DEAs as a mechanically active culture substrate. DEAs are membrane actuators, which decrease in thickness, and expand in area upon electrical stimulation (electric fields of ~100 $\mathrm{V\mu m^{-1}}$) [10]. This emerging class of soft actuators are compliant (~1 MPa of elastic modulus), can generate large in-plane deformation (>100 % [11]), provide ultra fast response time (<200 µs [12]), and have high energy density (>500 $\mathrm{J\,kg^{-1}}$) [13]. With this unique combination of properties, DEAs could provide unprecedented performance for deformable bioreactors. It has been demonstrated that DEAs can be miniaturized to dimensions capable of single-cell stimulation (100 µmx100 µm), and integrated into large arrays [14]. In addition, the actuator can be made of a transparent cytocompatible thin membrane (~30 µm), thus enabling cells to be cultured directly on top of the device, and inspected *in situ* using a high-resolution inverted microscope. However, interfacing DEAs with living cells presents some important challenges, including the need to provide a cytocompatible environment, and to ensure that the system is compatible with standard cell culture protocols and equipment. Many obstacles need to be overcome before this promising technology can be used for applications in cell biology.

1.2 Research objectives

The main objective of this thesis is to provide the first demonstration that DEAs can be interfaced with living cells, and used to control their mechanical environment. It advances knowledge in the field of DEAs by developing novel actuator designs, fabrication processes, and characterization techniques tailored for this new field of application. The concept of the DEA-based deformable bioreactor is presented in Fig. 1.1, where cells are cultured on top of the transparent DEA, and stretched upon actuation. To provide an interesting alternative to current technologies, the DEA-based deformable bioreactor has to meet the following requirements:

- The device should meet the performance of commercially available systems, and provide up to 20% strain and 5 Hz actuation frequency.
- The device should provide stable actuation performance for 2 h to 24 h, which corresponds to the duration of typical mechanotransduction experiments [4].
- To ensure a cytocompatible environment, the selected materials should be non-cytotoxic, and the electrically driven DEA should be safe for living cells.

- The device should be compatible with standard cell culture protocols, which include ethanol sterilization, days of incubation at 37 °C, 5 % CO_2 and 95 % relative humidity, and days of immersion in culture medium (aqueous solution used to support cell growth).
- The device should be optically transparent to enable high-resolution imaging of cells.

In addition, the application of the DEA-based deformable bioreactor must be demonstrated. In order to validate the technology, a biological experiment has to show that:

- Periodic actuation of the device can generate a stretch-induced cellular response.
- The periodic fringing electric field has no effect on the studied cellular mechanism.

The second objective of the thesis is to decrease the actuation voltage of DEAs, which is typically in the kV range, and therefore limiting the possible applications. Different approaches could be investigated, but I focus on reducing the thickness of the elastomer membrane. I develop novel fabrication processes, characterization techniques, and analytical model for thin DEAs. This work contributes to advancing knowledge in the field of DEAs, and makes important steps toward real-world applications of this emerging technology.

1.3 Thesis outline and contributions

This thesis builds on DEAs, and advances the field by developing and demonstrating a practical application in cell mechanobiology, where large actuation strain and fast response time are key advantages, and required forces are small (cells elastic modulus is 1-100kPa). In addition, it presents a technique to manufacture ultra-thin DEAs, demonstrating a practical approach to decrease the driving voltage (typically in the kV range), hence tackling one of the main obstacles hindering the development of commercial applications for DEAs.

State-of-the-art

The first two chapters of this thesis cover the fundamentals of DEAs, and give an introduction to mechanobiology and deformable bioreactors.

> **Chapter 2** summarizes the theory of DEAs, presents state-of-the-art devices to highlight key features of the technology, discusses the DEA materials and their impact on the actuation performance.
>
> **Chapter 3** presents an introduction to cellular mechanobiology, summarizes the techniques for mechanical stimulation of cells *in vitro*, and presents the state-of-the-art of miniaturized deformable bioreactors.

DEA-based Deformable Bioreactor

The main contribution of this thesis, is to provide the first demonstration that DEAs can be interfaced with living cells, and used to control their mechanical environment. It opens the door to a new and promising field of research, where real-world applications are possible for DEAs.

> **Chapter 4** presents the design and fabrication of a DEA-based deformable bioreactor. It details its unique and versatile design, which can generate compressive or tensile uniaxial strain, and provide optical transparency without the need for optically transparent electrodes. It also details the the choices that were made to provide a cytocompatible device, which can sustain ethanol sterilization, incubation, and immersion in culture medium.
>
> **Chapter 5** presents the actuation performance of the DEA-based deformable bioreactor, capable of generating between -10 % and 35 % uniaxial strain on a 1 mm x 0.5 mm area. It presents measurements of the strain profile, which show good uniformity, and strain measurements over cyclic actuation, which demonstrate stable actuation performance over more than 12 h and 50 000 actuation cycles. It also presents an analysis of the system dynamic response, which shows strain rates of 700 s^{-1}, 100 times faster than what commercial systems can achieve.
>
> **Chapter 6** presents a validation of the technology. It details a biological experiment where lymphatic endothelial cell (LEC)s were cultured on the DEA-based deformable bioreactor, and periodically stretched by 10 % at a 0.1 Hz frequency for 24 h. The results show stretch-induced alignment of cells, and confirm that the fringing electric field has no effect on cell viability or morphology. This experiment provides the first demonstration that DEAs can be interfaced with living cells, and used to control their mechanical environment.

Low-voltage DEAs

The second contribution of the thesis is the development of an ultra-thin low-voltage DEA. The fully-printed device is manufactured using commercially available and scalable techniques, presenting a practical approach towards low-voltage DEAs, a critical step for the development of real-world applications. Its fabrication process and actuation performance are presented in Chapter 7, which also investigate the stiffening impact of the electrodes in thin-DEAs.

- **Chapter 7** presents the fabrication process of a fully-printed 3 µm thick DEA, and demonstrates that the driving voltage can be significantly reduced by decreasing the membrane thickness to a few microns. It reports a radial actuation strain of 7.5 % at only 245 V, which corresponds to 125 % kV^{-1}, the highest reported value for a DEA. To investigate the stiffening impact of the electrodes, it presents a simple DEA model which includes their mechanical properties, and shows that the electrodes stiffness should not be neglected in the design and optimization of thin DEAs. It also presents a strain mapping algorithm based on optical correlation, which is used to provide experimental evidences of the stiffening impact of the electrodes on thin DEAs.

2 Fundamentals of dielectric elastomer actuators

2.1 Summary

In this chapter, I introduce the concept of DEA, a type of soft actuator which directly converts electrical energy into mechanical work [10], as opposed to more common soft actuators which use pneumatic [15] or thermal actuation [16]. I first present a selection of state-of-the-art devices, chosen to highlight some of the technology's key advantages. I then summarizes the theory behind the working principle of DEAs and their possible failure mechanisms. In the last section, I discuss the available materials, and explain how they can affect the device performance.

2.2 Introduction

A DEA consists of a soft dielectric elastomer (DE) membrane sandwiched between two compliant electrodes as presented in Fig. 2.1(a). When a voltage difference is applied between the electrodes, the resulting electrostatic pressure compresses the membrane in the out-of-plane direction, hence generating internal stresses that stretch the membrane in-plane. The resulting actuation is schematized in Fig. 2.1(b), where the membrane thickness decreases, and its surface area increases during actuation. This basic actuation principle can generate planar [17, 18], bending [19, 20], or bubble-like [21–23] expansion, depending on the actuator geometry. In addition to their highly compliant nature (∼1 MPa elastic modulus), DEAs can provide large strain (>100 % [10]), fast response time (<200 µs [12]), silent operation, high energy density (560 J kg^{-1} [13]),and low power consumption.

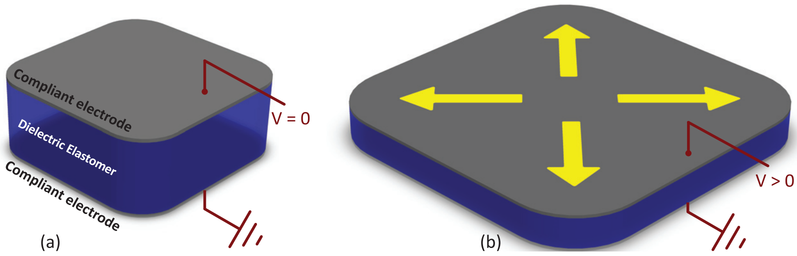

Figure 2.1 – (a) A DEA is composed of a soft DE membrane sandwiched between two compliant electrodes. (b) When a voltage difference is applied between the electrodes, the membrane thickness decreases, and its surface area increases.

2.3 Selected examples

In this section, I present a selection of state-of-the-art DEAs, chosen to highlight features that are most relevant to this thesis. I present examples of devices which provides: highly compliant systems (~1 MPa), large actuation strain (>100 %), fast response time (<1 ms), and optical transparency.

2.3.1 Highly compliant systems

DEAs are made of inherently soft materials (~1 MPa elastic modulus) such as elastomer and rubber. Their soft nature enables safe interaction with fragile objects, and compliant systems which can easily conform to arbitrary shapes. An example of application is the development of DEA-based grippers or manipulators [20, 24–27]. The example presented in Fig. 2.2(a) shows a multi-segment gripper developed for aerospace applications [25], which can wrap itself around objects of arbitrary shapes. Each individual finger can bend by more than 60° upon actuation, and generate up to 2.2 mN holding force. The multi-segment design can also be replaced by integrating oriented fibers in the membrane as presented in Fig. 2.2(b). The role of the fibres is to stiffen the membrane in specific directions, and to act as geometric hinges in the shape change [24]. One limitation of DEA-based grippers is their low holding force, typically in the mN range for single layer actuators. A clever solution is to use the device's fringing electric field for electroadhesion as shown in Fig. 2.2(c). In this example, the DEA's electrodes were patterned to increase the fringing electric field, effectively increasing the holding (shear) force of the device above 1 N [26].

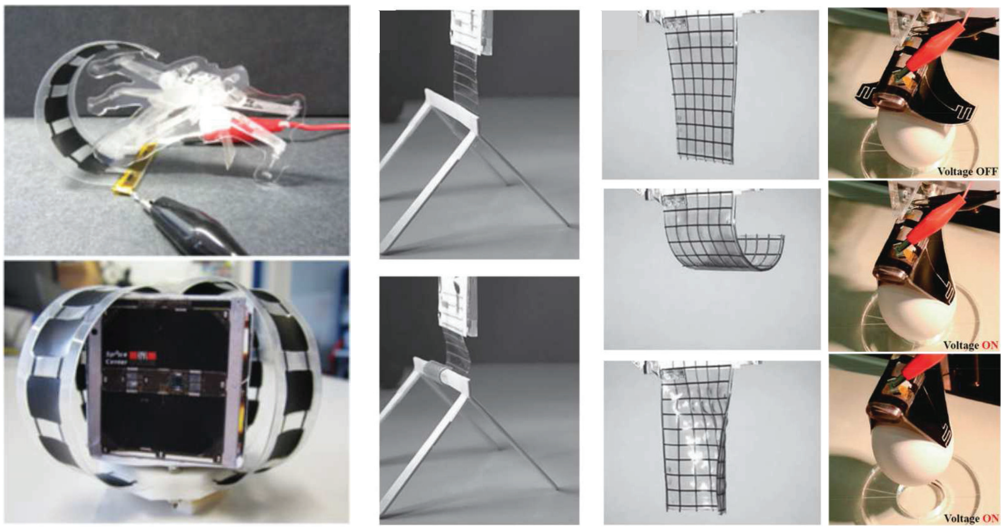

(a) (b) (c)

Figure 2.2 – (a)Rollable multisegment DEA-based gripper wrapped around objects of various shape and size to demonstrate conformability (Adapted from [25]). (b)Horizontal and vertical bending in a DEA-based gripper using embedded fibres that control the shape change (Adapted from [24]). (c)Versatile DEA-based soft gripper with intrinsic electroadhesion for improved holding force (Adapted from [26]).

2.3.2 Large actuation strain

DEAs have two main modes of actuation: surface expansion and thickness compression. Although both phenomenon occur concurrently, devices are often designed to use one or the other [28]. The surface expansion can occur in-plane or out-of-plane, and both configurations have demonstrated area expansion greater than 100 %. The largest reported strain for a DEA was achieved with the bubble-like actuator presented in Fig. 2.3(a). An acrylic elastomer membrane of 5 cm in diameter was coated with carbon grease electrodes, and mounted on a pressure chamber designed to safely harness the system electromechanical instability (EMI)(see section 2.4), demonstrating an area expansion of 1692 % [29]. For in-plane expansion, the largest actuation strain was reported on the device presented in Fig. 2.3(b), where an acrylic elastomer membrane of 3.5 cm in diameter was coated with carbon grease electrodes, and a set of weights were attached to its circumference to generate a constant radial tensile stress. In this configuration, the device could survive EMI and achieve an area strain of 488 % [11]. Those two configurations enable large deformation, but are less compatible with miniaturization [30]. The common alternative to external loads is to store mechanical energy in the actuator by prestretching the membrane and fixing it to a rigid frame. Using this approach, the miniaturized DEA presented in Fig. 2.3(c) could achieve 85 % linear actuation strain [14].

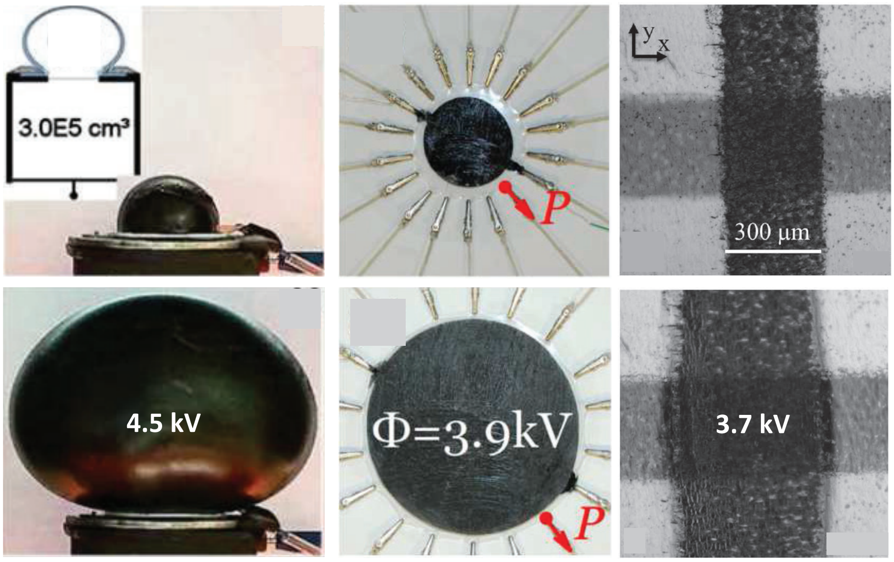

(a) (b) (c)

Figure 2.3 – DEAs can generate large actuation strain. (a)The largest strain was reported on a bubble-like actuator which used a pressure chamber to eliminate the device EMI, and achieved 1692 % area strain (Adapted from [29]). (b)For in-plane expansion, the largest actuation was achieved by attaching a set of weights to the actuator circumference. This configuration effectively suppressed EMI, and achieved 488 % area strain (Adapted from [11]). (c)External pressure source or dead load aren't practical for miniaturization. Instead, mechanical energy can be stored in the membrane by prestretching and fixing it to a rigid frame. This example show a miniaturized DEA which can achieve up to 85 % linear actuation strain (Adapted from [14]).

2.3.3 Fast response time

Despite their inherently soft nature, DEAs can provide fast electromechanical response. The actuation performance however strongly depends on the choice of materials, of both the soft dielectric membrane and the electrodes [31–34]. Response time can range from >1 s for acrylic elastomers, to <1 ms for silicone elastomers. An example of ultra-fast DEA is the tunable lens presented in Fig. 2.4(a), where an encapsulated liquid (lens) located at the center of a DEA is deformed upon actuation, hence modifying the system focal length [12]. The graph presented in Fig. 2.4(b) shows the normalized optical response as a function of frequency, and compares the performance obtained with acrylic and silicone elastomer membranes. The results clearly demonstrate the superior mechanical properties of silicone over acrylic elastomer, which exhibited significant viscoelastic losses. The device could be actuated at more than 1 kHz, making it the world's fastest tunable lens at the time of publication. Another example of fast DEA is the tubular actuator presented in Fig. 2.4(c), which was developed for active structral vibration control [35]. The actuator was made by Danfoss PolyPower A/S (Nordborg, Denmark), and essentially consisted of a silicone elastomer membrane with corrugated surface and electrode that was rolled on itself. The results presented in Fig. 2.4 show the dynamic response of the device, with the natural frequency of the system drifting from 30 Hz when loaded with a 100 g mass, to 20 Hz when loaded with a 500 g mass.

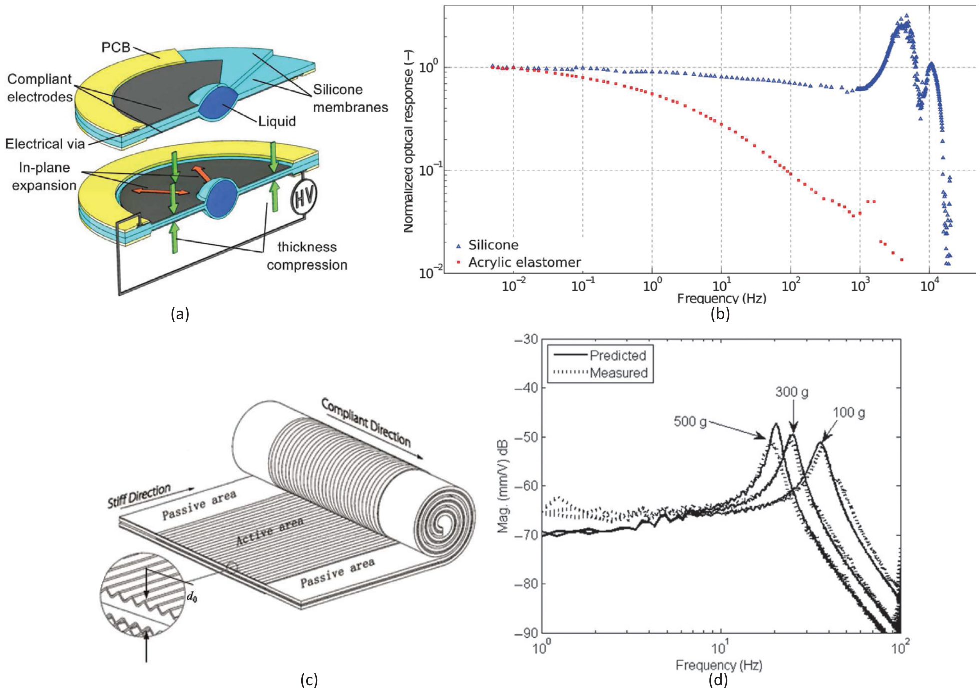

(a) (b) (c) (d)

Figure 2.4 – (a)Schematic of a fast DEA-driven lens, where an annular DEA compresses a central liquid encapsulation (lens), decreasing its radius of curvature and hence focal length. (b)Frequency response of the tunable lens, comparing the performance of silicone and acrylic elastomers. (Adapted from [12])(c)Schematic of the tubular actuator made by Danfoss Polypower A/S (Nordborg, Denmark) for active structural vibration control. (d)Frequency response of the actuator under increasing loads (Adapted from [35]).

2.3.4 Optical transparency

DEAs can be made almost completely [29,36,37] or partially [23,38,39] transparent to visible light, which enables many interesting applications. One of them is the development of tunable lenses, like the one presented in Fig. 2.4(a)-(b). This bioinspired design has the electrodes surrounding the lens (outside of the optical path), hence maximizing the optical quality of the system [40]. Another design is presented in Fig. 2.5(a), where the DEA covers one entire side of the lens, and is made with semi-transparent carbon nanotube (CNT) electrodes [41]. This alternative design maximizes the device tuning range, providing more than 100 % change in focal length. The semi transparent electrodes are however in the optical path of the system, and inevitably affect its optical quality. In other applications, optical defects are voluntarily patterned on top of a transparent DEA, like the laser speckle reducer presented in Fig. 2.5(b). This transparent device integrates an optical diffuser, moved in a circular motion by four independent DEAs, effectively destroying the coherence of the transmitted light [42]. This device is also an example of fast DEAs, with a reported actuation (resonance) frequency of 300 Hz. Instead of a diffuser, transmission [43,44] or reflection [45] diffraction gratings can be patterned on top of the DEA membrane. The example presented in Fig. 2.5(c) shows a DEA-based tunable transmission grating, with a continuous period tunability of 34.4 % [44].

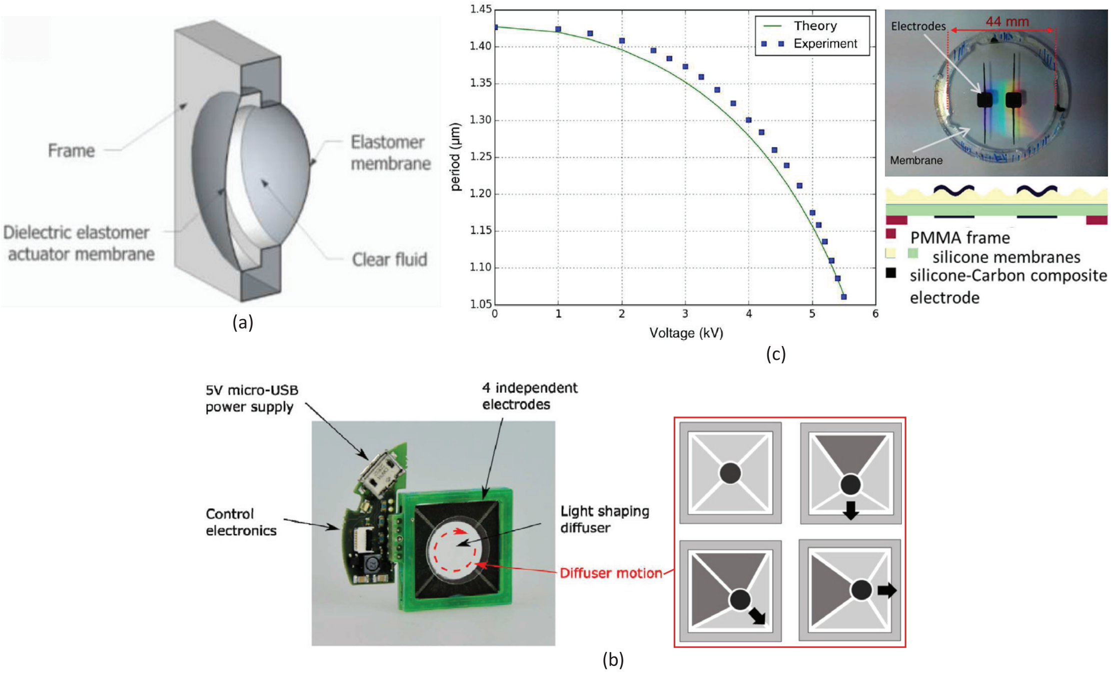
Frame
Elastomer membrane
Dielectric elastomer actuator membrane
Clear fluid
(a)
1.45
1.40
1.35
1.30
1.25
1.20
1.15
1.10
1.05
period (µm)
0
1
2
3
4
5
6
Voltage (kV)
Theory
Experiment
Electrodes
44 mm
Membrane
PMMA frame
silicone membranes
silicone-Carbon composite electrode
(c)
5V micro-USB power supply
4 independent electrodes
Control electronics
Light shaping diffuser
Diffuser motion
(b)

Figure 2.5 – (a)Tunable lens composed of a DE membrane, an encapsulated liquid, and a passive elastomer membrane. The passive membrane has a smaller radius of curvature, which increases upon actuation, hence increasing the device focal length (Adapted from [41]).(b)Laser speckle reducer developed by Optotune AG (Dietikon, Switzerland) composed of a diffuser surrounded by 4 independed DEAs used to generate a circular motion, and destroy the laser coherence(Adapted from [42]). (c)DEA-based tunable transmission diffraction grating continuously, with a continuous period tunability of 34.4 %(Adapted from [44]).

2.4 Working principle

2.4.1 Deformation response of dielectric elastomers

DEs are hyperelastic materials, and their response to mechanical stress is therefore not well described by linear elastic models. The stress-stretch relationship $\sigma = f(\lambda)$ of a DE subjected to an equibiaxial force P is schematized in Fig. 2.6 [46]. To understand the general shape of this curve, the material can be pictured as a bi-dimensional (2D) network of folded polymer chains, with cross-linking sites at every intersections. The elastic behaviour is provided by the polymer chains, which can unfold under tensile stress, allowing for the network to extend up to a limiting stretch value λ_{lim}, close to which the polymer network becomes increasingly stiff [47, 48]. For analytical and numerical analysis, the deformation response of rubber-like materials can be described using constitutive models. The Gent model is often used since it includes a limiting stretch parameter and can therefore predicts the material response at large stretch [49]. The Neo-Hookean and Yeoh models are also commonly used, but don't account for the presence of a limiting stretch.

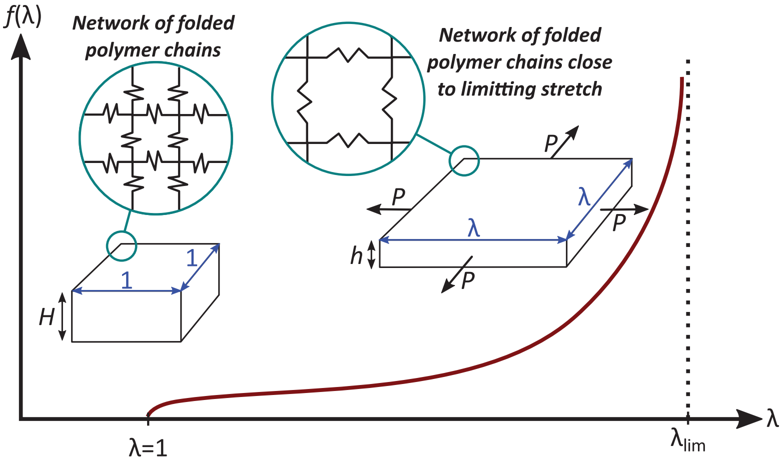
f(λ)
Network of folded polymer chains
Network of folded polymer chains close to limitting stretch
H
1
1
h
λ
λ
P
P
P
P
λ=1
λlim
λ

Figure 2.6 – Stress-stretch relationship $f(\lambda)$ of a DE membrane subjected to an equibiaxial force P (Adapted from [46]). The material elasticity comes from a network of folded polymers chains, which can extend under tensile stress, up to a limiting stretch λ_{lim}, close to which the polymer network becomes increasingly stiff.

2.4.2 DEA actuation

If we consider a DEA composed of an incompressible and isotropic DE membrane, sandwiched between two compliant electrodes of negligible stiffness, the stretch in the principal directions $(\lambda_x, \lambda_y, \lambda_z)$ can be written as:

$$\lambda_x \lambda_y \lambda_z = 1 \text{(volume conservation)} \tag{2.1}$$

$$\lambda^2 \lambda_z = 1 \text{(Equibiaxial actuation)} \tag{2.2}$$

$$\lambda^2 = 1/\lambda_z, \tag{2.3}$$

and the electrostatic stress generated in the membrane during actuation can be expressed as:

$$\epsilon E^2 = \epsilon \left(\frac{V}{h}\right)^2 \ [46] \tag{2.4}$$

where ϵ is the dielectric permittivity, h is the thickness, E is the electric field across the membrane thickness, and V is the applied voltage. Due to the constant-volume (Poisson ratio of 0.5) of the soft DE membrane, a thickness compression is accompanied by an area expansion. This particularity of soft dielectric elastomer transducers explains why the electrostatic pressure obtained in Eq. 2.4 corresponds to twice the pressure normally calculated for parallel plate capacitors [50]. If no external load is applied on the system, the equation of state is:

$$\epsilon \left(\frac{V}{h}\right)^2 = f(\lambda), \tag{2.5}$$

where $f(\lambda)$ is the stress-stretch function of the DE membrane, and λ is the lateral stretch as defined in Eq. 2.3. The membrane thickness h can be replaced by $h = H/\lambda^2$, where H corresponds to the initial membrane thickness, and the voltage-stretch relationship of the system can be written as:

$$V = \frac{H}{\lambda^2}\sqrt{\frac{f(\lambda)}{\epsilon}}. \tag{2.6}$$

From this equation, the general shape of the voltage-stretch response of DEAs can be obtained, and is presented in Fig. 2.7. The results show that the voltage increases with stretch, until it reaches a first maximum which corresponds to the point of electromechanical instability (EMI). At this point, there is a positive feedback between the membrane thinning and the increase in electric field, similar to the pull-in effect observed in parallel plate actuators [51]. Thanks to the hyperelastic properties of the membrane, and more precisely to its mechanical stiffening close to the material limiting stretch, the actuator can jump to another stable region of the curve (i.e positive slope). This stable position is however at much higher stretch, and the EMI jump therefore often induces dielectric breakdown.

Dielectric breakdown is one of the main failure mechanism of DEAs. It occurs when the electric field in the membrane exceed the material dielectric strength E_B, at which point there is an electrical discharge between the two electrodes, which irreversibly damages the actuator [52]. Some types of electrodes have however demonstrated self-clearing capabilities [53, 54], allowing an actuator to recover from this type of failure. The breakdown voltage V_B can be calculated as a function of stretch ($V_B = E_B/h = V_B H/\lambda^2$), and plotted with $V(\lambda)$ as presented in Fig. 2.7. Dielectric breakdown occurs at the intersection of the two curves, and can be induced by the EMI jump as illustrated in this example.

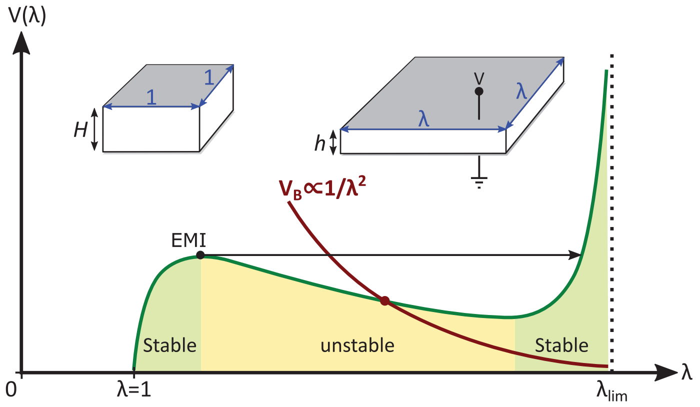

Figure 2.7 – The green curve corresponds to the voltage-stretch response of a DEA under no external load, and the red curve corresponds to the breakdown voltage V_B (Adapted from [46]). The actuation voltage V increases with stretch λ, until it reaches the point of EMI, where there is a positive feedback between the membrane thinning and the increase in electric field. At this point, the system jumps to a stable position of much higher stretch, often exceeding the membrane dielectric strength.

The unstable region of the DEA response can be suppressed by two methods. The first one is to modify the shape of $f(\lambda)$ by decreasing λ_{lim}. This effectively stiffens the membrane at lower stretch, and ensure that the mechanical restoring force of the system is high enough to avoid positive feedback between the membrane thinning and the increase in electric field. For synthetic elastomers, λ_{lim} can be decreased by increasing the cross-link density [55], or using interpenetrating network [21]. The second method is to apply an external force P on the membrane during actuation. In this configuration, the equation of state can be rewritten as:

$$\frac{P}{\lambda h} + \epsilon \left(\frac{V}{h}\right)^2 = f(\lambda), \tag{2.7}$$

and the voltage-stretch relationship can be rewritten as [46]:

$$V = \frac{H}{\lambda^2}\sqrt{\frac{f(\lambda) - P\lambda/H}{\epsilon}}. \tag{2.8}$$

The force P can be constant or vary during actuation, like in the case of a prestretched membrane fixed on a rigid frame. To illustrate the effect of an external load, the voltage-stretch response of a DEA under a constant force P_{pre} is presented in Fig. 2.8. Due to the applied force, the initial stretch state λ_{pre} is closer to λ_{lim}, which has a similar effect to decreasing λ_{lim}. In addition, Eq. 2.8 shows that the applied force P_{pre} artificially modifies the shape of $f(\lambda)$, decreasing the driving voltage and suppressing the $V(\lambda)$ peak at the origin of the EMI. This is an important result, which enabled unprecedented strain levels, and was critical to the development of DEAs [10]. For practical reasons, the external force is typically applied on DEAs by simply prestretching the membrane, and fixing it to a rigid frame. In this configuration, the external force P however decreases as the actuation strain increases.

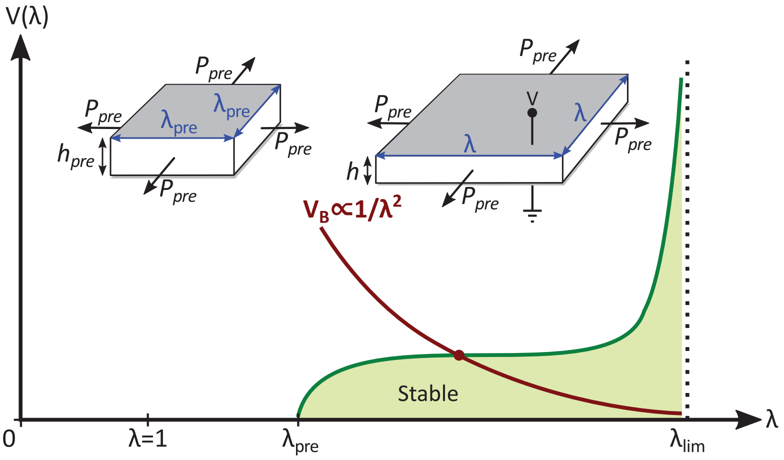

Figure 2.8 – The green curve corresponds the voltage-stretch response of a DEA under constant load P_{pre}, where the initial stretch λ_{pre} is set by the external force, and the red curve corresponds to the breakdown voltage V_B (Adapted from [46]). In this configuration, the EMI is completely suppressed, hence enabling large actuation strain.

Another important strain limiting mechanism of DEAs is loss of mechanical tension. This reversible process is characterized by a buckling motion and/or the formation of wrinkles on the electrodes [56, 57]. It doesn't cause immediate failure (i.e. dielectric breakdown), but limits the maximum actuation strain. The condition of loss of tension is when the in-plane mechanical stress reaches zero [58, 59], which happens when the actuation force of the DEA can't overcome the resulting reaction force, and it becomes energetically favourable to deform out-of-plane. The reaction force can be from a rigid frame [56], from embedded stiffening fibres [57, 58], or from a passive zone in the device membrane [14]. An interesting example is presented in Fig. 2.9, where radial wrinkles are formed on the electrodes. The loss of mechanical tension isn't induced by the surrounding rigid frame, or the central passive zone of the membrane, but by the compressive hoop stress generated during actuation.

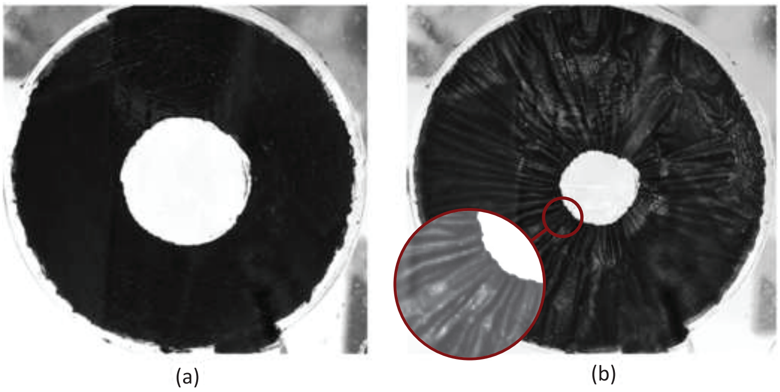
(a)
(b)

Figure 2.9 – An annular DEA showing loss of mechanical tension and the formation of radial wrinkles (Adapted from [60]). Loss of mechanical tension doesn't necessarily induce failure (i.e. dielectric breakdown), but it limits the actuation strain of the actuator.

2.5 Materials

2.5.1 Dielectric elastomers

To maximize the actuation strain of DEAs, the DE membrane has to exhibit two important properties: It should have a low Young's modulus, and a high dielectric strength. A wide range of elastomers have been tested as DEA materials [61], including natural rubber [62], acrylic elastomers [63], silicone elastomers [64], polyurethane [65], and thermoplastics [66]. Most reported devices however use the VHB acrylic elastomer film commercialized by 3M, or some of the commercially available two-part (i.e. addition curing) silicone elastomers.

The VHB is available in film as shown in Fig. 2.10(a), and provides an adhesive surface, making the fabrication of the actuator straightforward: The film is typically prestretched, fixed on a rigid support using its natural adhesion, and patterned with carbon-powder or carbon-grease electrodes. In addition, the material provides a unique combination of low Young's modulus and high dielectric strength, which enables large actuation strain [11, 29]. The film is however only available in predefined thickenesses of 0.5 mm and 1 mm, which makes the membrane thickness and prestretch interdependent, and limits the design possibilities. Moreover, the soft acrylic elastomer is also viscoelastic, and provides poor dynamic response when compared with alternative materials like silicone elastomers.

A wide range of silicone elastomers are readilly available, offering different Young's modulus, dielectric strength, maximum stretch at break, viscoelasticity and dielectric permittivity [64]. Based on the application requirements, other parameters can also be considered such as the material's optical transparency or biocompatibility. Silicone elastomers exhibit lower actuation strain than VHB, but provides faster mechanical response due to their low viscoelasticity [12]. In addition, silicones are available in their uncured state, and can be formed into membrane of the desired thickness. A wide range of techniques have been demonstrated to produce DE film of all thicknesses (sub-µm to 100 µm), including blade casting (Fig. 2.10(b)) [67], spray coating [68], spin coating [69], and molecular beam evaporation [69]. More recently, Wacker Chemie AG and Parker Hannifin Corporation have put on the market silicone elastomer films for DEA applications, with thicknesses ranging from 20 µm to 400 µm.

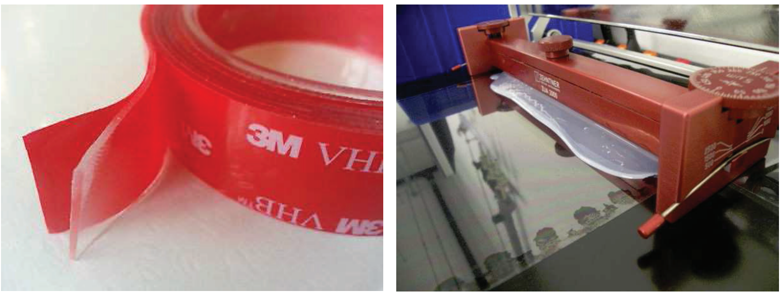

(a) (b)

Figure 2.10 – (a)VHB acrylic elastomer commercialized by 3M which comes in 0.5 mm and 1 mm thick films. (b)Two-parts silicone elastomer being formed into a membrane of the desired thickness using a blade-casting applicator. Once formed in to a membrane, the silicone elastomer is heat-cured, and peeled from the casting substrate.

Important efforts have been made in the recent years to develop new materials, tailored for DEA applications [61, 64]. One of the main focus has been to increase the dielectric permittivity and the electromechanical sensitivity of the DE membrane, hence decreasing the driving voltage of DEAs [70, 71]. Another focus has been to eliminate the EMI by modifying the mechanical properties of the DE membrane, using interpenetrating network to lock prestrain in the membrane [21], or tuning the stress-strech relationship by controlling the crosslinking density [55]. Although significant progress has been made in this field, material engineering has proven to be very challenging, and most actuators are still fabricated using commercially available acrylic or silicone elastomers.

2.5.2 Stretchable electrodes

The ideal electrode has a resistivity and a Young's modulus equal to zero, which ensures that the DEA performance is only determined by the properties of the DE membrane. In practice however, there is typically a trade-off to be made between those two properties, meaning that low resistivity electrodes often have a greater stiffening impact, and vice-versa. Depending on the specific application, other properties such as resistance to mechanical abrasion, optical transparency, and biocompatibility of the electrode can also be required. Most DEAs made of carbon- or metal-based electrodes [72, 73]. Other technologies like conductive polymers [74] and ionogels [37] have also been reported, but are less commonly used.

Carbon-based electrodes

Carbon particles can be simply deposited on the membrane as presented in Fig. 2.11(a). The loose carbon particles provide minimal stiffening impact, but are sensitive to static charges, difficult to pattern, and can easily detach from the surface. As an alternative, carbon particles can be incorporated into a viscous medium and painted on the membrane as presented in Fig. 2.11(b). With the carbon particles incorporated in a viscous medium like oil, the electrodes are much easier to handle and to pattern. The oil however induce viscous losses, and can diffuse in the membrane, thus affecting its mechanical and electrical properties. Instead of a viscous medium, carbon particles can be incorporated into an elastomer matrix, and cured on the membrane as presented in Fig. 2.11(c). Before curing, the electrodes are easy to handle and to pattern. After curing, they offer structural stability, and won't transfer upon mechanical contact. The Young's modulus is however higher, and the electrodes thickness should be minimized in order to limit mechanical stiffening [32].

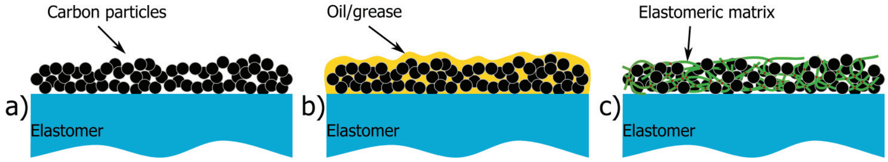

Figure 2.11 – Three main types of carbon-based electrodes: (a)Carbon particles deposited on the surface. (b)Carbon particles embedded in a viscous medium. (c)Carbon particles embedded in an elastomer matrix, and cured once on the membrane. (Adapted from [72])

The carbon electrodes are mainly based on carbon black or graphite particles, but the use of CNTs has also been reported [38, 75]. Due to their high electrical conductivity, thin layers of CNTs can be used, providing semi-transparent electrodes with self-clearing capabilities (i.e. in case of dielectric breakdown, the electrodes are locally vaporized, hence electrically insulating the breakdown area).

In this thesis, I use carbon particles embedded in an elastomer matrix as electrodes, building on the laboratory expertise [67]. To prepare the electrode material, carbon powder is dispersed in uncured silicone elastomer using ball mixing. This conductive ink is then patterned on the DEA membrane using pad-printing as presented in Fig. 2.12: 1)The equipment consists of a cliché engraved with the desired electrode design, a reservoir filled with conductive ink, and a silicone pad. 2)Sliding the reservoir over the cliché fills the engraved pattern with conductive ink, 3)which is then transferred from the cliché to the DEA membrane via soft-contact from the silicone pad. 4)Once transferred on the membrane, the electrode is then heat cured to crosslink the elastomer matrix. With this technique, 2-3 µm thick electrodes can be patterned with a ~100 µm lateral resolution. (Chapter 7 details how the same technique can be used to print ~µm thick silicone elastomer membrane for DEA applications.)

Other approaches can be used to pattern conductive rubber electrodes. The electrode material can be diluted and spray coated on the membrane through a shadow mask [76]. It can also be screen printed [77], or transferred on the membrane using a micro-patterned elastomer stamp [78]. Another technique is to cast and cure the electrode material on a sacrificial substrate, pattern it by laser engraving, and bond it to the DEA membrane before dissolving the sacrificial substrate [79].

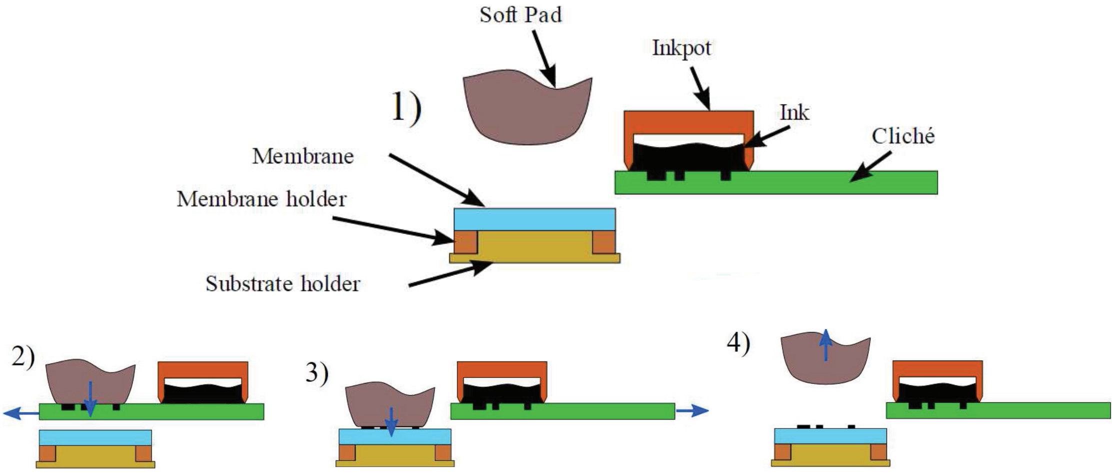

Figure 2.12 – Pad-printing is used in this thesis to pattern carbon-elastomer composite electrodes. 1)The equipment is composed of a cliché engraved with the desired electrode design, a container filled with conductive ink, and a soft silicone pad. 2)Sliding the reservoir over the cliché fills the engraved pattern with conductive ink, 3)which is then transferred from the cliché to the DEA membrane using the silicone pad. 4)Once the electrodes are patterned on the membrane they are heat cured to crosslink the elastomer matrix.(Adapted from [30])

Metal-based electrodes

For metallic electrodes, the simplest solution is to evaporate a thin metallic film on the DE membrane. The metallic layer provides a thickness dependant electrical conductivity, and optical transparency. It can however stiffen the actuator by more than two orders of magnitude [80], and doesn't enable more than a few percent strain before cracking and losing conductivity. This approach is therefore better suited for bending actuators like the one presented in Fig. 2.13(a) [69], where small strain levels can generate large bending angles. One alternative is to pattern the metallic film [81], minimizing its stiffening impact, and improving the maximum deformation. An example is presented in Fig. 2.13(b), where a spiral pattern was used to optimize the out-of-plane displacement of a DEA diaphragm [82]. Another approach to improve the actuation strain of metallic electrodes, is to use a corrugated substrate as presented in Fig. 2.13(c) [83]. A similar configuration can also be obtained by evaporating a thin metallic film on a stretched substrate, and then relax it to induce wrinkles in the stiff electrodes [84]. In this configuration, the actuator can expand by more than 20 % before loosing conductivity. Finally, some more unconventional approaches have also been proposed, like the implantation of gold ions at the surface of the membrane [39], the use of encapsulated liquid metals [85], or photopatternable platinum salt electrodes [86]. Those last techniques can provide interesting performance, but at the cost of more complex fabrication processes.

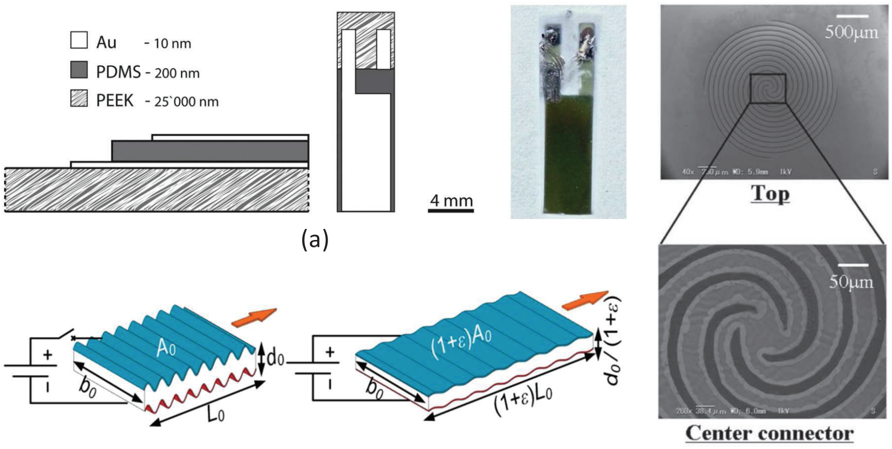

(a)

(c)

(b)

Figure 2.13 – Metallic electrodes provide low resistivity, are semi-transparent, but can significantly stiffen the DEA. (a)Bending actuators are a possible application where low strains can generate large deformations.(Adapted from [69]). (b) Metallic electrodes can be patterned to decrease their stiffening impact, here enabling large out-of-plane deformation of a suspended DE diaphragm (Adapted from [82]). (c)Corrugated metallic electrodes can be used to enable large (>20 %) uniaxial strain (Adapted from [83]).

Electrodes stiffening impact

During actuation, the DEA electrodes expand with the membrane, and their mechanical deformation contributes to the energy balance of the system. Practically, it implies that the actuation strain of DEAs decreases with stiffer electrodes. This effect was often neglected in early designs, where thick membranes, and electrodes with almost no resistance to deformation (carbon power or carbon grease) were used. However, by decreasing the membrane thickeness to reduce the driving voltage, or by using conductive rubber electrodes instead of carbon powder to improve manufacturability, the mechanical impact of the electrodes increases significantly. A few studies have investigated this effect, and experimentally demonstrated the electrodes stiffening impact on DEAs performance [32–34]. This topic however remains mostly overlooked, particularly in the development of analytical models. In Chapter 7, I present an analytical model that accounts for the electrodes mechanical stiffness, developed to help designing and optimizing thin DEAs.

2.6 Conclusion

In this chapter, I introduced the concept of DEA, discussed the key features of this technology, and presented a selection of state-of-the-art devices. I summarized the theory required to understand the voltage-stretch response of DEAs, and explained the main strain-limiting mechanisms: EMI, dielectric breakdown and loss of mechanical tension. Most importantly, prestretch was identified as a key parameter to eliminate EMI, and achieve large actuation strain. In the last section, I presented the main DEA materials, and discussed how the choice of DE and electrodes can affect the actuator performance.

3 Introduction to cell mechanobiology

3.1 Summary

In this chapter, I introduce the concept of cellular mechanobiology, an emerging field of science that studies how cells can sense and respond to their mechanical environment. I present examples of how cellular activity can be regulated by mechanical stimuli, and explain the importance of gaining insight into the underlying mechanotransduction mechanisms. At the interface between biology and engineering, this multidisciplinary research area heavily relies on *in vitro* models. I review the main techniques for mechanical stimulation of cells *in vitro*, highlight the limitations of current technologies, and detail recent advances in miniaturized deformable bioreactor.

3.2 Introduction to cell mechanobiology

Cells in the human body are constantly exposed to a complex and dynamic mechanical environment. Looking at the circulatory system for instance, muscle contraction generates tensile and contractile stress in cardiac tissues, whereas the resulting blood flow generates shear stress on the artery walls. It has been demonstrated that cells can sense their mechanical environment, and translate this information into a biochemical response [2–4]. This is achieved via mechanotransduction mechanisms, and can influence fundamental cell functions such as mobility [87], proliferation [88–90], apoptosis [91], and differentiation [88, 92]. Impairment of these cellular functions contribute to the underlying causes of various diseases, including atherosclerosis [93] and cancer [94]. To illustrate the omnipresence of mechanical stimuli in the human body, a non-exhaustive list of internal stimuli and the possible mechano-associated disseases are presented in Fig. 3.1 [8].

The idea that the development of the human body can be affected by its mechanical environment can be traced as far back as 1892, in a study where J. Wolff demonstrated bone remodelling under different loading conditions. Observations at the cellular level had to wait for the invention of the voltage clamp, which enabled biologists to measure ion current through the cellular membrane.Using this technique, stretch-induced depolarization of nerve cells was reported in 1950 [95], providing the first demonstration of mechanosensentivity at the cellular level. The underlying mechanisms were however still unknown, and it’s only in 1984 that a first mechanotransduction mechanism was successfully identified. Using the patch clamp technique, researchers could demonstrate the existence of mechanically-gated transmembrane ion channel [96]. Since then, the biomechanics of various organs and tissues have been investigated, with tangible outcomes like the development of better diagnosis and treatment for cardiovascular and respiratory diseases [2].

Despite considerable progress in mechanobiology over the past few decades, the fundamental mechanisms of cellular mechanotransduction remain largely unclear. Advances in this field could lead to better diagnosis and treatments for some of the leading causes of death in the world, including heart diseases and cancers, and provide valuable insights for other emerging fields like tissue engineering. There is therefore great interest in new tools and technologies for mechanotransduction studies, particularly for the development of microengineered platforms, which can provide accurate stimulation and sensing in high-throughput experiments [97].

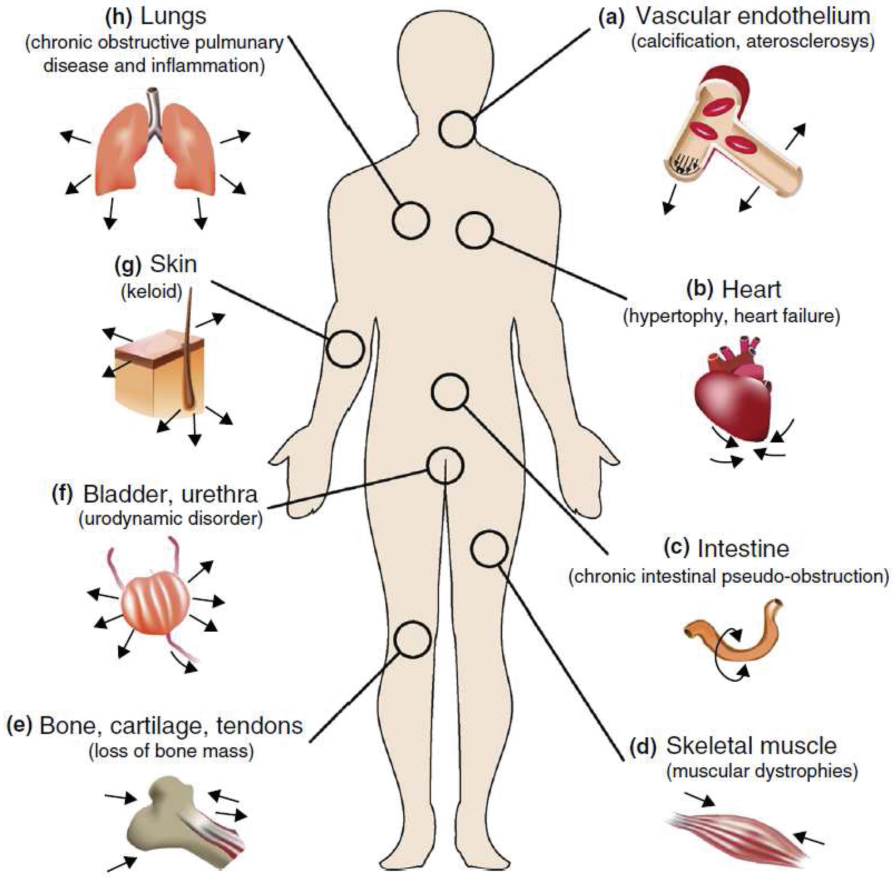
(h) Lungs
(chronic obstructive pulmunary disease and inflammation)
(a) Vascular endothelium
(calcification, aterosclerosys)
(g) Skin
(keloid)
(b) Heart
(hypertopy, heart failure)
(f) Bladder, urethra
(urodynamic disorder)
(c) Intestine
(chronic intestinal pseudo-obstruction)
(e) Bone, cartilage, tendons
(loss of bone mass)
(d) Skeletal muscle
(muscular dystrophies)

Figure 3.1 – Cells in the human body are exposed to a complex and dynamic mechanical environment. Impairment in their ability to sense and respond to mechanical stimuli can contribute to the underlying causes of various diseases. This figure presents a non-exhausitve list of the internal mechanical stimuli in the human body, and report some of the possible mechano-associated diseases (Adapted from [8])

3.3 Techniques for mechanical stimulation of cells *in vitro*

Due to the complexity of the *in vivo* environment, mechanotransduction studies heavily rely on *in vitro* models. In order to overcome the limitation of standard static culture dishes, several techniques have been developed to apply controlled mechanical loads on cultured cells. The main approaches capable of providing precise and dynamic stimulation are summarized in Fig. 3.2. They can be separated in three types, based on the scale at which they are designed to work: sub-cellular, single-cell and cell population.

At sub-cellular scale, one of the most common techniques is atomic force microscopy (AFM), where a sharp tip with a radius of curvature on the orders of nanometers is located at the end of a cantilever. The tip is brought in contact with the cell membrane as presented in Fig. 3.2(a), and used to generate a local deformation field. With this approach, it is also possible to extract information on the membrane stiffness by tracking the cantilever displacement and bending angle [98]. A second approach is magnetic twisting cytometry, which uses functionalized magnetic micro-beads that attaches to the cell membrane. Once they are attached to the membrane as shown in Fig. 3.2(b), an external magnetic field is used to generate a twisting moment on the beads, hence twisting the membrane. The analysis is slightly complex, but can provide information on the mechanical properties of the membrane. Local stimulation of cell *in vitro* has been used for mechanotransduction experiments [99, 100], and to characterize the mechanical properties of the cellular membrane [101, 102].

At cellular scale, mechanical stimulation can provide insight on how the cytoskeleton network respond to stress for example. A common approach is micropipette aspiration, where a suspended cell (i.e. not attached to a substrate) is deformed using suction as presented in Fig. 3.2(c). Information on the mechanical properties of the cell can also be obtained by analysing the evolution of its shape during suction, and the technique can be easily combined with electrophysiology studies (i.e. monitor the transmembrane electrical potential). A second approach is optical tweezers, used to manipulate functionalized silica micro-beads that attach to the cell membrane as presented in Fig. 3.2(d). The beads are trap at the focal point of a highly focussed laser, and their position can be controlled by steering the laser beam. Two beads are typically required, one on each side of the cell, and are used to apply compressive or tensile stress. Information on the cell mechanical properties can be obtained by analysing the evolution of its shape, but similar to magnetic twisting cytometry, the mechanical analysis can be complex. Mechanical stimulation of single-cells has been used for mechanotransduction studies [103, 104], and to characterize the mechanical properties of cells [105, 106].

At population scale, experiment are more representative of the *in vivo* environment. A common approach is shear-flow experiments, in which a flow of culture medium is used to generate shear stress on cultured cells as presented in Fig. 3.2(e). The flow is typically generated with a cone-and-plate viscometer system, a parallel-plate flow chamber, or a wave bioreactor. The shear stress can be easily calculated and controlled with the system geometry and flow rate. Another common approach is to culture cells on a deformable substrate which can be actively deformed as presented in Fig. 3.2(f). The cell-to-substrate adhesion ensures that any mechanical deformation generated in the substrate is effectively transferred to the cells. This type of experiment is typically done using a thin elastomer membrane, functionalized with fibronectin or collagen to promote cell adhesion, and deformed using pneumatic or mechanical actuation, providing precise control over the applied stretch. Mechanical stimulation of cell population has been used to study biological responses such as stretch-induced morphological changes [88, 107] and gene expression [88]. Cell monolayers are used in most cases but there is growing interest in three-dimensional (3D) cultures [108, 109] which provide better model of the in vivo environment.

In this work, I focus on deformable bioreactors (Fig. 3.2(f)), and demonstrate the use of DEAs as a mechanically active culture substrate. The generation of tensile and compressive stress on cell populations is challenging, and available technologies are often limited in terms of performance. There is therefore great interests for new approaches to mechanical stimulation of cell populations *in vitro*. Particularly for techniques which enable miniaturization and parallelization. In the next section, I present the state-of-the-art of deformable bioreactors.

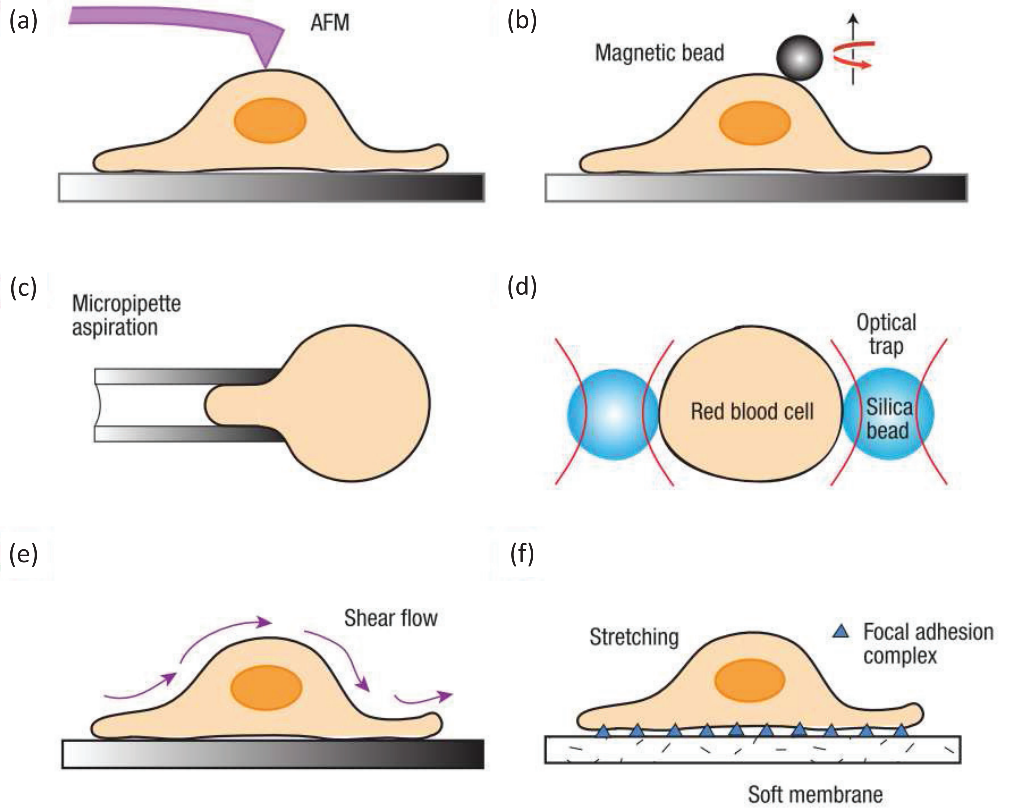

Figure 3.2 – Various approaches have been developed for the mechancial stimulation of cells *in vitro*. This schematic presents the the main approaches to deform cells locally:(a)AFM and (b)magnetic twisting cytometry, to deform single cells:(c)micropipette aspiration and (d)optical trapping, or to deform small cell populations:(e)shear flow stress and (f)substrate stretching.(Adapted from [2])

3.4 Deformable bioreactors

A deformable bioreactor is a mechanically active culture substrate, where precise and controlled strain can be applied to living cells. The strain is generated in the culture substrate, and transmitted to cells through their focal adhesions, which are large macromolecules that provides mechanical binding between the cells and the membrane (or the extracellular matrix *in vivo*) [110]. Several techniques have been used to deform soft culture substrate, including pneumatic, mechanical, magnetic and electrostatic actuation [8, 9, 97, 111, 112]. The systems have to be compatible with sterilization protocols, sustain days of incubation at 37 °C,5 % CO_2, and 95 % relative humidity, and days of immersion in growth medium. The important performance metric for deformable bioreactors are the strain type, amplitude and frequency. In addition, there is great interest in the development of miniaturized systems (hand-sized), enabling parallel experiments, and compatible with transmission optical microscopy. In this section, I present the main types of strain generated by deformable bioreactors, review the commercially available systems, and discuss the recent advances in miniaturized deformable bioreactors.

3.4.1 Types of strain applied to cells

The cells mechanical environment *in vivo* can be described in terms of shear stress and strain. For experiments on cell populations *in vitro*, shear stress is reproduced using shear-flow, and strain is reproduced using deformable bioreactors. Different types of strain can be applied to cell cultures, and Fig. 3.3 summarizes the most common ones.

- Uniaxial strain can be unconstrained as presented in Fig. 3.3(a), in which case the tensile strain is accompanied by a compressive strain in the transversal direction due to the Poisson effect. Uniaxial strain can also be constrained as presented in Fig. 3.3(b), limiting or suppressing the transversal compression, hence providing better strain uniformity. Uniaxial systems are often less complex, easier to control, and easily adapted for parallel studies. In addition, they provide an accurate description of the vascular environment *in vivo*, physiologically more relevant than multiaxial strain [113].

- Multiaxial strain can be biaxial as presented in Fig. 3.3(c), where the external force is applied along two perpendicular axis, or equiaxial as presented in Fig. 3.3(d), where the force is applied radially. (The equiaxial case is often distinguished from the equibiaxial [9] because strain profiles can differ significantly at the membrane boundary) Multiaxial systems can provide highly uniform strain profiles, and are physiologically relevant for studies on connective tissues [113, 114]. In addition, the biaxial systems provide high flexibility in terms of strain profile.

- Equiaxial strain can also be applied to cells through an out-of-plane deformation of the membrane as presented in Fig. 3.3(e). This configuration is found in many miniaturized systems, using pressure or mechanical actuation to induce buckling of a suspended membrane. Although enables compact designs (see section 3.4.3), the vertical motion of the membrane makes cell imaging difficult. In addition, the fixed boundary condition induces a radial strain gradient that intrinsically limit strain uniformity.

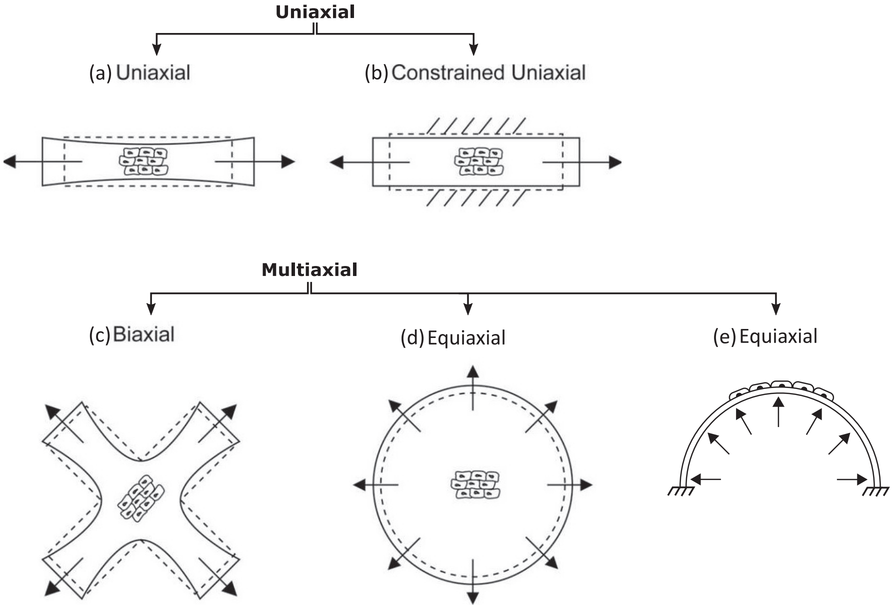

Figure 3.3 – Schematic of the different types of strain applied to cells by deformable bioreactors. Uniaxial strain can be (a)unconstrained, and exhibit compressive strain in the transversal direction, or (b)constrained in the transversal direction, and provide better uniformity. Multiaxial strain can be (c)biaxial, with force being applied along two perpendicular directions, or (d)equiaxial, with force being applied radially. (Equi-biaxial and equiaxial are often distinguished [9], mainly because their strain profiles are different close to the membrane boundaries) (d) Equiaxial strain cal also be applied to cells by out-of-plane deformation of the membrane, a configuration which is found in many miniaturized deformable bioreactors. (Adapted from [9])

3.4.2 Commercially available systems

There are currently three companies that provide deformable bioreactors. The available systems are relatively simple to use and reliable. They are however bulky, slow, and often incompatible with optical microscopy.

The most important one is Flexcell International Corporation [5], which specializes in equipment for research in mechanobiology and tissue engineering. Their system is presented in Fig. 3.4(a), and its working principle is schematized in Fig. 3.4(b). An elastic culture membrane is mounted on top of a pneumatic chamber, which includes a central loading post, on top of which the membrane can slide without sticking. When vacuum is created below the membrane, its suspended region is pulled out-of-plane, thus generating in-plane deformation in the area located over the loading post. The Flexcell system can generate up to 20 % equiaxial strain, and up to 33 % if the loading post is removed, which however induces out-of-plane displacement and lower strain uniformity. Culture membranes with anisotropic stiffness are also available, enabling up to 12 % uniaxial strain. In terms of actuation frequency, the system can be driven between 0.01 Hz and 5 Hz, thus covering the range of biologically relevant frequencies.

Another company in the field of mechanobiology is CellScale Biomaterials Testing [6], which proposes systems to generate equiaxial or uniaxial strain on cultured cells. The equiaxial device is presented in Fig. 3.4(c), and is composed of an electric motor, attached to a flexible frame, which supports an elastic culture substrate. The flexible frame is presented in Fig. 3.4(d), and is designed to transform the uniaxial force (red arrows) generated by the motor, into radial force (blue arrows) that stretches the culture membrane equiaxially. The maximum strain and actuation frequency aren't accessible in the product information, and therefore can't be compared with alternative technologies. The company also proposes a system of similar dimension, which can be mounted on top of an inverted microscope, and apply uniaxial strain on 24 culture chamber in parallel.

A similar device is proposed by Strex USA [7], and presented in Fig. 3.4(e). The system consists in a series of elastic culture chambers, like the one shown in Fig. 3.4(f), and pulled in parallel by a linear motor. The system provides 20 % strain, at a maximum frequency of 1 Hz.

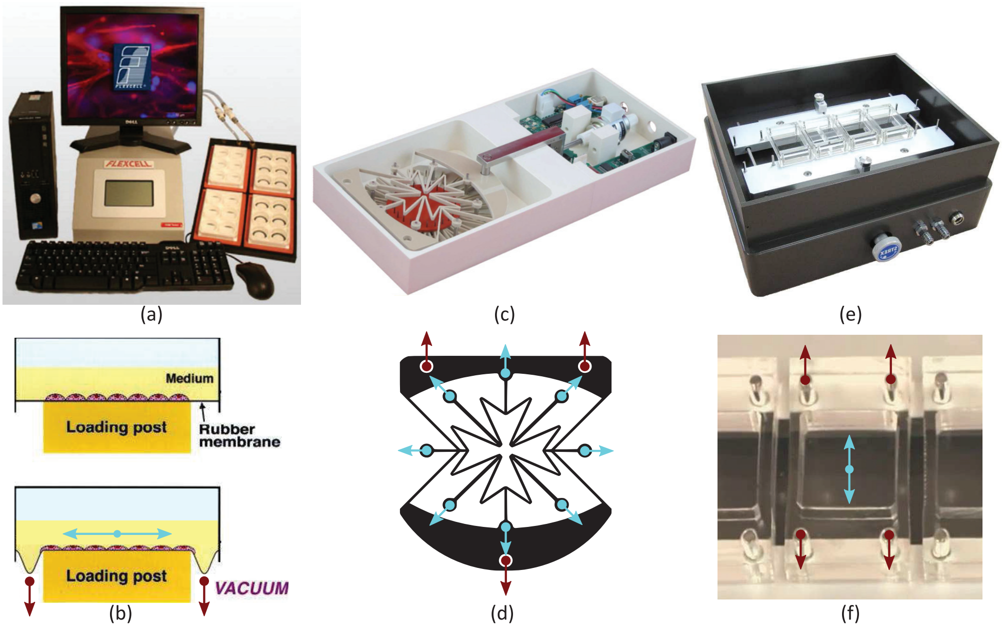

(a) (c) (e)
(b) (d) (f)

Figure 3.4 – Deformable bioreactors are commercialized by three main companies. (a)Flexcell International Corporation proposes a system based on pneumatic actuation, which provides uniaxial or equiaxial strain (Adapted from [5]). (b)The Flexcell device is composed of a culture membrane, suspended on top of a vacuum chamber with a central loading post. Using vacuum, the membrane is pulled against the post, and stretched in-plane (Adapted from [5]). (c)CellScale Biomaterials Testing proposes systems based on mechanical actuation, which provides uniaxial or equiaxial strain (Adapted from [6]). (d)The equiaxial device is composed of a suspended membrane, attached to a flexible frame, which gets pulled by a linear motor. The frame transform the linear force of the motor (red arrows), into an equiaxial force that stretches the membrane radially (blue arrows) (Adapted from [6]). (e)Strex USA also provide a system based on mechanical actuation, which provides uniaxial strain (Adapted from [7]). (f)The Strex device is composed of a series of elastic culture chambers, pulled in parallel by a linear motor. A similar system is also proposed by CellScale (Adapted from [7]).

3.4.3 Miniaturized systems

Commercial deformable bioreactors have enabled mechanical stimulation of cells *in vitro*, and demonstrated the importance of mechanotransduction studies. They are however bulky and low throughput, which limit their applications. Because of their size, commercial systems also don't make efficient use of precious reagents and cells [115]. To address those limitations, significant effort has been made over the past decade to miniaturize deformable bioreactors. In this section, I review the main approaches and classify them by actuation mechanisms.

Pneumatic actuation

Most miniaturized deformable bioreactors are based on pneumatic actuation, and therefore don't integrate any active element. The culture chambers are made of PDMS, fabricated using standard techniques for microfluidics, and connected to an external source of pressure or vacuum. With this approach, devices are easy to manufacture and reliable. The size of the culture chamber is also greatly reduced, but the entire system often remains bulky because of the external pump (can require up to 0.1 atm [116]) and valves. In addition, arrays require complex systems of pneumatic connections, and are therefore not practical. The solution is often to have a single pressure input, and a stiffness gradient across the array (ex. suspended membrane of increasing diameter).

A first design is presented in Fig. 3.5(a). Developed by the Wyss Institute at Harvard Univisersity, one of the leaders in the field of lab-on-a-chip, the device is composed of a suspended culture membrane, bounded by two pneumatic side-chambers [117]. When vacuum is created in the side-chambers, it generates uniaxial strain in membrane. With this device, the authors reproduced the lung functions on a chip, and stretched an alveolar-capillary interface by 15 % for 4 h at 0.2 Hz. The same design has also been used to reproduce the human gut on a chip [118], it has been fabricated in an array of 24 deformable culture chambers [13], and implemented with electrical stimulation capabilities to study both stimuli (i.e. electrical and mechanical) on a single device [119]. Interesting variations of the side-chamber design have been proposed, including the device presented in Fig. 3.5(b), where the suspended culture membrane is surrounded by four pneumatic chambers [116]. This configuration enables biaxial deformation, which greatly improve the device flexibility in terms of strain profiles, and demonstrated up to 25 % uniaxial strain . Another variation is presented in Fig. 3.5(c), where a circular membrane is surrounded by a cylindrical pneumatic chamber, and can generate up to 10 % equiaxial strain [48].

Another approach is to have the pneumatic chamber located below the culture membrane. In this configuration, a positive pressure will induce out-of-plane deflection as presented in Fig. 3.5(d) [115]. This device is an example of how a strain gradient can be generated using a single pressure input: From left to right, the membranes decrease in diameter and therefore an increase in stiffness. As a result, the first membrane deforms significantly more than the last one under the same pressure. Many devices are based on the same design [121, 122], and can generate up to 20 % equiaxial strain. Out-of-plane equiaxial deformation however provides low strain uniformity, and the vertical displacement makes optical imaging difficult. A different geometry is presented in Fig. 3.5(e), where a transparent loading post is pusched against the

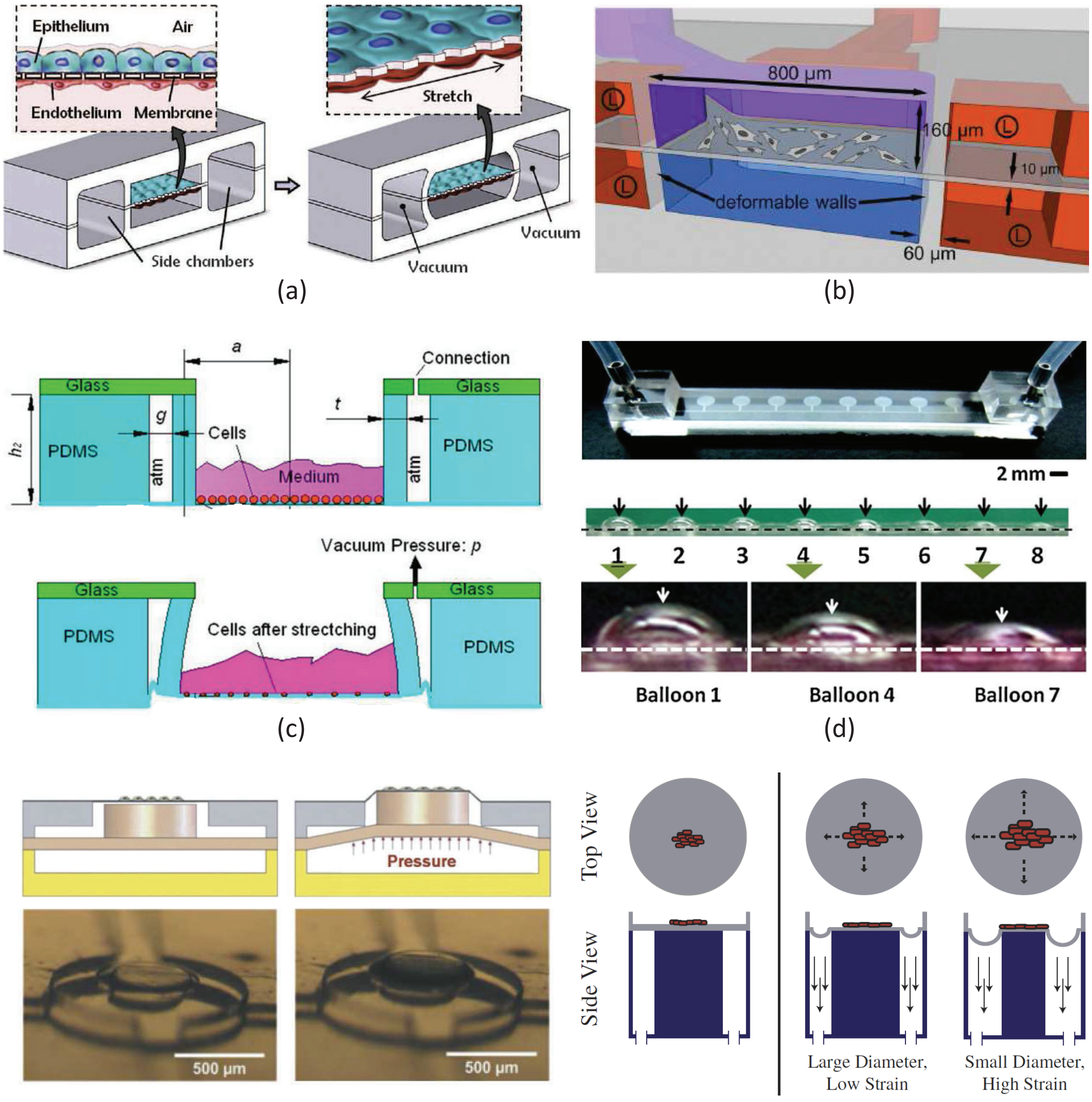
Epithelium
Air
Endothelium
Membrane
Side chambers
Stretch
Vacuum
Vacuum
800 µm
160 µm
10 µm
deformable walls
60 µm
L
a
Connection
Glass
Glass
g
t
h2
PDMS
Cells
PDMS
atm
Medium
atm
Vacuum Pressure: p
Glass
Glass
PDMS
Cells after stretching
PDMS
2 mm
1
2
3
4
5
6
7
8
Balloon 1
Balloon 4
Balloon 7
Pressure
500 µm
500 µm
Top View
Side View
Large Diameter, Low Strain
Small Diameter, High Strain

(a) (b) (c) (d) (e) (f)

Figure 3.5 – Most miniaturized deformable bioreactors are based on pneumatic actuation. Taking advantage of the techniques developed for microfluidics, the devices are easy to manufacture and reliable. A PDMS structure, composed of a suspended membrane and pneumatic side-chambers, can be used to generate (a)uniaxial strain (Adapted from [117]), (b)biaxial strain (Adapted from [116]), or (c)equiaxial strain (Adapted from [48]). With the pneumatic chamber located below the culture membrane, it is easy to generate (d)out-of-plane equiaxial strain (Adapted from [115]), (e)equiaxial strain using a moving loading post (Adapted from [108]), or (f)equiaxial strain using a fixed loading post (Adapted from [120]). To avoid the need for individual addressing, which can be complicated for arrays of pneumatic actuators, a strain gradient can be induced by the system geometry. This effect is shown in (f), where posts of increasing diameter induce decreasing strain levels for a same pressure input.

membrane as the pressure increases [108]. This design provides up to 6 % equiaxial strain, with better uniformity than the deflecting membrane, but still induces vertical displacement. An interesting alternative is presented in Fig. 3.5(f), where the transparent loading post is fixed, and the membrane is pulled against it using vacuum. This design, which is a miniaturized version of the system proposed by Flexcell [5], provides up to 6 % equiaxial strain, and keeps the membrane out-of-plane position stable.

Piezoelectric actuation

One of the first miniaturized deformable bioreactor was proposed by Kamotani et al. in 2008 [123]. The device is presented in Fig. 3.6(a), and is composed of an array of 24 suspended culture membranes, placed on top of a refreshable Braille display. The pins of the Braille display are individually controlled by piezoelectric actuators, and can be pushed against the culture membrane to generate radial strain. Using this device, the authors stretched endothelial cells by 25 %, for 12 h at 5 Hz. This approach provides a simple and compact design, but exhibits a non-uniform strain profile, and provides no control on the strain rate.

Thermal actuation

A few examples of thermal actuation have been reported, where small temperature variations in the culture substrate can induce large deformation. This approach provides simple devices, typically controlled with a simple heater, but which are often limited in terms of response time. In addition, it is challenging to develop materials that work over a range of temperature compatible with living cells. A first example is presented in Fig. 3.6(b), where cells are cultured on a creased hydrogel film, and stretched uniaxially by inducing swelling in the culture substrate [124]. The authors have demonstrated that the swelling ratio of the hydrogel film can be controlled with temperature, and generated 15 % uniaxial strain on living cells, by increasing the temperature from 26 °C to 38 °C over 10 min. A second example is presented in Fig. 3.6(c), where a liquid crystal elastomer was used as the culture substrate, a material known to exhibit reversible and large deformation under temperature change. The authors demonstrated up to 30 % uniaxial strain with this approach, but could only apply 5 % strain at frequencies below 1.6 Hz on living cells (to avoid excessive heating).

Magnetic actuation

Magnetic actuation has also been investigated [90, 125], using devices similar to the one presented in Fig. 3.6(d). The system is composed of an array of magnetic micropillars, patterned on a deformable culture membrane, and actuated with an external magnetic field [90]. This approach enables remote actuation, and is therefore compatible with *in vivo* applications. The device fabrication and control system are however complex compare to alternative actuation mechanisms. Under horizontal magnetic field, the micropillars all bend in the field direction, hence stretching cells attached on one end to a pillar, and on the other end to the passive membrane as shown in Fig. 3.6(e). With this approach, 5 % uniaxial stain was demonstrated on living cells [90], and in a different experiment, living cells were sitmulated at 10 Hz for up to 48 h [125].

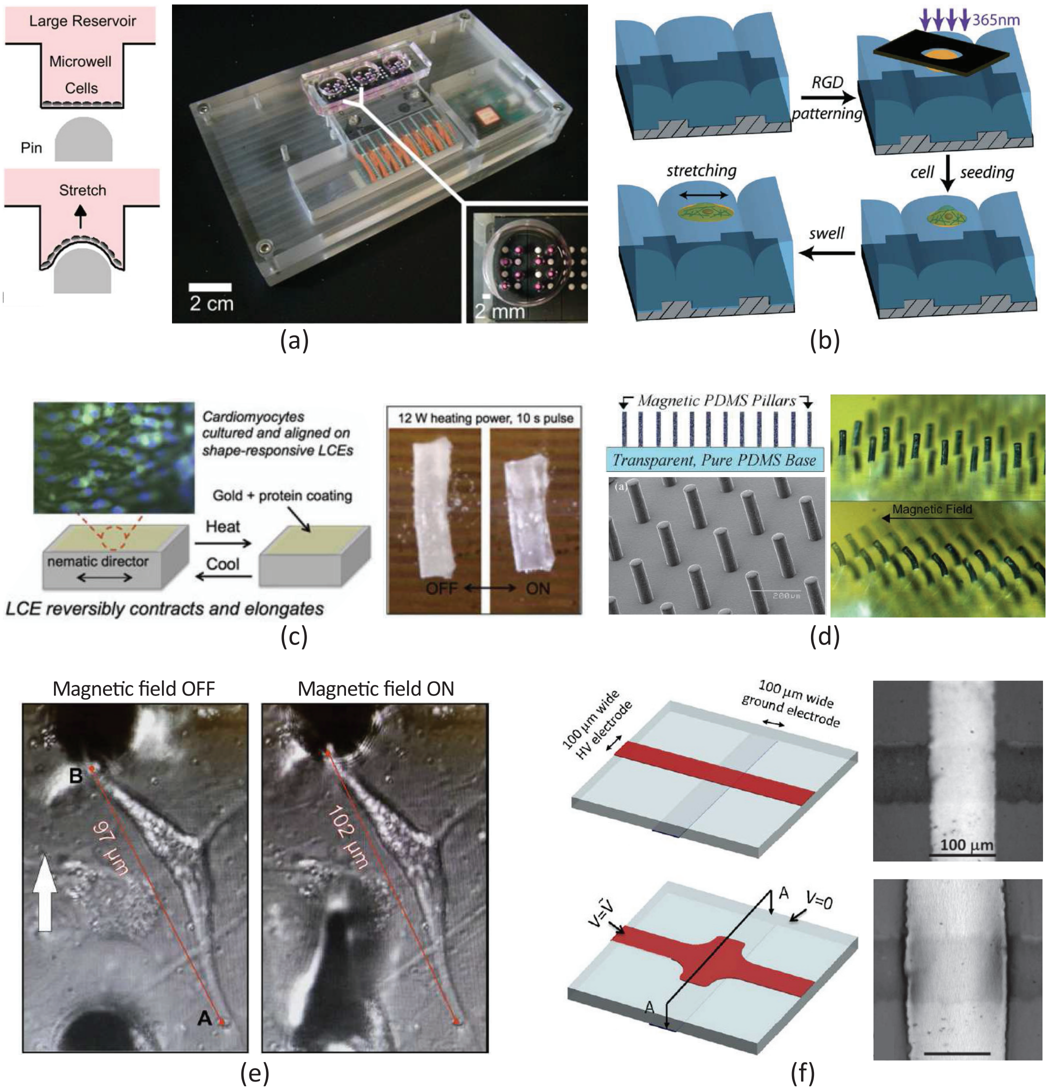
Large Reservoir
Microwell
Cells
Pin
Stretch
2 cm
2 mm
(a)
365nm
RGD
patterning
cell
seeding
stretching
swell
(b)
Cardiomyocytes cultured and aligned on shape-responsive LCEs
Gold + protein coating
Heat
Cool
nematic director
LCE reversibly contracts and elongates
12 W heating power, 10 s pulse
OFF
ON
(c)
Magnetic PDMS Pillars
Transparent, Pure PDMS Base
Magnetic Field
(d)
Magnetic field OFF
Magnetic field ON
B
A
97 µm
102 µm
(e)
100 µm wide HV electrode
100 µm wide ground electrode
V=Ṽ
V=0
A
A
100 µm
(f)

Figure 3.6 – In addition to pneumatic deformable bioreactors, alternative actuation mechanisms have been reported. (a)One of the first integrated solution was proposed by Kamotani et al. in 2008, and used a piezoelectrically actuated braille display to deform an array of suspended culture membranes (Adapted from [123]). Thermal actuation was used to generate uniaxial strain in culture substrate made of (a)crease hydrogel with a temperature-dependent swelling ratio ((Adapted from [124]), and (b)liquid crystal elastomers, known to exhibit large and reversible deformation under temperature change ((Adapted from [126])). Magnetic actuation was also reported, using (d)an array of magnetic micropillars, patterned on a PDMS membrane, and actuated using an external magnetic field((Adapted from [127]). The magnetic pillars bend in the direction of the magnetic field, (e)hence stretching cells with one end attached to a pillar, and the other end attached to the passive membrane((Adapted from [125]). (f)The use of DEA has been proposed, and a design for uniaxial stretching of single cells has been reported, but this technique has never been tested with cells (Adapted from [14]).

Electromechanical actuation

The use of DEAs for mechanical stimulation of cells *in vitro* was proposed by a group at ETH Zurich [128], which however never published on the topic. Prior to my arrival at the LMTS, an array of micro-DEAs was developed to apply periodic uniaxial tensile strain on small areas (100 µmx100 µm) of a larger cytocompatible membrane [14, 129]. The design of the actuator is presented in Fig. 3.6(f), where gold-implanted electrodes are patterned on both sides of a silicone elastomer membrane. Upon actuation, due to the membrane uniaxial prestretch, the actuator generates up to 80 % uniaxial strain. This work demonstrated the great potential of DEAs for mechanical stimulation of cells *in vitro*. It showed that large uniaxial strain can be generated on a (semi)transparent device, that single-cell stimulation is possible, and that arrays of actuators can be fabricated for high-throughput studies. It however didn't provide any demonstration that DEAs can be interfaced with living cells, and used to control their mechanical environment. Amongst other limitations, the device showed limited lifetime when actuated in aqueous solutions, a critical requirement for biological applications.

3.5 Conclusion

In this chapter, I introduced the concept of cellular mechanobiology, and explained how the development of miniaturized deformable bioreactors is of great interests for biologists. The large size of commercially available systems limits their applications, and wastes precious reagents and cells. I presented the state-of-the art of miniaturization deformable bioreactors, and detailed a wide range of systems, based on pneumatic, piezoelectric, thermal, magnetic and electromechanical actuation. It appears from this overview of the reported technologies, that DEAs could provide a unique combination of features, including large actuation strain, fast response time, optical transparency, arrays of actuators for high-throughput experiments, and a simple and compact control system.

4 DEA-based deformable bioreactor - Design and fabrication

4.1 Summary

In this chapter, I first summarize the fundamental requirements of deformable bioreactors, highlight the challenges of interfacing DEAs with living cells, and justify the main material and design choices that were made. I then present a versatile DEA design capable of generating compressive or tensile uniaxial strain on cells *in vitro*, and detail the device fabrication process.

The DEA-based deformable bioreactor I developed is presented in Fig. 4.1. The device is composed of a transparent silicone elastomer membrane, with stretchable electrodes patterned on both sides of the membrane, hence forming the DEA element. Cells are cultured on top of the device, and exposed to mechanical stimulation upon actuation (uniaxial tensile strain in the presented device). The electrode-gap is designed to provide optical transparency, and enables in situ high-resolution imaging of cells using transmission light microscopy.

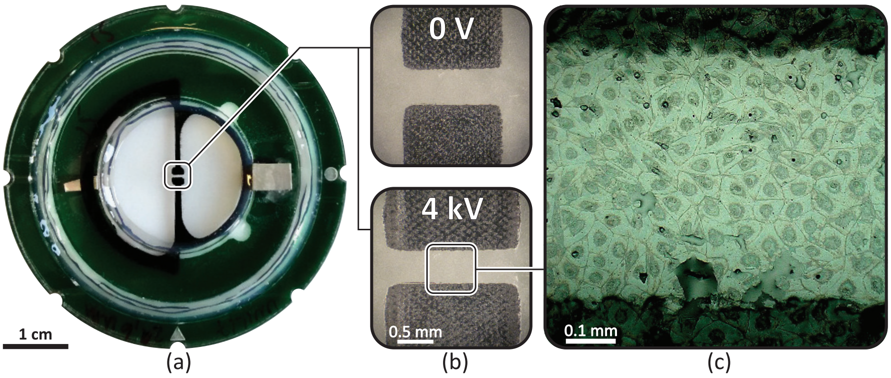

(a) (b) (c)

Figure 4.1 – (a) Picture of the DEA-based deformable bioreactor, composed of a transparent silicone elastomer membrane, prestretched, and fixed on a rigid plastic frame. Stretchable electrodes are patterned on both sides of the membrane, hence forming a DEA element which can provide local mechanical stimulation. (b) Close-up pictures of the DEA element show that uniaxial extension is generated upon electrical stimulation. (c) The generated strain is transferred to a cell monolayer which is cultured on top of the silicone membrane.

4.2 Requirements and design considerations

4.2.1 Key requirements

The main requirements and objectives for the DEA-based deformable bioreactor are summarized in Table 4.1. The system has to be cytocompatible, and sustain standard cell culture protocols such as sterilization and incubation. The materials therefore have to be non-cytotoxic, and their properties shouldn't be affected by immersion in ethanol or culture medium. Another key requirement is the optical transparency of the system. More precisely, the device has to be compatible with transmission light microscopy, which is the standard technique for live cell imaging. In terms of mechanical stimulation, requirements can vary significantly between experiments or types of cell, and there is no absolute range of biologically relevant parameters. In this work, I decided to focus on the generation of uniaxial strain, a type of strain which is well adapted to describe the vascular system [130]. For the strain amplitude and frequency, I defined the objectives based on the performance of commercially available systems, which can deliver between -20 % and 20 % strain, at frequencies below 5 Hz [5–7]. Depending on the studied mechanisms and types of cell, mechanotransduction experiments can require from 2 h [116], to more than 24 h [4] of periodic mechanical stimulation. Based on the duration of the reported studies, the objective for the DEA-based deformable bioreactor is to provide stable actuation performance for 2 h to 24 h of periodic actuation.

Table 4.1 – A summary of the key requirements and objectives for the DEA-based deformable bioreactor.

Parameter	Requirement/Objective
Biocompatibility	Essential
Sterilization compatible	Essential
Incubator compatible	Essential
Optical transparency	Essential
Strain types	uniaxial compressive/tensile
Strain amplitude	$-20\,\%$ to $20\,\%$
Actuation frequency	0.1 Hz to 5 Hz
Working lifetime	2 h to 48 h
Growth medium immersion	>3 days

4.2.2 Membrane material

To achieve large actuation strain, the DEA membrane is typically chosen for its dielectric and mechanical properties, selecting materials of high dielectric strength and low Young's modulus [81]. Standard materials include the VHB acrylic elastomer film commercialized by 3M, and silicone elastomers such as the Sylgard 186 commercialized by Dow Corning. For the DEA-based deformable biroeactor, the membrane materials also have to support cell growth, provide high optical transparency, and sustain standard cell culture protocols. Silicone elastomers are an interesting choice since they can be cytocompatible, chemically inert, and provide high optical transparency. They also exhibit fast, repeatable and stable mechanical response due to their good mechanical properties (i.e. low viscoelasticity and creep). Despite providing lower actuation strain than acrylic elastomers, silicone-based DEAs can generate more than 100% linear strain [10], which largely exceed typical requirements of deformable bioreactors (< 20%). In addition, silicone elastomers offer more design flexibility since they are readily available in their uncured state, and can be casted to the desired film thickness, thus enabling individual control of membrane thickness and prestretch.

The DEA-based deformable bioreactor was fabricated using a silicone elastomer membrane. This choice was mainly motivated by the superior mechanical properties of silicones, and by the possibility to cast the material into membranes of the desired thickness.

4.2.3 Electrode material

To achieve large actuation strain, the electrode material is typically selected to provide minimal stiffening impact on the actuator, and to remain conductive during actuation (i.e. under stretch) [32, 72]. Several electrode technologies meeting those criteria have been reported and are summarized in Chapter 2, including carbon powder, carbon nanotubes, silver nano-wires, carbon grease, carbon-loaded elastomer, implanted gold ions, and conductive hydrogels. In addition to provide high electrical conductivity and low mechanical stiffness, the electrodes of the DEA-based deformable bioreactor have to be cytocompatible (or else isolated from the cell culture). The main challenge is however for the electrodes to sustain standard cell culture protocols such as sterilization and incubation. The use of carbon-grease, carbon powder, carbon nanotubes, or silver nano-wires is therefore not suitable. Those types of electrode indeed risk of getting dissolved or washed away by ethanol during sterilization, or during incubation when cells are immersed in culture medium.

Although alternative technologies could have been used, such as as conductive hydrogels or gold implanted electrodes, I decided to fabricate the DEA-based deformable bioreactor using carbon-loaded silicone elastomer electrodes. The choice was mainly motivated by the laboratory's expertise with this technology, and because they can be easily and reproducibly patterned with high resolution (minimum feature size of 100 µm) using pad-printing [30].

4.2.4 DEA immersion in a conductive liquid

When interfacing DEAs with living cells, one important aspect to consider is that the cells have to stay immersed in culture medium, an aqueous solution designed to support cellular growth. It is however important for the DEA-based deformable bioreactor to have only one side immersed in culture medium, keeping the opposite side in air. In this configuration, the device can be easily mounted on top of a standard inverted optical microscope, hence enabling in situ live cell imaging. Another aspect to consider, is that due to the presence of various salts in solution, the culture medium is electrically conductive, and consequently acts as a blanket electrode. Although we could not observe any diffusion of ionic species from the culture medium in the DEA membrane, nor any effect of the device electric field on cell viability, a design with completely overlapping electrodes (as presented in Fig. 4.2) is preferable. In this configuration, the electric field is mostly confined between the DEA electrodes, thus limiting the cells exposure to the device fringing electric field.

The DEA-based deformable bioreactor was designed with completely overlapping electrodes (i.e. no exposed feed lines, an element often present in DEA designs). The electrode on the cell culture side was connected to ground, and only this side was immersed in culture medium, hence enabling optical monitoring to be done from the opposite (high-voltage) side. For experiments where the fringing electric field would become problematic, it is possible to almost suppress it using a three electrodes configuration: A high-voltage electrode is sandwiched between two DEA membranes, and covered on both sides by ground electrodes of slightly larger surface area. The device fringing electric field is almost suppressed in this configuration [131], but the need for a second membrane and ground electrode makes the fabrication more complex, and was therefore not implemented in this work.

4.3 Design for uniaxial tensile and compressive strain

4.3.1 Role of prestretch

The cells *in vivo* mechanical environment is often better described by anisotropic strains, notably in the vascular system [130]. There is therefore a lot of interest for systems capable of generating uniaxial strain on cells *in vitro*. While expanding-DEAs typically generate equibiaxial actuation, techniques to produce uniaxial actuation have been reported, including the use of stiffening fibres embedded in the membrane [132], the use of anisotropic boundary conditions [129], and the use of non-equibiaxial membrane prestretch [14]. Amongst those approaches, optimization of the membrane prestretch is the most suitable technique: It can provide large actuation strain, it is simple to implement, and it is compatible with miniaturization (i.e. not limited by the size of the stiffening fibres). Figure 4.2 presents the DEA design that I developed to generate tensile or compressive uniaxial strain. The actuation anisotropy is induced by placing one axis of the membrane under high prestretch λ_H, and the transversal axis under low prestretch λ_L. This configuration significantly stiffens the membrane along λ_H, hence greatly limiting the actuation along this axis. The second benefit of λ_H is to suppress electromechanical instability in the system, by taking advantage of the materials hyperleastic properties [133]. For small values of λ_L, the maximum strain is limited by loss of mechanical tension in the membrane. The amplitude of λ_L has to be determined carefully, as higher λ_L increases the maximum strain, but also decreases the actuation anisotropy and stiffens the membrane. For high values of λ_L, as the membrane stiffness increases, the maximum strain eventually becomes limited by the dielectric strength of the material.

4.3.2 Uniaxial tensile strain

With the anisotropic prestretch configuration presented in Fig. 4.2, a simple rectangular DEA design could be used to generate uniaxial tensile strain. It is however important that the actuator also provides high optical transparency, a key requirement for deformable bioreactors. While a few stretchable transparent electrode technologies have been reported [73], opaque carbon-based electrodes are often preferred due to their superior electrical and mechanical properties. The actuator geometry that I developed addresses the transparency requirement, without the need for transparent electrodes. The design is presented in Fig. 4.2, where stripe electrodes aligned with λ_H are patterned on both sides of the membrane, leaving a central gap of dimensions g x w located at a distance L from the membrane boundary. When a voltage difference is applied, the electrodes expand laterally, effectively stretching the gap width w, generating uniaxial tensile strain in this fully transparent region of the device. As general design rules, the electrodes width should be at least 10 times smaller than the membrane in order to maximise actuation strain [46], and a high w/g ratio maximises strain uniformity in the gap. Experimental results presented in Chapter 5 validate the design, demonstrating that a uniform strain profile is effectively generated in the passive electrode-gap.

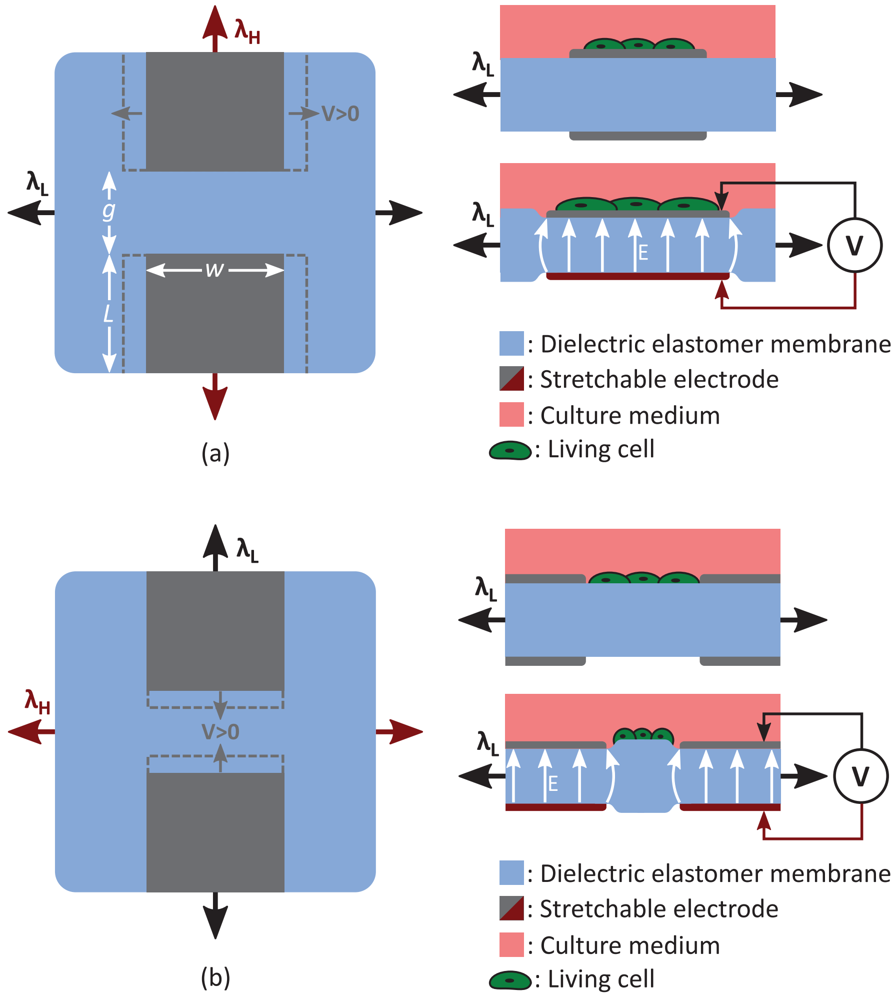
λH
λL
V>0
g
w
L
λL
λL
E
V
: Dielectric elastomer membrane
: Stretchable electrode
: Culture medium
: Living cell
(a)
λL
λH
V>0
λL
λL
E
V
: Dielectric elastomer membrane
: Stretchable electrode
: Culture medium
: Living cell
(b)

Figure 4.2 – DEAs are composed of a dielectric elastomer membrane, sandwiched between two stretchable electrodes. When a voltage difference is applied, the electrostatic pressure compresses the membrane in the out-of-plane direction, which is accompanied by a lateral expansion due to the material incompressibility. To achieve uniaxial expansion, we induce stiffness anisotropy in the membrane by defining high λ_H and low λ_L prestretch axes. Our actuator is composed of stripe electrodes of length L, with a central gap of length g and width w. The gap area undergoes (a) uniaxial tensile strain when the electrodes are aligned with λ_H, or (b) uniaxial compressive strain when the electrodes are aligned with λ_L.

4.3.3 Uniaxial compressive strain

The same electrode geometry can also be used to generate uniaxial compressive strain. As presented in Fig. 4.2(b), it only requires the electrodes to be aligned with λ_L instead of λ_H. When a voltage difference is applied, the stripe electrodes expand along their length L, effectively compressing the transparent gap. If the membrane is fixed on a rigid frame, the gap compression is equal to the electrode elongation $\delta g = 2\delta L$. Assuming uniform strain on the electrode and in the gap, the ratio between the electrode tensile strain $\epsilon_L = \delta L/L$, and the gap compressive strain $\epsilon_g = \delta g/g$, is determined by the device geometry $\epsilon_L/\epsilon_g = 2L/g$. A design with a high L/g ratio will therefore generate a localized strain field (i.e. low tensile strain in the electrode, and high compressive strain in the gap), and minimize the electromechanical stress in the actuator, an interesting property which can improve the stability and lifetime of the actuator. Based on the conclusion of this simplistic analysis, I maintained a ratio of $1/10$ between the gap and the electrode length. Experimental results presented in Chapter 5 demonstrate that a uniform compressive strain profile is generated in the electrode-gap, but not along the electrode. Further improvement of the design therefore requires the use of numerical methods (e.g finite element analysis) to better describe the actuator response.

4.4 Fabrication process

Here I present the fabrication process of the DEA-based deformable bioreactor, and highlight some of its unique features such as the passivation layers and an oil backing. The membrane and the electrode fabrication is based on standard processes from the Microsystem for Space Technology Laboratory (EPFL, Switzerland). Those fabrication steps are therefore not detailed here, but can be accessed in the form of a scientific video article [67].

To begin, a silicone elastomer membrane is placed under non-equibiaxial prestretch ($\lambda_H = 2.7$, $\lambda_L = 1.2$) and assembled between two poly(methyl methacrylate) (PMMA) rigid frames, as presented in Fig. 4.3(a). A pressure sensitive silicone adhesive (ARclear, Adhesive Research), and a cytocompatible silicone sealant (Silpuran 4200, Wacker) are used to fix the membrane in place. The silicone sealant provides a gradual transition between the hard plastic frame and the soft elastomer membrane. This transition is essential to avoid stress points that could otherwise rupture the highly prestretched membrane.

Carbon-loaded silicone elastomer electrodes are patterned on both sides of the 30 µm thick membrane as presented in Fig. 4.3(b), and covered by a thin film of cytocompatible silicone elastomer (LSR4305, Bluestar Silicones) as presented in Fig. 4.3(c). Both materials are applied using pad-printing, and heat cured on the membrane at 80 °C for 1 h. The electrodes are 1-2 µm thick, and the silicone passivation layer is 2-4 µm thick. Covering the electrodes with a passivation layer has many advantages: It improves the stability of the electrodes resistance over cyclic actuation, it decouples the actuator performance and biocompatibility requirements (i.e. the DEA membrane can be selected based on its actuation performance, and the passivation based on its biocompatibility), and it provides a culture interface with uniform mechanical and chemical properties.

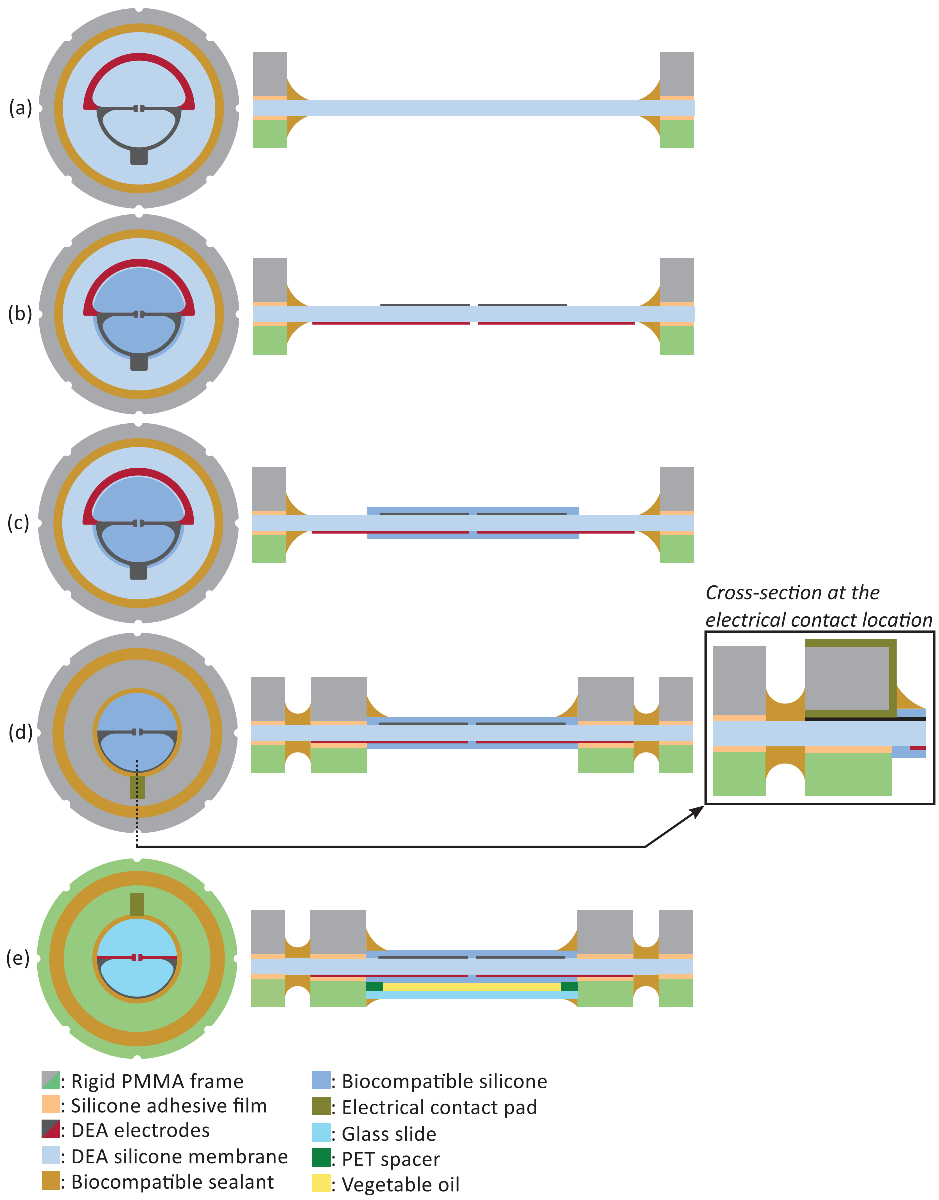
(a)
(b)
(c)
(d)
(e)
Cross-section at the electrical contact location
: Rigid PMMA frame
: Silicone adhesive film
: DEA electrodes
: DEA silicone membrane
: Biocompatible sealant
: Biocompatible silicone
: Electrical contact pad
: Glass slide
: PET spacer
: Vegetable oil

Figure 4.3 – For the fabrication of the DEA-based deformable bioreactor: (a) A silicone elastomer membrane is prestretched, and fixed between two rigid PMMA frames using silicone adhesive film and cytocompatible sealant. Using pad-printing, we pattern carbon black-elastomer composite electrodes on both sides of the membrane. (b) Using pad-printing, we cover the electrodes with a thin layer of cytocompatible silicone, leaving an area exposed for electrical contact. (c) A second set of rigid plastic PMMA frames is fixed on the membrane, creating electrical contact between the DEA electrodes and metallic contact pads patterned on the PMMA frames. The top frame creates a volume used as a cell culture chamber, while the bottom frame creates a volume used for an oil encapsulation. (d) A polyethylene terephthalate (PET) spacer and a glass slide are stacked on the backside of the membrane, the resulting interstice is filled with vegetable oil, and sealed.

A second set of rigid PMMA frames are fixed on the membrane as presented in Fig. 4.3(d), making electrical contacts with the DEA element. Reliable electrical connections between soft stretchable electrodes and rigid components (outside circuitry) can be challenging to achieve. Here I use conductive metallic tape, which is wrapped around the PMMA frames, and pressed in contact with the soft DEA electrodes. Since the assembly slightly compresses the membrane, it is important that the DEA electrodes don't overlap under the PMMA frames: Compression of the active area increases the electric field during actuation, and can induce premature dielectric breakdown. A ring of cytocompatible silicone sealant is used to provide a gradual transition between the hard plastic frame and the soft elastomer membrane, and seal what will be the cell culture chamber.

The second set of PMMA frames creates two reservoirs, one on each sides of the membrane. The top reservoir is the cell culture chamber, designed to contain culture medium and support cell growth. In order to avoid exposing cells to electric field, the top electrodes and the culture medium are both connected to ground. The bottom reservoir is used to create an encapsulated oil backing, bounded on one side by the silicone membrane, and on the other side by a glass slide as presented in Fig. 4.3(e). The oil backing isolates the cells culture from the backside environment, otherwise only separated by a 30 µm thick silicone elastomer membrane, a material known for its high gas permeability. With this physical barrier, the culture environment is similar to what would be obtained on a standard cell-culture dish. In addition, with a total spacing of only 310 µm between the cells and the glass slide, the device can be mounted on an inverted optical microscope for high resolution imaging of cells. The dimensions of the fabricated device are reported in Fig.4.4 and Table 4.2 for the tensile and compressive designs.

Table 4.2 – Electrode geometry of the tensile and compressive designs

Design	L	g	w
Tensile	19.5 mm	0.5 mm	1.5 mm
Compressive	18 mm	2 mm	2 mm

Another important role of the oil backing is to protect the device from the effects of cyclic actuation. When actuated in air for a few thousands cycles, the formation of cracks can be observed at the surface of the passivation layer. The degradation is superficial and doesn't affect the actuation performance. It however induces light scattering and makes optical imaging through the membrane difficult. To demonstrate the effect of oil immersion, devices were cycled between 0 % and 10 % strain at a 1 Hz frequency during 4 h, with and without the oil backing. The picture presented in Fig. 4.5(a) shows that oil immersion effectively suppresses the formation of cracks, which are however clearly visible after actuation in air as presented in Fig. 4.5(b).

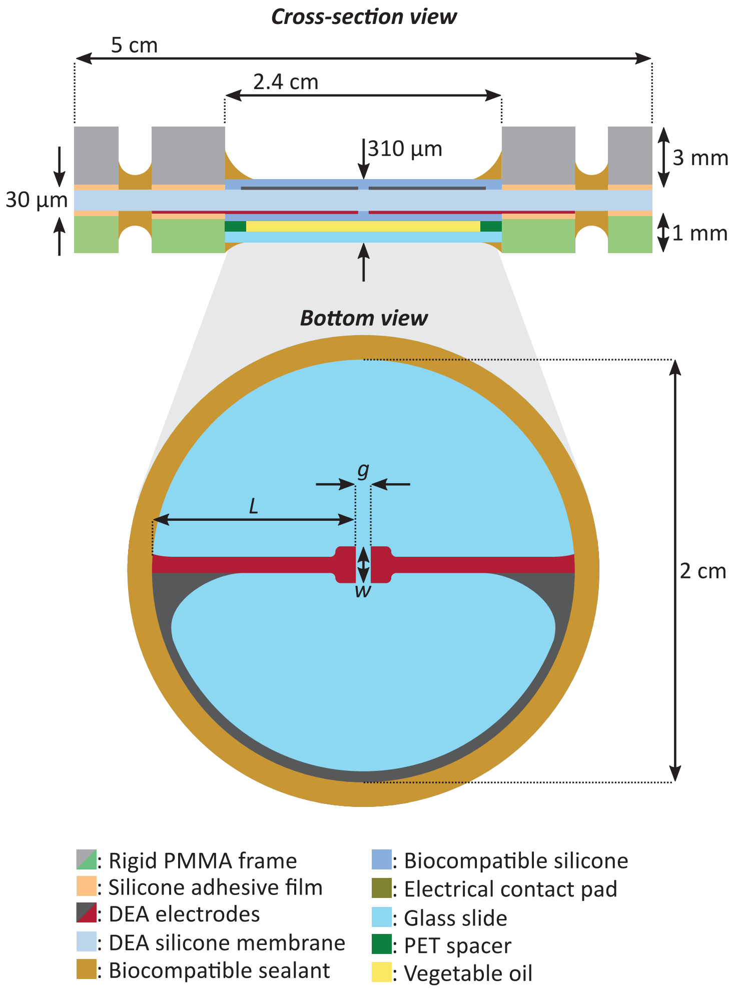
Cross-section view
5 cm
2.4 cm
310 µm
3 mm
30 µm
1 mm
Bottom view
g
L
w
2 cm
: Rigid PMMA frame
: Silicone adhesive film
: DEA electrodes
: DEA silicone membrane
: Biocompatible sealant
: Biocompatible silicone
: Electrical contact pad
: Glass slide
: PET spacer
: Vegetable oil

Figure 4.4 – Dimensions of the fabricated DEA-based deformable bioreactor.

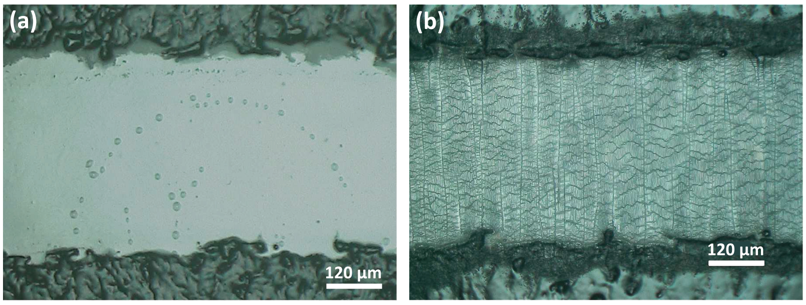
(a)
120 µm
(b)
120 µm

Figure 4.5 – When actuated in air, the formation of cracks can be observed at the surface of the passivation layer. To demonstrate that crack formation can be suppressed by oil immersion, two devices were actuated in culture condition (i.e. topside immersed in growth medium) from 0 % to 10 % strain at a 1 Hz frequency for 24 h. (a)The bottom side of the first device was immersed in safflower oil and presents no cracks, (b) while bottom side of the second device was kept exposed to air and presents a dense pattern of superficial cracks at its surface.

Different types of immersion liquids can be used to prevent crack formation, including aqueous solutions such as the cell culture medium. It is however impossible to immerse both sides of the device in aqueous solutions, since it would be the equivalent of fully covering both sides of the membrane with electrodes. This configuration would completely modify the actuation mode of the device, transforming the it into a bubble-like actuator. The challenge is therefore to find a non-conductive and non-cytotoxic liquid which doesn't diffuse through the device membrane. Several liquids were tested, including Sylgard 184 catalyst, Sylgard 186 catalyst, safflower oil, microscope calibration liquid, glycerol and ethylene glycol. Amongst the tested liquids, only the safflower oil and microscope calibration liquid didn't diffuse through the device, and safflower oil was selected mainly for its well known composition, biocompatibiltiy, and low cost.

4.5 Conclusion

In conclusion, I presented in this chapter a versatile DEA design capable of generating compressive or tensile uniaxial strain, and which provides optical transparency without the need for transparent electrodes. A picture of the fabricated device is presented in Fig. 4.6(a), with the possible strain types presented in Fig. 4.6(b), and a cross-section of the system presented in Fig. 4.6(c). I detailed in this chapter the fabrication process of the DEA-based deformable bioreactor, discussed the main challenges and solutions to interfacing DEAs with living cells, and highlighted some of the device unique features such as the passivation layers and oil backing. The fabricated device is made of cytocompatible materials, it can be sterilized in ethanol, immersed in culture medium, and incubated for weeks without any adverse effects. In addition to be compatible with standard cell culture protocols, its design enables *in situ* high-resolution optical imaging of cells. Table 5.1 summarize the requirements and results of the DEA-based deformable bioreactor.

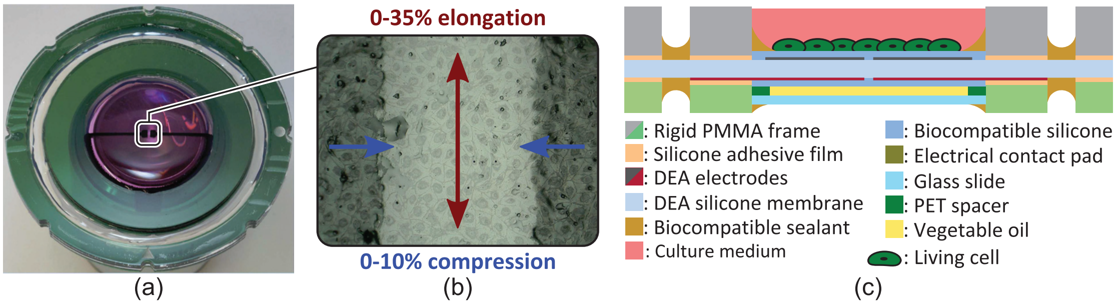

Figure 4.6 – (a)Picture of the fabricated device, which can (b)generate up to 10% uniaxial compressive strain, or 35% uniaxial tensile strain.(c)Cells are cultured on top of the device, where they are exposed to in-plane deformation upon actuation of the DEA.

Table 4.3 – Summary of the DEA-based deformable bioreactor results. Parameters highlighted in grey have been addressed in the design and fabrication steps.

Parameter	Requirement/Objective	Results
Biocompatibility	Essential	✓
Sterilization compatible	Essential	✓
Incubator compatible	Essential	✓
Optical transparency	Essential	✓
Strain types	uniaxial compressive/tensile	✓
Strain amplitude	−20 % to 20 %	−10 % to 20 %
Actuation frequency	0.1 Hz to 5 Hz	1 kHz bandwidth
Working life-time	2 h to 48 h	24 h
Growth medium immersion	>3 days	>2 weeks

5 DEA-based deformable bioreactor - Actuation performance

5.1 Summary

In this chapter, I analyse the actuation performance of the DEA-based deformable bioreactor. The first section characterizes the strain amplitude, anisotropy and uniformity of the tensile and compressive designs. The results demonstrate that -10 % to 35 % uniaxial strain can be generated in a transparent area (0.5 mm x 1.5 mm) of a larger cytocompatible membrane. The second section presents stability measurements, and demonstrates stable actuation strain over a period of 12 h of cyclic actuation. The last section analyses the system static and dynamic response, and demonstrates strain rate in the excess of 700 s^{-1}, two orders of magnitude higher than typical pneumatic based systems [5].

The results presented in this chapter are part of a manuscript in preparation, which details the device fabrication process, analyses the main performance metrics, and highlight the unique possibilities enabled by its ultra-fast response time. The system dynamics was studied with the help of Matthias Imboden and Samuel Rosset, both from the Microsystems for Space Technologies Laboratory (EPFL, Switzerland). Part of the results obtained on the tensile design, namely the voltage-strain curve and the strain profile measurements, have already been published in Lab on a Chip [134].

5.2 Actuation strain

One of the main requirement of the DEA-based deformable bioreactor is to generate compressive and tensile uniaxial strain. In order to evaluate the device performance, I measured its actuation strain by tracking the electrode boundaries at increasing driving voltages. Due to the highly non-equibiaxial prestretch of the membrane, preferential actuation is expected along the direction of low prestretch λ_L. In addition to measure strain along the direction of low prestretch λ_L, I also measured strain in the direction of high prestretch λ_H, and evaluated the actuation anisotropy. The results obtained for the tensile and compressive designs are presented in Fig. 5.1.

For the tensile design, a maximum strain of 35 % is achieved along λ_L at 185 Vμm^{-1}, accompanied by a -9 % strain along λ_H. Those results clearly illustrate the effect of the membrane non-equibiaxial prestretch, with an absolute strain 4 times higher along λ_L than λ_H. The maximum strain is limited by loss of mechancial tension in the membrane, and not by the

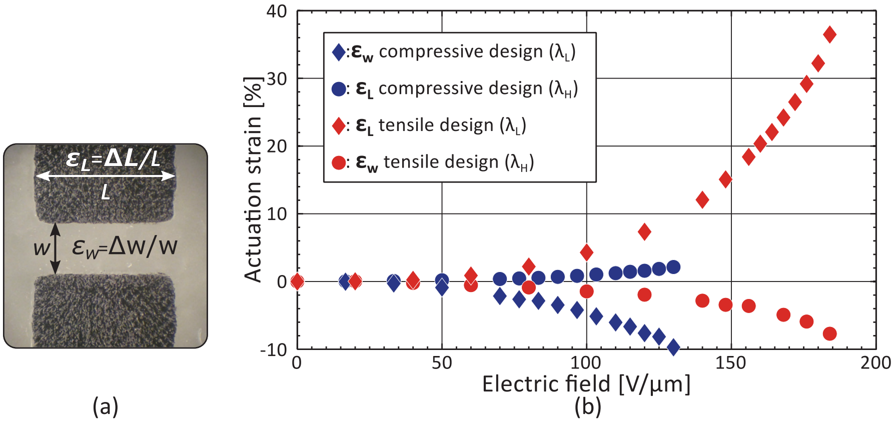

(a)

(b)

Figure 5.1 – The actuation strain of the compressive and tensile designs was measured as a function of the applied electric field. (a)The strain was calculated by tracking the electrode boundaries, thus giving a measurement of the averaged in the gap ($\epsilon_w = \Delta w / w$) or on the electrode ($\epsilon_L = \Delta L / L$). (b) The results show a maximum tensile strain of 35 %, and a maximum compressive strain of 10 %, both limited by loss of mechanical tension. Comparing strain along λ_H and λ_L gives a measure of the strain anisotropy, and shows that the actuation strain is 4 to 5 times lower along λ_H.

material dielectric strength or by electromechanical instability [46, 47, 59]. Although higher strain could be achieved by increasing λ_L, this would also decrease the actuation anisotropy, and shift the response curve towards higher electric field. Considering that 35% strain is already satisfying the objective that was set for the system (20%), it is therefore preferable to keep the current prestretch state, and operate at lower electric field.

For the compressive device, a maximum strain of -10 % is achieved along λ_L at 140 Vμm^{-1}, accompanied by a 2 % strain along λ_H. Similar to the tensile design, the absolute strain is 5 times higher along λ_L than λ_H due to the membrane non-equibiaxial prestretch. The maximum strain is limited by loss of mechanical tension, and not by the material dielectric strength or by electromechanical instability [46, 47, 59]. In order to increase the maximum strain, and reach the -20 % strain objective, several value of λ_L were tested, but provided marginal improvement.

An interesting aspect of the tensile design, is that loss of mechanical tension was observed in the active area. During actuation, the electrode is expected to be under small tensile stress, and the gap to be under high compressive stress. Loss of mechanical tension should therefore occur in the gap area, and not on the electrode. This result suggests that the strain distribution on the device is more complex than imagined, and that some areas of the electrode are under compressive stress during actuation. Further improvement of the device performance would therefore require a better understanding of the system though finite element analysis and experimental validation.

The results presented in Fig. 5.1 were obtained by tracking the electrode boundaries, and therefore give a measure of the average strain. While this technique is convenient, as it requires only minimal equipment and data processing, it can however hide valuable information. I consequently developed an image processing algorithm, which can measure the strain profile using pictures of the device in its actuated and unactuated states. The technique is based on digital image correlation (DIC), and is detailed in Chapter 7.

Using this technique, I measured the strain profile of the tensile design at 130 Vμm^{-1}, which gives an average strain of 11 % when calculated by tracking the electrode boundaries. The y-strain ϵ_{yy} (aligned with the low prestretch λ_L direction) profile is presented in Fig.5.2(a), and the x-strain ϵ_{xx} (aligned with the high prestretch λ_H direction) profile is presented in Fig.5.2(b). Cross-sections of the strain profiles are presented in Fig.5.3, where the region corresponding to the electrode gap is highlighted in grey. The cross-section **A** shows uniform tensile strain on the electrode, with a clear drop at its boundaries, and is in agreement with the measured 11 % average strain. The cross-section **B** shows uniform tensile strain in the gap, with a profile similar to the one observed directly on the electrode. The transition at its boundaries is however softer, mainly due to the low compressive strain generated in the gap along the x-axis as shown by the cross-section **C**.

Using the same technique, I measured the strain profile of the compressive design at 130 Vμm^{-1}, which gives an average strain of 10 % when calculated by tracking the electrode boundaries. The x-strain ϵ_{xx} (aligned with the low prestretch λ_L direction) profile is presented in Fig.5.4(a), and the y-strain (aligned with the high prestretch λ_H direction) profile is presented in Fig.5.4(b). Cross-sections of the the strain profiles are presented in Fig.5.5, where the region corresponding to the electrode gap is highlighted in grey. The cross-section **B** shows uniform compressive strain at the centre of the gap, with smooth transition at its borders, mainly due to the active area which was extending on each sides of the gap for this device (to electrically connect both sides of the electrode). The cross-section **C** shows uniform compressive strain in the gap, with a sharp transition at its boundaries, and is in agreement with the measured 10 % average strain.

The strain profile of the compressive device also reveals an interesting aspect of the design. The cross-sections **A** and **C** show tensile strain exceeding 20 % on the electrode, with a non uniform profile along their length. This result is in agreement with the fact that the loss of mechanical tension occurs on the electrode, and not in the gap as initially expected. It confirms that the simplistic model (i.e. assuming uniform strain on the electrode) that guided the electrode design isn't valid, and that further improvement of the device performance would require a better understanding of the system.

In summary, the results presented in this section validate two important aspects of the device: 1) The transparent electrode-gap effectively deforms with the DEA electrodes upon actuation. In other words, the design I developed provides optical transparency, and is compatible with transmission light microscopy, a key requirement of the DEA-based deformable bioreactor. 2) A uniform strain profile is generated in the transparent electrode-gap, and its amplitude can be approximated by simply tracking the electrode boundaries.

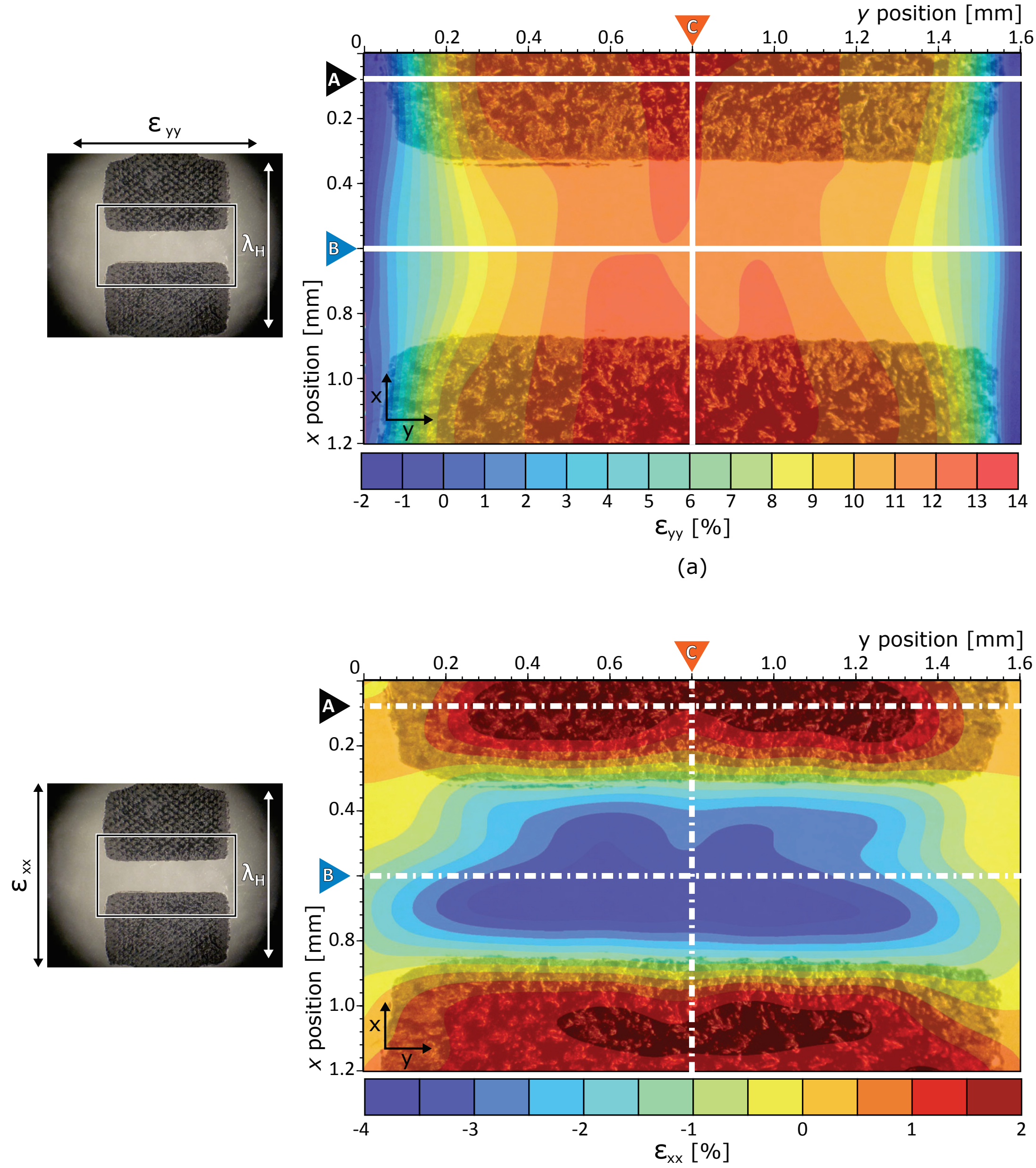

(a)

(b)

Figure 5.2 – Strain profile of the tensile design. Using the device surface topography and DIC, I measured the displacement field in the electrode gap, and calculated the corresponding strain profile. (a) The y-strain ϵ_{yy} profile is overlaid on a picture of the device. (b) The x-strain ϵ_{xx} profile is overlaid a picture of the device.

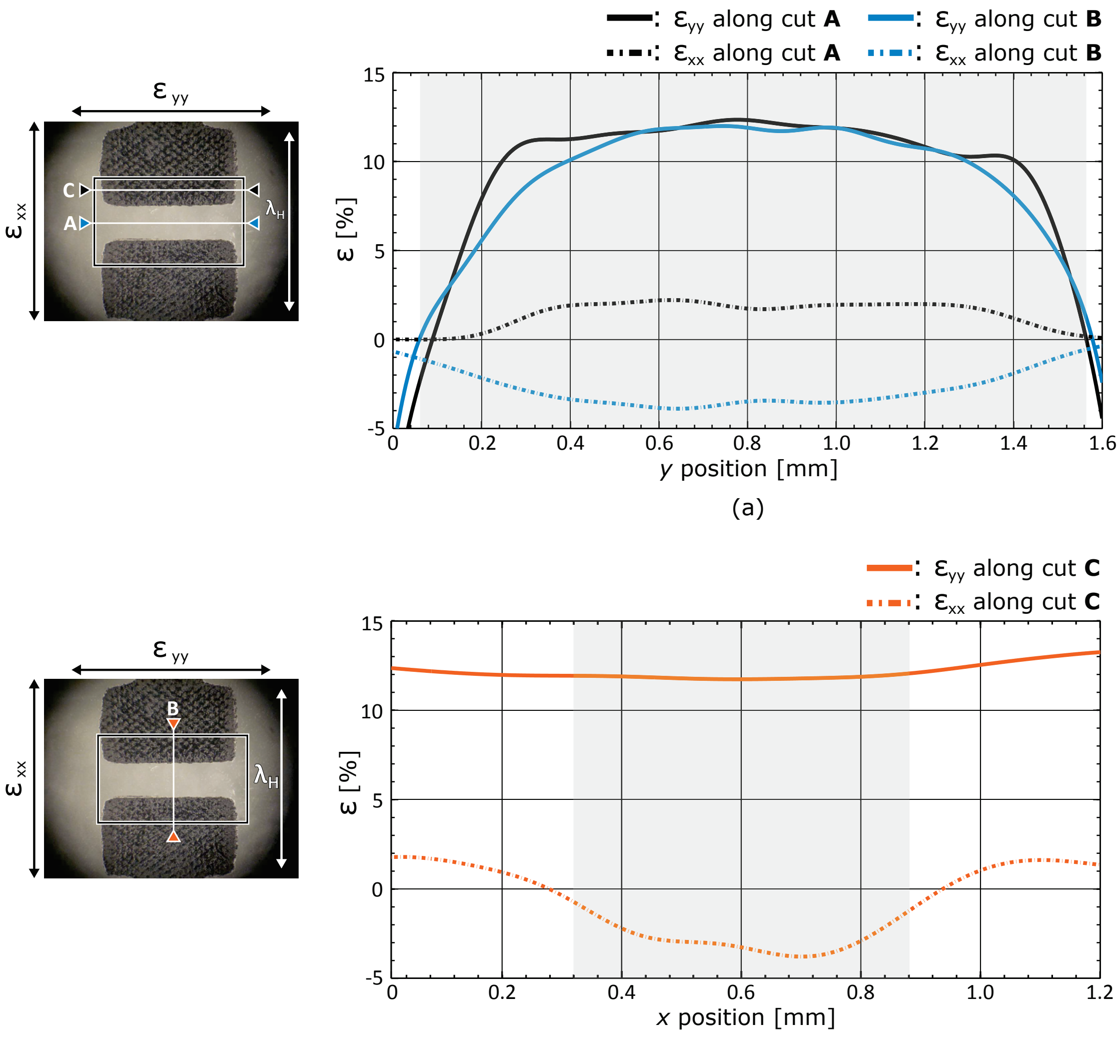

(a)

(b)

Figure 5.3 – Strain profile of the tensile design. Using the device surface topography and DIC, I measured the displacement field in the electrode gap, and calculated the corresponding strain profile. (a) ϵ_{yy} and ϵ_{xx} profiles along the cuts **A** and **B**, with the gap region highlighted in grey. (b) ϵ_{yy} and ϵ_{xx} profiles along the cut **C**, with the gap region highlighted in grey.

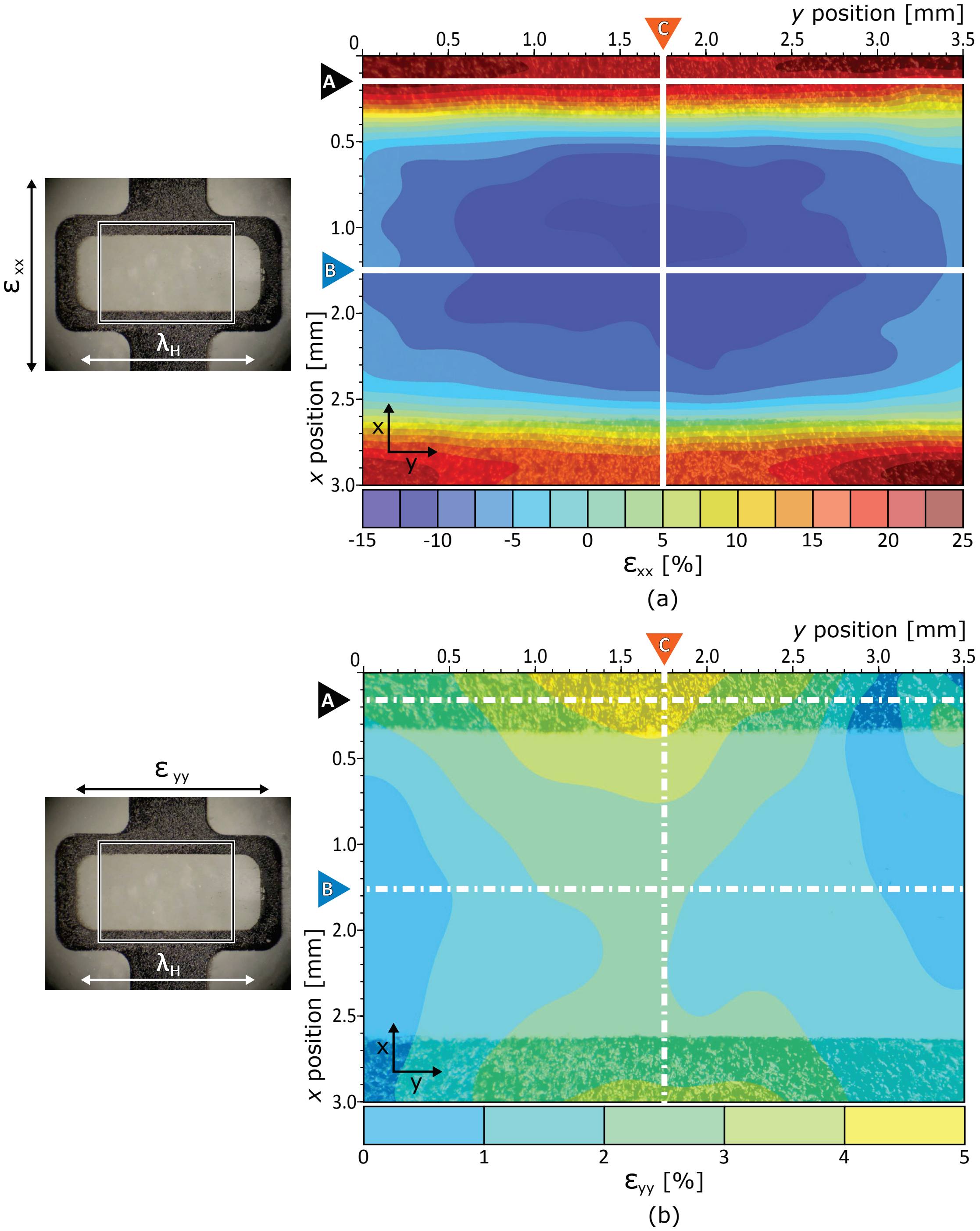

Figure 5.4 – Strain profile of the compressive design. Using the device surface topography and DIC, I measured the displacement field in the electrode gap, and calculated the corresponding strain profile. (a) The x-strain ϵ_{xx} profile is overlaid on a picture of the device. (b) The y-strain ϵ_{yys} profile is overlaid a picture of the device.

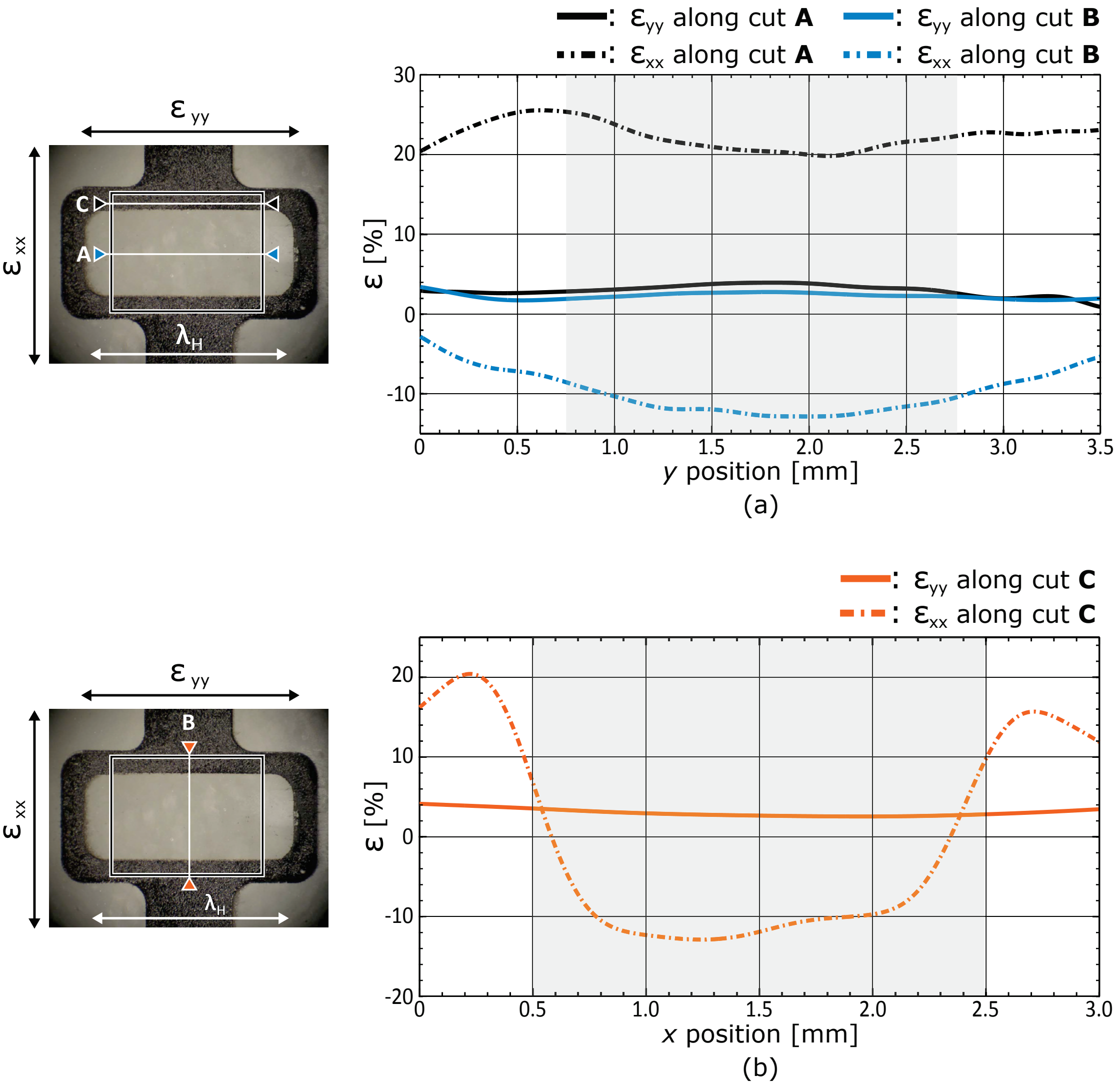

Figure 5.5 – Strain profile of the compressive design. Using the device surface topography and DIC, I measured the displacement field in the electrode gap, and calculated the corresponding strain profile. (a) ϵ_{yy} and ϵ_{xx} profiles along the cuts **A** and **B**, with the gap region highlighted in grey. (b) ϵ_{yy} and ϵ_{xx} profiles along the cut **C**, with the gap region highlighted in grey.

5.3 Stability and lifetime

Another important requirement of the DEA-based deformable bioreactor is to provide stable actuation performance. During a mechanotransduction experiment, the device is periodically actuated, and has to generate a controlled mechanical stimulation. It is therefore important to know if the device strain-voltage curve is stable over cyclic actuation, and for how long it can be actuated before failure.

In order to evaluate the system stability and lifetime, a device was filled with growth medium (see Fig. 5.6(a)), mounted on an optical microscope, and periodically actuated. The driving signal was generated with a data acquisition (DAQ) device, controlled via LabView and connected to a high-voltage amplifier (609E-6, TREK Inc., USA). The LabView interface also controlled a camera installed on the microscope, periodically acquiring pictures of the device in its actuated and unactuated states, and calculating the corresponding strain by tracking the electrode boundaries. For this experiment, I used a device generating tensile strain, and actuated it using a 1 Hz square wave signal with a 50 % duty cycle, switching between 0 $\mathrm{V\mu m^{-1}}$ and 130 $\mathrm{V\mu m^{-1}}$ (corresponding to 3.7 kV for the characterized device).

The strain evolution is presented in Fig. 5.6(b). The results show that the DEA-based deformable bioreactor provides stable actuation performance and long lifetime in cell culture conditions, with limited drift over more than 12 h and 50 000 actuation cycles.

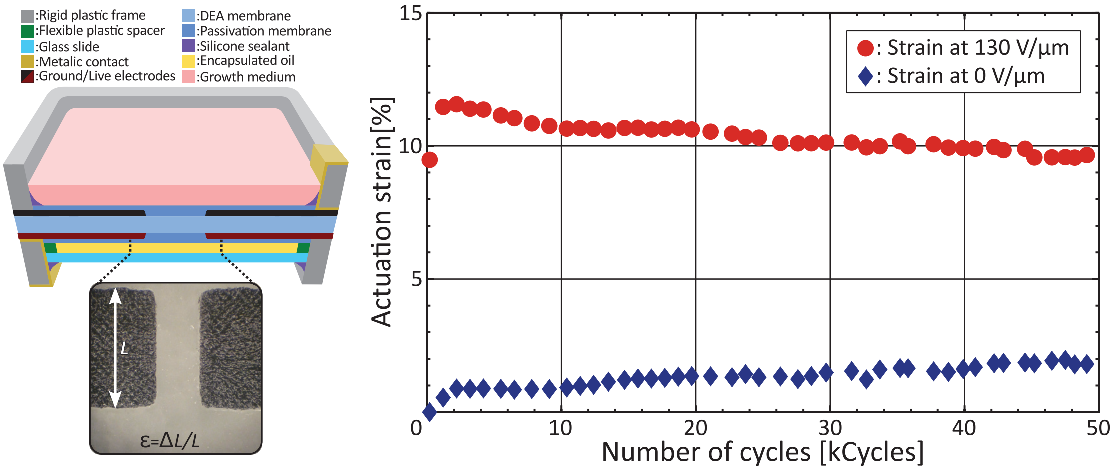

(a) (b)

Figure 5.6 – The actuation stability of our deformable bioreactor was evaluated over cyclic actuation. (a)The device (tensile design) culture chamber was filled with cell growth medium, and the DEA element was actuated at a 1 Hz frequency during 12 h. A square-wave driving signal with a 50 % duty cycle was used, switching between 0 V/µm and 130 V/µm, and periodically measuring strain. (b)The results show small drifts in the actuated and unactuated states, demonstrating the stable actuation performance and long lifetime of the device in cell culture conditions.

The strain in the unactuated state quickly increases by 1 % over the first 1000 cycles, and then slowly increases by an additional 1 % over the rest of the experiment. Measurements in the actuated state show a similar trend, with a quick 2 % strain increase over the first 1000 cycles.

Over the rest of the experiment, the strain however decreases, slowly returning back to its initial value. A possible contribution to those effects is elastic deformation: Periodic stretch can induce irreversible macromolecular chain scission [135] in the membrane, softening the active area, which as a result expands due to the membrane prestretch. Another possible contribution is delayed elastic-deformation [135]: Some molecular phenomena can have mechanical relaxation time slower than the actuation period, causing the apparition of a remaining strain, which however disappears once the actuator is at rest.

The experiment was stopped due to the device failure by dielectric breakdown. Most of the characterized devices worked for more than 12 h, but only a few could reach 24 h. One hypothesis is that ions can diffuse from the culture medium (which contains salt in solution) into the membrane, increasing leakage current and eventually inducing a short-circuit in the system. Similar stability and lifetime measurements were however obtained for devices operated in air, hence suggesting that the diffusion of ionic species in the membrane isn't the main limitation. Another possible explanation is that defects in the membrane are the principal cause of failure. Defects in the form of air bubbles, dust particles or silicone filler aggregates can indeed be found in the membrane. They locally modify the electrical and mechanical properties of the membrane, an effect which can even be further amplified by the membrane high-prestretch, creating weak points that can eventually lead to the device failure.

5.4 Dynamic response

Another important requirement of the DEA-based deformable bioreactor is to work at frequencies ranging from 0.1 Hz to 5 Hz, similar to commercially available systems [5]. In this section, I present measurements that were made on the tensile design, and which provide insights in the dynamic response of the system. A more detailed analysis would however be required to precisely identify the underlying physical mechanisms, and further optimize the system response time. The results presented in this section were obtained with the help of Samuel Rosset and Matthias Imoboden, both from the Microsystems for Space Technology Laboratory (EPFL, Switzerland).

The actuation of the tensile design was first characterized in static conditions. The device was placed under a microscope, connected to a high-voltage power supply, and actuated with a 4 kV step function which maintained the voltage applied for 300 s. The device static response was analysed by tracking the electrode boundaries and calculating the corresponding strain. The results are presented in Fig.5.6, and show the evolution of the normalized strain over time. The device reaches 90 % of its maximum strain after 7 s, and its maximal strain within 100 s, approximately 10 times faster than standard acrylic elastomer DEAs [136].

The device response time wasn't limited by the power supply, which could reach 4 kV within 1 ms, or by the electrical time constant of the device, which was smaller than 0.1 µs. The actuation was mostly limited by viscoelastic effects in the membrane, the passivation and the electrodes. Simple control system theory could be applied to greatly improve the response time, adjusting the driving signal to compensate for the system viscoelasticity. This technique has alread been demonstrated for silicone-based DEAs, and improved the response time by more than two orders of magnitude [136].

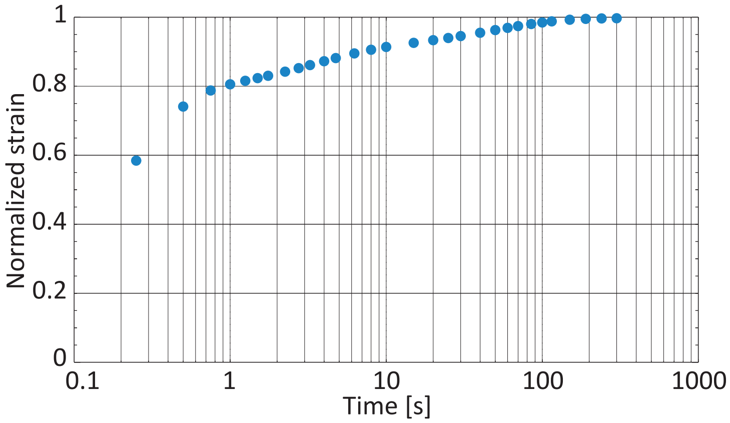

Figure 5.7 – The tensile design was characterized under static conditions. The device was actuated with a 4 kV step function for 300 s, during which pictures of the device were periodically acquired, and used to calculate the corresponding strain. The response time was limited by the device mechanical time constant, reaching 90 % of the final strain after 7 s, and the final strain (15 %) after 100 s.

The tensile design was then characterized under dynamic conditions. The device was placed under a microscope , connected to a high-voltage power supply (609E-6, TREK Inc., USA), and cycled between 0 V and 4 kV at increasing frequencies f. In order to achieve a sinusoidal strain profile, and based on the device strain-voltage curve, the device was actuated with a signal of the form $(A(sin(2\pi f t) + 1))^{1/3}$ (Although the theory of DEA predicts a quadratic relationship $\epsilon \propto V^2$ between strain ϵ and voltage V, our device is better described by a cubic relationship $\epsilon \propto V^3$, hence the the driving signal of the form $sin^{1/3}$). A high-speed camera (Phantom V210, Vision Research Inc., USA) was used to image the device at 10 000 fps, track the electrode boundaries during actuation, and calculate the corresponding strain.

The results are summarized in Fig. 5.8, where the maximum and minimum strains are presented as a function of the driving frequency. It shows that the minimum strain stays above 1%, and that the amplitude of this remaining strain appears to be independent of the frequency. This effect is probably due to a mechanical softening of the membrane, similar to the results presented in Fig. 5.6, and is therefore not related with the device response time. The results also show that the maximum strain decreases at higher frequencies, going from 16% at 0.1 Hz, down to 7% at 2 kHz. Based on those measurements, the device bandwidth (- 3 dB) is equal to 1 kHz. Another interesting metric is the maximum strain rate of the device, which can be easily calculated by multiplying the strain by $2\pi f$, where f is the frequency. The maximum strain rate is obtained at 2 kHz, and correspond to 700 s^{-1}, more than 100 times faster than what conventional systems can deliver [5].

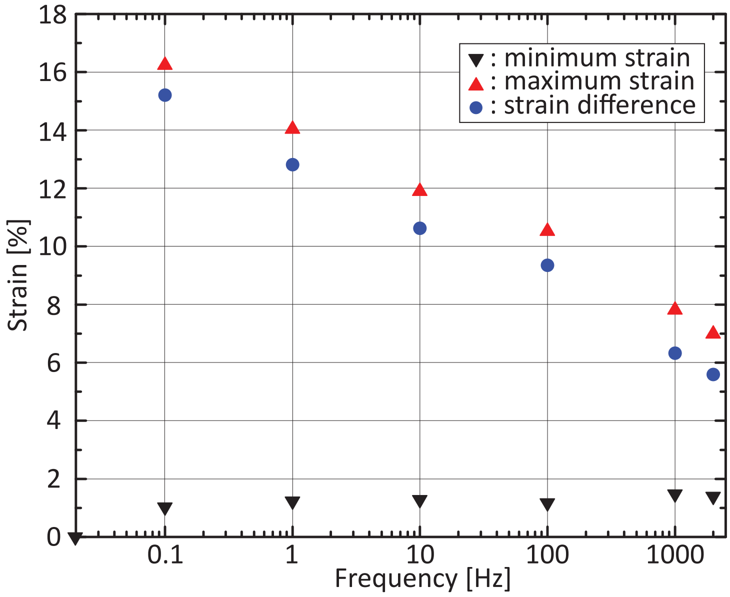

Figure 5.8 – In order to evaluate the system dynamic response, the tensile design was actuated with a sinusoidal signals oscillating between 0 V and 4 kV at increasing frequencies. A high-speed camera was used to acquire pictures of device during actuation, and calculate the corresponding strain. The results show that the maximum amplitude decrease at higher frequencies, reaching half of the static strain at 300 Hz. It also shows a strain rate of 220 s^{-1} at 2 kHz, for a maximum strain of 5 %.

The cells *in vivo* mechanical environment is influenced by a wide range of physiological processes, with time scales ranging from 0.1 cycle/s in the lymphatic system [137], to 10 cycle/s during atrial fibrillation [138]. This environment is typically represented *in vitro* with simple sinusoidal or trapezoidal strain profiles. The *in vivo* environment is however much more complex, and the slow repeating cycles often contain high-frequency information. Those higher-frequency features can play a critical role, such as the systole and diastole stages of the cardiac cycle [139], but are often not reproduced *in vitro* due to the speed limitations of available systems. The ultra-fast dynamics of the DEA-based deformable bioreactor solves this problem, and enables the generation of accurate strain profiles.

The example of the human heart clearly demonstrates how small differences in a strain profile can be linked to important physiological conditions. The strain profile of a normal heart is presented in Fig. 5.9(a)(adapted from [139]), and compared with a heart affected by diastolic dysfunction, a condition linked with pulmonary hypertension, pulmonary oedema, and valve diseases. Although one of them is linked to a deadly condition, both profiles are similar: A 1 s cycle which includes a first peak followed by a lower plateau. The main differences are actually encoded in the higher frequency features, and this information is typically not reproduced *in vitro*. In order to demonstrate the unique advantage of the DEA-based deformable bioreactor's ultra-fast response time, I reproduced the normal and diastolic strain profiles using the tensile design. The result are presented in Fig. 5.9(b), and show that both profiles could be accurately reproduced.

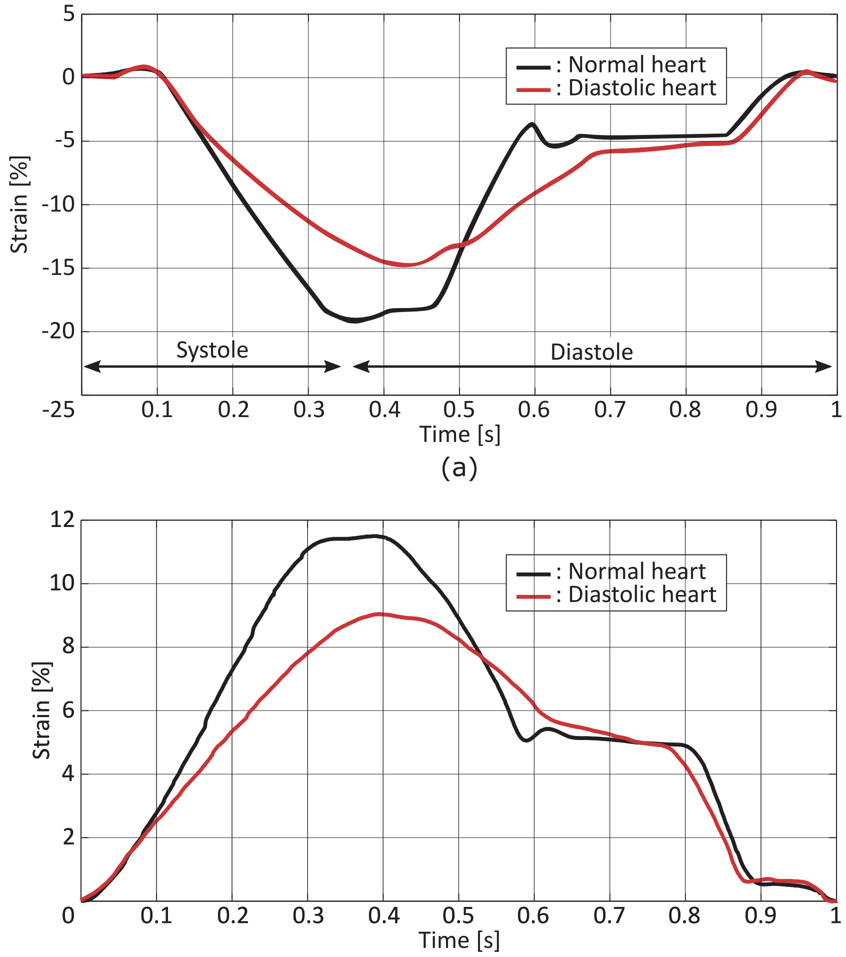

(a)

(b)

Figure 5.9 – The cells *in vivo* mechanical environment is often mimicked using a sinusoidal stimulation profile, mainly due to the limited strain rate of available systems. (a)The comparison between the strain profile of a healthy heart, and a heart affected by diastolic dysfunction, however clearly shows that small variations can have important physiological implications. (Adapted from [139]) (b) As a demonstration of the DEA-based deformable bioreactor ultrafast response time, the healthy and diastolic strain profiles were reproduced with the tensile design, showing that the device can provide accurate *in vitro* mechanical environment.

5.5 Conclusion

In this chapter, I characterized the actuation performance of the DEA-based deformable bioreactor. In the first section, I analysed the actuation strain of the device. I showed that the compressive design can achieve -10 % uniaxial strain, and that the tensile design can achieve 35 % uniaxial strain. I also demonstrated that both designs exhibit uniform strain profiles in the transparent electrode-gap, hence validating one of the device's key feature. In the second section, I evaluated the device performance over periodic actuation. Its response (10% strain) varied by less than 2% strain over more than 12 h and 50 000 actuation cycles, demonstrating the system's stability and lifetime. In the last section, I analysed the static and dynamic response of the device, and demonstrated that it can achieve strain rates in the excess of 700 s^{-1}, 100 times faster than standard pneumatic-based systems [5].

Table 5.1 – Summary of the DEA-based deformable bioreactor results. Parameters highlighted in grey have been experimentally validated.

Parameter	Requirement/Objective	Results
Biocompatibility	Essential	✓
Sterilization compatible	Essential	✓
Incubator compatible	Essential	✓
Optical transparency	Essential	✓
Strain types	uniaxial compressive/tensile	✓
Strain amplitude	−20 % to 20 %	−10 % to 20 %
Actuation frequency	0.1 Hz to 5 Hz	1 kHz bandwidth
Working life-time	2 h to 48 h	24 h
Growth medium immersion	>3 days	>2 weeks

6 DEA-based deformable bioreactor - Technology validation

6.1 Summary

In this chapter, I demonstrate that the DEA-based deformable bioreactor can be used for mechanical stimulation of cells *in vitro*. Using the tensile design shown in Fig. 6.1, I cycled a population of lymphatic endothelial cells (LECs) between 0 % and 10 % strain at a 0.1 Hz frequency for 24 h. In order to assess the effect of the device fringing electric field, the experiment was repeated with an immobilized device, thus exposing cells to periodic electric field, but suppressing the mechanical stimulation. The results show no effect of the electric field, and a clear stretch-induced alignment of LECs, providing the first demonstration that DEAs can be interfaced with living cells and used to control their mechanical environment.

The work presented in this chapter was done with the help of Cansaran Saygili and Tatiana V. Petrova from the Vascular and Tumor Biology Laboratory (UNIL, Switzerland), who did the cell preparation, the straining and the microscopy. The results of this collaborative work were published in Lab on a Chip [134].

6.2 Lymphatic endothelial cells (LECs)

The human lymphatic system is composed of lymphatic organs such as the thymus and spleen, a vast network of lymphatic vessels, and a clear liquid called lymph which is circulating in this open system. The internal wall of the lymphatic vessels are covered in LECs, continuously exposed to shear flow stress caused by the lymph circulation, and to tensile strain from the peristalsis motion of the lymph vessels. The main functions of the lymphatic system is to drain and filter interstitial fluid (lymph) from tissues. It also plays a critical role in the body's immune system, by producing and transporting different types of white blood cells. There is consequently great interests in *in vitro* models designed to study the mechanisms regulating lymphatic vascular growth, repair and functions. Progress in this field could lead to better diagnosis, prognosis, and treatment of cancer, but while recent work have investigated the effect of mechanical stimulation on LECs [130, 140], many important questions still remain.

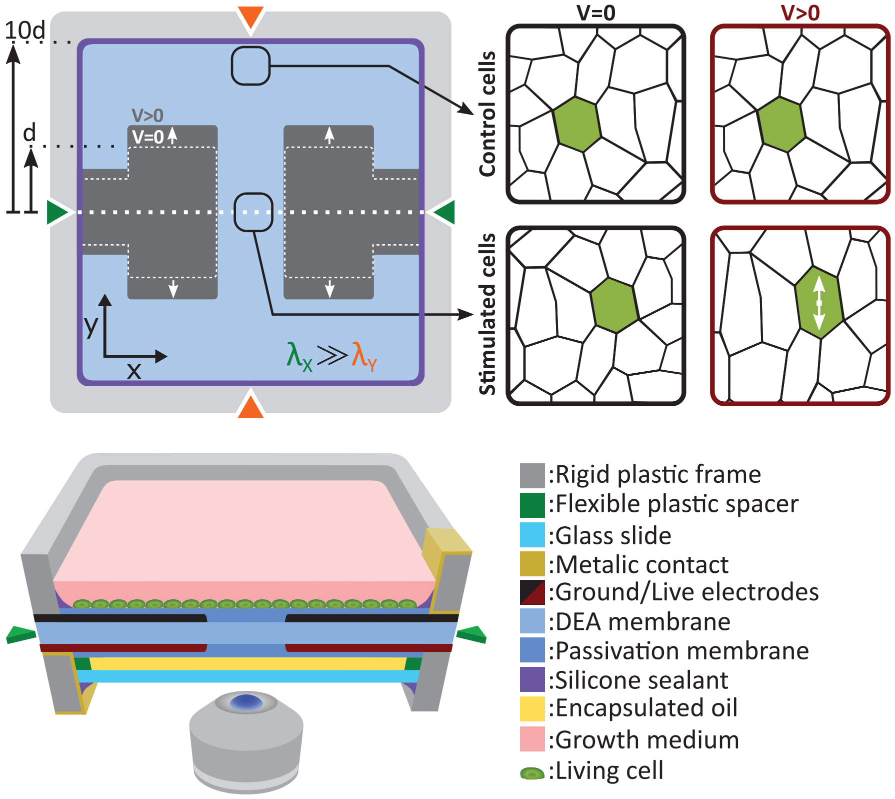
10d
d
V>0
V=0
y
x
$\lambda_X \gg \lambda_Y$
V=0
V>0
Control cells
Stimulated cells
:Rigid plastic frame
:Flexible plastic spacer
:Glass slide
:Metalic contact
:Ground/Live electrodes
:DEA membrane
:Passivation membrane
:Silicone sealant
:Encapsulated oil
:Growth medium
:Living cell

Figure 6.1 – Schematic diagram of the DEA-based deformable bioreactor. The cross-section shows a DEA composed of a silicone elastomer membrane sandwiched between two stretchable electrodes. The membrane is under non-equibiaxial prestretch and the actuator provides uniaxial tensile strain. The actuator is coated on both sides by a layer of cytocompatible elastomer. The cell culture is located on top of the device, while an oil encapsulation protects the other side. Cells located at the gap and on the electrodes experience uniaxial tensile strain during actuation, whereas cells outside this region can be used as a static control population.

6.3 Materials and methods

6.3.1 Cell culture protocol

The culture chamber of the DEA-based deformable bioreactor was incubated with fibronectin ($6\,\mu g/cm^2$) in phosphate buffered saline (PBS) for 1 hour at room temperature to promote cell adhesion. The device was next filled with endothelial cell growth medium (Lonza) and incubated at 37 °C for 24 h. Pre-conditioning of poly(dimethylsiloxane) in growth medium containing fetal bovine serum was reported to modify surface chemistry and significantly improve cell attachment [141]. Human LECs were cultured as described previously [140], and seeded on the fibronectin-coated device ($60\,kcells/cm^2$). A confluent LECs monolayer was obtained within 24 h of incubation at 37 °C, 5 % CO_2 and 95 % relative humidity.

6.3.2 Mechanical stimulation of LECs

After reaching a confluent cell monolayer, the device was mounted on an inverted microscope as presented in Fig.6.2. A portable incubator was used to control temperature, CO_2 and humidity levels in the culture chamber. An opening in the incubator provided optical access for the microscope objective, while the oil backing kept the cell culture isolated from the room environment. After the incubator reached equilibrium, the device was connected to a high-voltage power supply, and cycled between 0 % and 10 % uniaxial strain at a 0.1 Hz frequency with a 50 % duty cycle for up to 24 h. A low-pass filter was connected between the power supply and the device in order to smooth the device driving signal. The filter had a cut-off frequency of 1 Hz, while the actuator has a cut-off frequency greater than 10 Hz, typical for silicone-based DEAs [31]. The strain level and frequency were selected to reproduce the mechanical environment of LECs in the lymphatic valves [137]. While acute cell response can occur within the first few hours of mechanical stimulation, long term effect are often more representative of the *in vivo* environment. For that reason I designed a 24 h experiment, during which the microscope was programmed to periodically acquire pictures from different locations of the cell monolayer, monitoring the mechanically stimulated and static control areas of the device.

6.3.3 Effects of fringing electric field on LECs

When the electrodes of a DEA are completely overlapping as presented in Fig.6.1, the electric field generated by the actuator is mostly confined within the membrane. Cells located at the border of the electrode are however not perfectly shielded. In order to confirm that morphological changes observed on LECs upon stretching are not induced by fringing electric field, I repeated the stretching experiment with an immobilized device. In order to suppress the actuation I replaced the oil backing by a glass slide directly bonded to the membrane. The cells on the immobilized device are exposed to the same electric field, while not being mechanically stimulated, effectively decoupling the electric field exposure from the mechanical stimulation.

6.3.4 Staining and microscopy

After stopping the mechanical stimulation, cells were fixed with a solution of 4 % paraformaldehide (Sigma-Aldrich) in PBS, permeabilized with 0.1 % Triton X-100 (Applichem) and blocked with blocking buffer (0.5 % BSA, 5 % donkey serum, 0.01 % sodium azide, 0.1 % Triton X-100 in PBS). Phalloidin and Hoechst were diluted in blocking buffer as stated in product sheet and used to stain F-actin and deoxyribonucleic Acid (DNA). Cells were incubated with this solution for 1 h at room temperature, washed with 0.1 % Triton X-100 in PBS, and kept immersed in PBS. Fluorescence imaging was performed through the oil backing using a confocal Zeiss LSM 880 microscope with a 20X objective lens (Plan-Apochromat 20x/0.8 DIC M27 (WD=0.55mm)), and processed using Imaris software.

6.3.5 Characterization of cells morphology

Confocal microscope images obtained for F-actin and DNA staining were used to quantify cells morphology. Using ImageJ, I calculated the alignment relative to stretch direction and the elongation of LECs. For each cell I determined a long axis and defined a perpendicular short axis. The orientation was calculated as the angle created (clockwise) between the stretch direction and the long axis. The elongation was calculated as the ratio between lengths of the long and short axis.

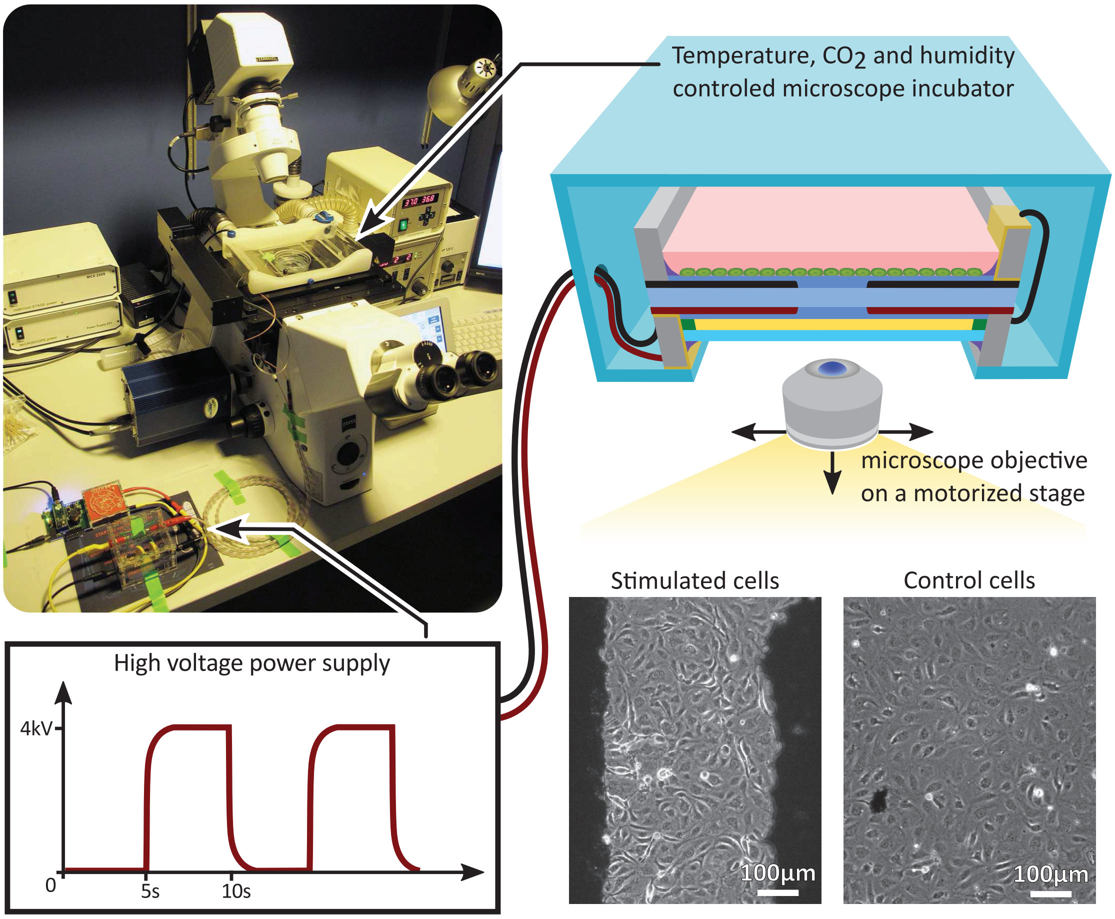
Temperature, CO2 and humidity
controled microscope incubator
microscope objective
on a motorized stage
Stimulated cells
Control cells
100µm
100µm
High voltage power supply
4kV
0
5s
10s

Figure 6.2 – The DEA-based deformable bioreactor was mounted on an inverted microscope during the stretching experiment. The microscope was programmed to periodically acquire pictures from different locations of the cell culture. A portable incubator was used to maintain the culture chamber at at controlled temperature, CO_2 concentration and humidity level. The device was cycled between 0 % and 10 % uniaxial strain at a 0.1 Hz frequency with a 50 % duty cycle for up to 24 %.

6.4 Results and discussion

6.4.1 Characterization of the deformable bioreactor

The experiment was made using the tensile design, for which the actuation performance are detailed in Chapter 2, and summarized here. The fabricated device is presented in Fig. 6.3(a). Stretchable electrodes appear in black on a transparent elastomer membrane, whereas the rigid frames used to hold prestretch and create a culture chamber appear in green with a silver pad for electrical connection. The average strain generated in the gap was measured by tracking the electrodes boundaries as described in Fig. 6.3(b). The actuation strain is presented in Fig. 6.3(c) as a function of the electric field applied across the membrane. The actuation strain is limited to $\epsilon_{yy} = 35\%$ by loss of mechanical tension, and not by electromechanical instability [46, 47, 59]. An electric field of 130 V/µm, which corresponds to a driving voltage of 3.9 kV for a 30 µm thick membrane, is required to reach $\epsilon_{yy} = 10\%$. The actuation is not perfectly uniaxial, and the tensile strain ($\epsilon_{yy} = 10\%$) is accompanied by a transversal compressive strain $\epsilon_{xx} = -2.5\%$, providing a strain ratio equal to $\epsilon_{yy}/\epsilon_{xx} = 4$.

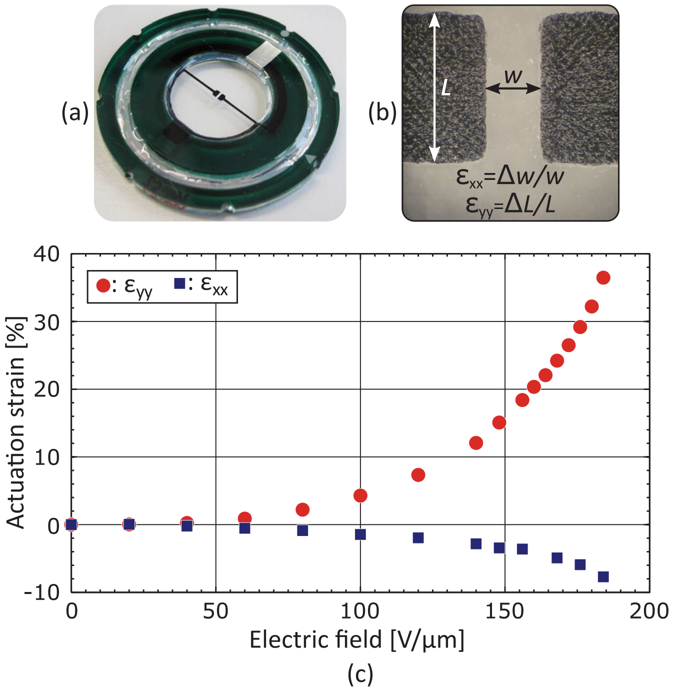

Figure 6.3 – (a) Picture of a fabricated DEA-based deformable bioreactor, where the stretchable electrodes appear in black, on a transparent membrane, held by a green rigid plastic frame. (b) Picture of the electrode gap, with the equations used to calculate the average strain generated in the gap upon actuation. (c) Average strain in the gap as a function of the electric field applied across the 30 µm thick membrane. The actuation is limited to $\epsilon_{yy} = 35\%$ by loss of mechanical tension, and is accompanied by a transversal compression of $\epsilon_{xx} = -7.5\%$. At a driving voltage of 3.9 kV, the device reaches $\epsilon_{yy} = 10\%$ and $\epsilon_{xx} = -2.5\%$.

6.4.2 Stretch-induced alignment of lymphatic endothelial cells

Figures 6.4(a)-(b) presents fluorescence micrographs acquired in the stimulated and static control areas of the device, respectively. The measurements were made after 24 h of cyclic actuation between 0 % and 10 % strain at a 0.1 Hz frequency. The signal obtained from the DNA staining is shown in blue, while the signal obtained from the F-actin staining is shown in green. The DNA is concentrated in the nucleus and can be used to identify and count cells, whereas F-actin is particularly abundant beneath the cell membrane and can be used to characterize cells morphology. The results show that the cells in the stimulated region tend to be more elongated and to align perpendicular to the applied strain, while cells in the static control tend to have a random orientation.

I characterized cell morphology in the stimulated and static control areas. Figure 6.4(c) presents the orientation distribution with respect to the strain axis. Green ellipses and black arrows on the left schematize cells and the strain axis respectively. Results show random distribution in the control area and preferential orientation around 100° in the stimulated area. Stretch-induce alignment has been reported for different types of cells [4] and is expected for LECs. The alignment is however typically perpendicular to strain which would corresponds to an orientation of 90° in Fig.6.4(c). The strain axis is difficult to precisely identify when analysing the fluorescence micrographs, and the 10° offset is probably due to a misalignment of the sample during imaging. Figure 6.4(c) presents the elongation distribution. The elongation coefficient corresponds to the ratio between the long and short axis of a cell, and the green ellipses on the left schematize the corresponding shapes. Results show that stimulated cells are more elongated, and that the elongation is perpendicular to the direction of strain.

In addition to LECs, I also cultured and stretched bronchial smooth muscle cells, fibroblasts, osteoblasts and cardiomyocytes. The device showed no visible effect on cell viability but strain rate was identified as a sensitive parameter. In some experiments, fast actuation of the device induced cell detachment and the driving signal had to be modified in order to limit strain rate. The fast response of DEAs can also be an advantage over alternative technologies, providing the possibility to accurately reproduce arbitrairy strain profiles, and model extreme environments to look at the effect of head trauma on neurones for example.

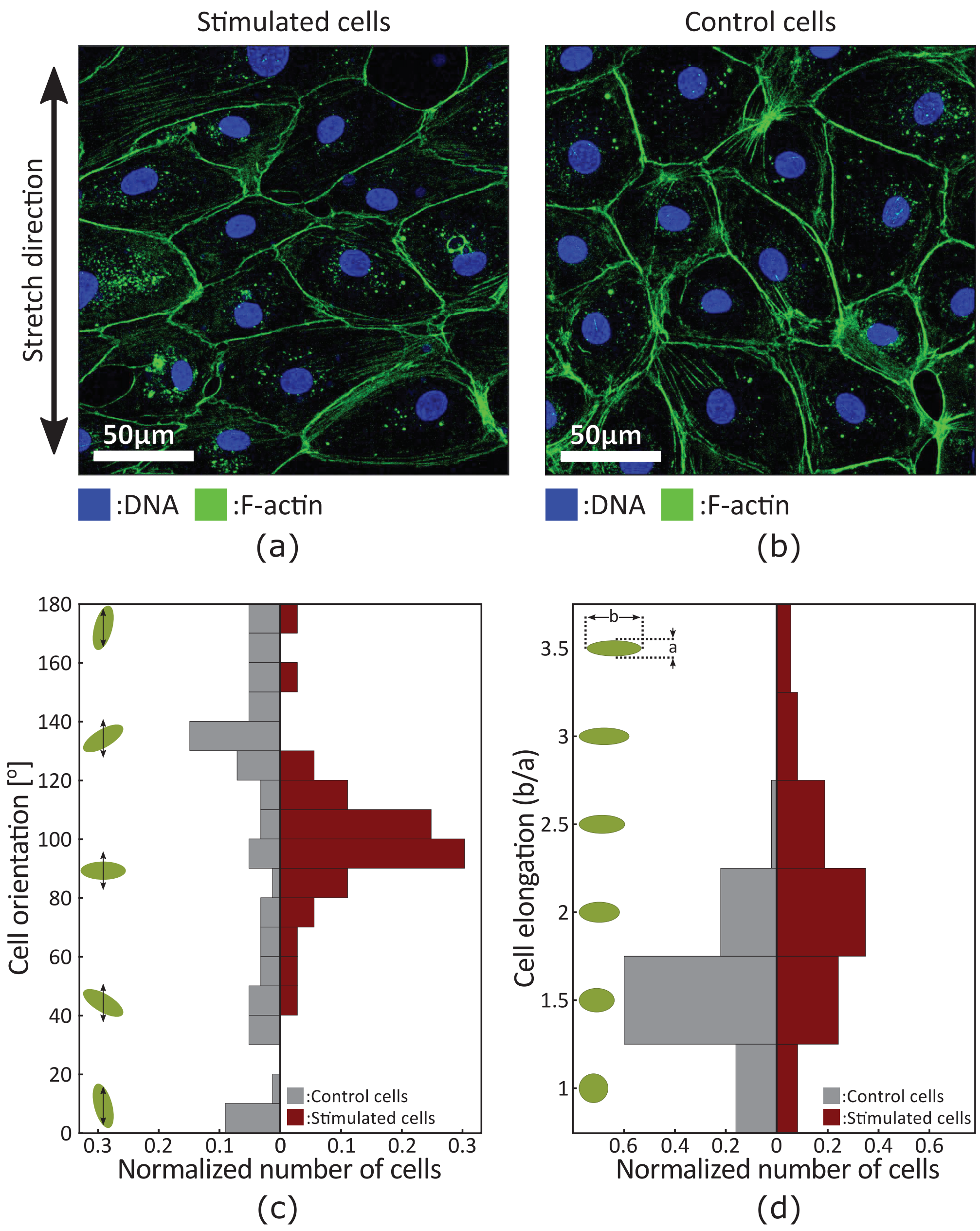

Figure 6.4 – Fluorescent micrographs acquired in the (a) stimulated and (b) static control areas show stretch-induced alignment of LECs. Measurements were done after 24 h of cyclic actuation between 0 % and 10 % strain at a 0.1 Hz frequency. (c) Orientation distribution of cells in the static control and stimulated areas. The green ellipses and the black arrows schematize the cells and the strain axis respectively. Results show clear alignment of LECs perpendicular to strain. (d) Elongation distribution of cells in the static control and stimulated areas. Elongation is calculated as the ratio between the long and short axis of cells, and the green ellipses shematize the corresponding cell shapes. Results show stretch-induced elongation of LECs.

6.4.3 Effect of fringing electric field on LECs

In this section, I present a control experiment designed to study the effect of the device fringing electric field on LECs morphology. The objective is to show that the device fringing electric field doesn't induce alignment or elongation of LECs, and confirm that the results of the test experiment presented in Fig. 6.4 were induced by periodic mechanical stimulation.
For this control experiment, I replaced the oil-backing by a glass slide which was directly bonded to the membrane. Figure 6.5 presents the device strain-voltage curves before and after immobilization, and shows that the glass slide almost completely suppresses the actuation. In this configuration, the cells are still exposed to the same electric field, while not being mechanically stimulated, effectively decoupling the electric field exposure from the mechanical stimulation. The device was connected to a high-voltage power supply and cycled between 0 V and 4.3 kV at a 0.1 Hz frequency with a 50 % duty cycle for 24 hour. The 4.3 kV actuation voltage corresponds to an electric field of 145 Vμm^{-1}, and generated 10 % strain before immobilization, hence reproducing the conditions of the test experiment.

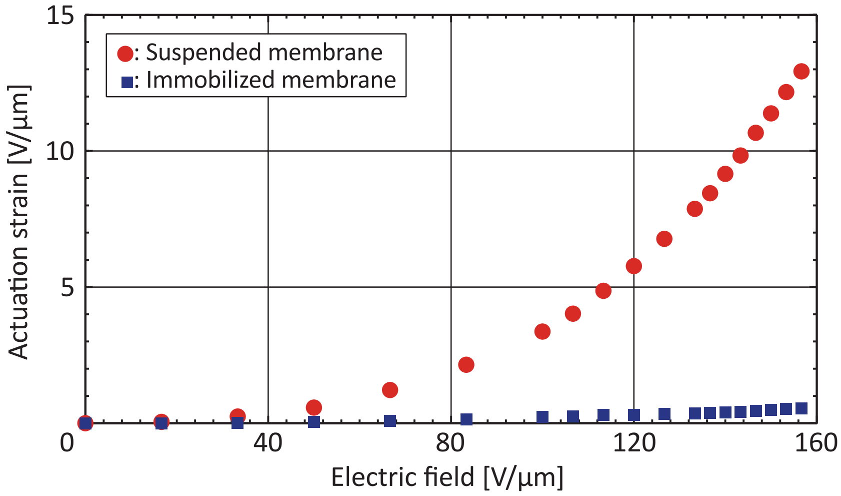

Figure 6.5 – Actuation strain of our DEA-based deformable bioreactor before and after immobilization. The actuation strain at 145 Vμm^{-1} decreases from 10 % for the suspended membrane, to 0.5 % for the immobilized membrane. The immobilization was achieved by replacing the oil backing by a glass slide directly bonded to the membrane.

Figure 6.6(a)-(b) present fluorescence micrographs acquired in the stimulated and control areas of the device after the 24 h experiment. The signal obtained from the DNA staining is shown in blue, while the signal obtained from the VE-cadherin (AF1002, R& D Systems) staining is shown in green. The DNA is concentrated at the nucleus and can be used to identify and count cells, whereas VE-cadherin is concentrated at the cells junctions and can be used to characterize cell morphology. The results show no visible difference in cell morphology between the stimulated and control cells.

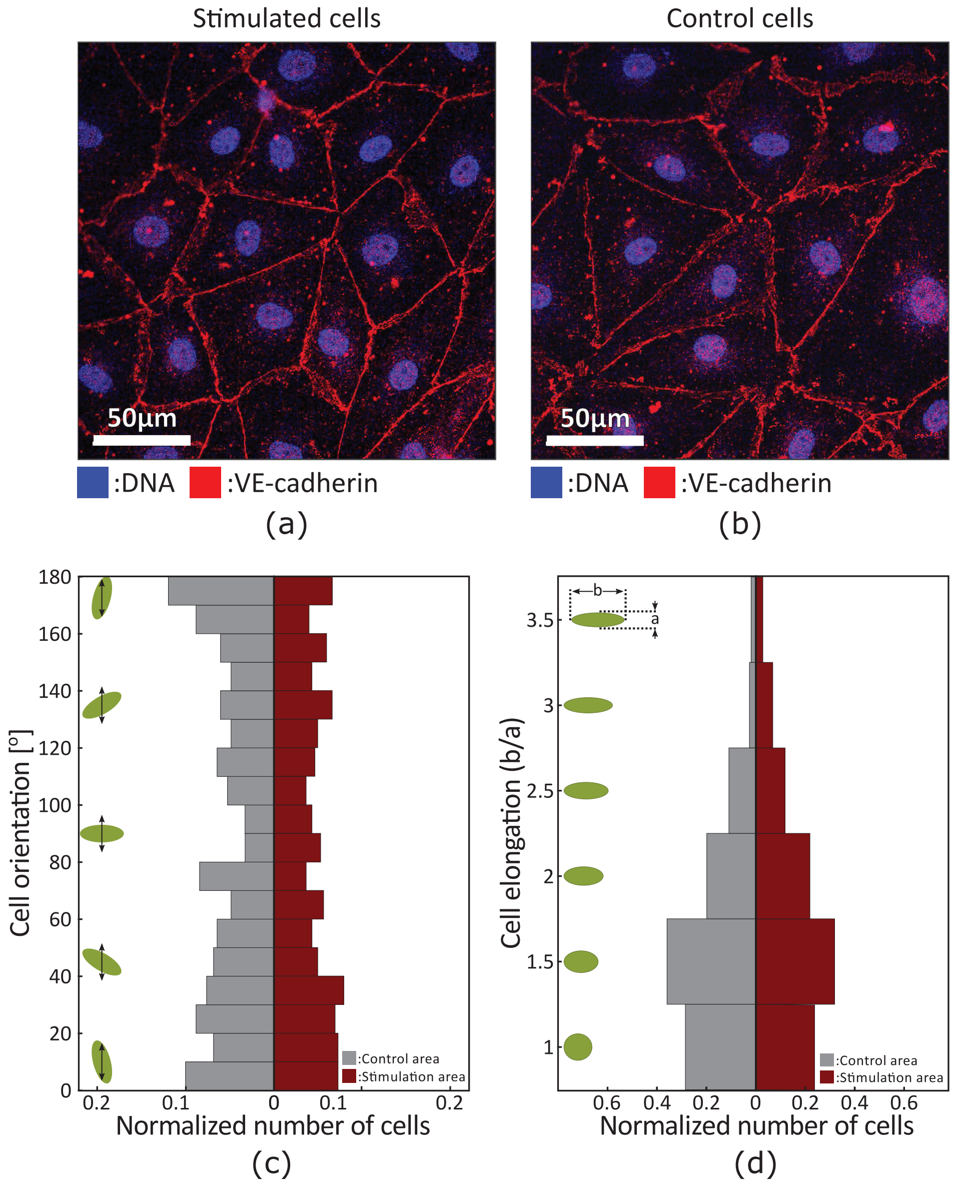

(a) (b)

(c) (d)

Figure 6.6 – Fluorescent micrographs acquired in the (a) stimulated and (b) control areas show no difference in cell morphology. Measurements were done after 24 h of cyclic actuation between 0 $\mathrm{V\mu m^{-1}}$ and 145 $\mathrm{V\mu m^{-1}}$ (corresponds to 10 % strain before immobilization) at a 0.1 Hz frequency. (c) Orientation distribution of cells in the control and stimulated areas. The green ellipses and the black arrows schematize the cells and the strain axis respectively. Results show random orientation in both areas, confirming that the device fringing electric field has no effect on LECs morphology. (d) Elongation distribution of cells in the control and stimulated area. Elongation is calculated as the ratio between the long and short axis of cells, and the green ellipses schematize the corresponding cell shapes. Results show similar distribution in both areas, confirming that the device fringing electric field has no effect on LECs morphology.

Figure 6.6(c) presents the orientation distribution with respect to the strain axis. Green ellipses and black arrows on the left schematize cells and the strain axis respectively. The results show a random orientation of LECs in the stimulated and control areas. Figure 6.6(d) presents the elongation distribution. The elongation coefficient corresponds to the ratio between the long and short axis of a cell, and the green ellipses on the left schematize the corresponding shapes. The results show similar distribution in the stimulated and control areas.

This control experiment demonstrates that the fringing electric field of the DEA-based deformable bioreactor has no effect on LECs morphology, and confirms that the morphological changes observed in the test experiment were stretch-induced.

6.5 Conclusion

In summary, I demonstrated in this chapter the first use of a DEA-based deformable bioreactor for mechanical stimulation of cells *in vitro*. As a proof of concept I cycled a monolayer of LECs between 0 % and 10 % uniaxial tensile strain at a 0.1 Hz frequency for 24 h. Using fluorescence imaging I analysed cells morphology in the stimulated and static control areas. Results showed stretch-induced alignment and elongation of LECs under uniaxial tensile strain, providing the first validation that DEAs can be interfaced with living cells and used to control their mechanical environment.

7 Printing low-voltage DEAs

7.1 Summary

In this chapter, I demonstrate the fabrication of a fully printed thin DEA, reducing the driving voltage below 300 V while keeping high actuation strain. DEAs are capable of strains greater than 100 %, and response time below 1 ms, but they require driving voltage in the kV range, limiting the applications. One way to reduce the driving voltage of DEAs is to decrease the dielectric membrane thickness, which is typically in the 20-100 µm range, as reliable fabrication becomes challenging below this thickness.

I report here the use of pad-printing to produce µm thick silicone membranes, on which I pad-print µm thick compliant electrodes to create DEAs. I achieve a lateral actuation strain of 7.5% at only 245 V on a 3 µm thick pad-printed membrane. This corresponds to a ratio of 125%/kV^2, the highest reported value to date for DEAs.

To quantify the increasing stiffening impact of the electrodes on DEA performance as the membrane thickness decreases, I compare two circular actuators, one with 3 µm- and one with 30 µm-thick membranes. The results show that the strain uniformity of the 3 µm-DEA is indeed affected by the mechanical impact of the electrodes.

I also present a simple DEA model that includes realistic electrodes of finite stiffness, rather than assuming zero stiffness electrodes as is commonly done. The simulation results confirm that the stiffening impact of the electrodes is an important parameter that should not be neglected in the design of thin-DEAs.

This work presents a practical approach towards low-voltage DEAs, a critical step for the development of real world applications. The results presented in this chapter were published in Applied Physics Letters [142] and in the SPIE proceedings of the Electroactive Polymer Actuators and Devices (EAPAD) conference [134].

7.2 Decreasing the driving voltage of DEAs

Stretchability, biocompatibility, optical transparency and silent operation are all key advantages of DEAs, making this technology an ideal candidate for a wide range of applications ranging from well-established fields such as optics [40, 45] and fluidics [143, 144] to emerging fields such as mechanobiology [14] and soft-robotics [24, 26, 145]. With voltages typically in the kV range, DEAs are however limited in terms of real-world applications, where cost and size of high-voltage electronics is an important drawback.

For small deformation and ignoring the electrodes stiffness, lateral $S_x = S_y$ and vertical S_z strains can be approximated [40] by:

$$S_x = -\frac{S_Z}{2} = \epsilon\frac{E^2}{2Y} = \epsilon\frac{V^2}{2t^2 Y} \tag{7.1}$$

where ϵ is the dielectric permittivity of the membrane, Y is its Young's modulus, E is the electric field between the two electrodes, V is the applied voltage and t is the membrane thickness. The driving voltage of DEAs can be reduced by optimizing the material properties of the elastomer membrane, or by reducing its thickness. The Young's modulus and dielectric permittivity of elastomers can be engineered [64] using techniques such as the addition of plasticizers [55] and fillers [146, 147]. It is only recently that significant improvement was reported over typical DEA materials, synthesizing an elastomer with high dielectric permittivity and low Young's modulus [71]. The reported actuator was however based on a 180 µm thick membrane and required 1 kV to reach a lateral strain of 7 %. A different and complementary approach consists in decreasing the elastomer membrane thickness. While typical actuators are 20 µm to 200 µm in thickness, several techniques can be used to make sub-micron elastomer membranes [69, 148–151]. It is however challenging to achieve thickness uniformity and breakdown field compatible for use with DEAs. Bending actuators composed of gold electrodes patterned on a 4 µm-thick membrane obtained by spin-coating, and a 200 nm-thick membranes produced by molecular beam evaporation have been demonstrated, but exhibited limited actuation strain [69].

I present here the use of pad printing to produce fully printed DEAs with membrane thickness of only a few microns. Pad printing is an industrial printing process mostly used to print inks on 3D surfaces otherwise difficult to print on. The technique transfers a pattern from a cliché onto a substrate via a silicone pad. With a clever choice of materials, and by carefully adjusting the printing parameters such as pad pressure and number of stamping steps, I can produce uniform silicone membranes of 1 µm to 10 µm in thickness. To make a DEA I first pad-printed two elastomer membranes, on top of which I next pad-printed compliant electrodes based on a carbon black-elastomer composite ink [67]. I finally assembled the two membranes back to back and applied a 10 % equibiaxial prestretch. The total membrane thickness after prestretch was 3 µm, ten times thinner than typical DEAs. Using this device, I report a lateral actuation strain of 7.5 % at only 245 V. It corresponds to a strain-to-voltage-squared ratio of 125 % kV^{-2}, the highest reported value for DEA to date by more than an order of magnitude.

To investigate the mechanical impact of the micron thick electrodes on the device performance I developed an energy-based model that includes the electrodes mechanical properties, a parameter typically neglected for standard DEAs but which should not be overlooked for thin DEAs. I also developed a strain-mapping algorithm based on optical correlation and analysed the strain profile of our actuator. Results show that the electrode stiffness is indeed a critical parameter, and gives insight on how to design and optimize thin DEAs.

7.3 Fabrication process of printed DEAs

Thin DEAs for low voltage applications present significant challenges. The fabrication of high quality membranes that can sustain high electric field is difficult below 20 µm where the presence of membrane defects and thickness variations become critical. The fabrication of thin DEAs has also been limited by the need for a technique to pattern stretchable electrodes on extremely soft membranes without inducing any mechanical damage, and with limited stiffening impact.

I report a fabrication process that overcomes those technical limitations. Our process is based on pad printing, an established technology mostly used in the industry to print 2D ink patterns on three dimensional surfaces. Pad printing machines use a cliché (steel plate engraved with the desired design) whose recessed features are filled by an ink pot sliding on its surface. A silicone pad is pressed against the cliché and then removed, thus picking up the ink from the cliché. The pad is next pressed against the printing substrate and removed, thus transferring the ink from the pad to the substrate (see Section 2.5.2). Pad printing uniform layers of high-viscosity materials such as silicone elastomers is not trivial. It is with a clever choice of materials, and by carefully adjusting the printing parameters such as pad pressure and number of stamping steps, that I was able to print uniform silicone membranes of 1 µm to 10 µm in thickness.

The thin DEA fabrication process that I developed based on pad printing is detailed in Fig.7.1.

(i) A substrate of high-quality PET foil was coated with a water soluble sacrificial layer of poly(acrylic) acrid (PAA). The sacrificial layer was obtained from a solution of 5 % PAA, 15 % water and 80 % isopropyl alcohol (IPA) applied by bar coating on a A4 sheet of PET. The substrate was next laser cut into 50 mm diameter circular pieces.

(ii) Using a pad printing machine (TMP-101, Teca-Print AG, Switzerland) a silicone layer was printed on the substrate. Several silicones such as the Sylgard 184 (Dow Corning, USA), Sylgard 186 (Dow Corning, USA) and Silbione LSR 4305 (Bluestar Silicones, France) were successfully printed. The more viscous silicones required the addition of solvent (OS-2, Dow Corning, USA) which led to lower quality membranes. The best results were obtained with Sylgard 184 for which no solvent was required due to its low viscosity (3500 $\mathrm{mPa\,s^{-1}}$ compared to 65 000 $\mathrm{mPa\,s^{-1}}$ for Sylgard 186, and 40 000 $\mathrm{mPa\,s^{-1}}$ for LSR 4305) and self-levelling properties. The substrate was allowed 30 min to self-level after printing, significantly improving the silicone layer uniformity. The substrate was then heat-cured at 80 °C for 60 min.

(iii) A stretchable electrode was pad printed on the cured silicone layer and heat-cured at 80 °C for 60 min. I used a carbon black-elastomer composite ink developed in our laboratory which provides stable mechanical and electrical properties and has a limited stiffening impact. Pad printing could not be used to apply electrodes on suspended thin membranes i.e. I had to print the electrodes before releasing the membrane and had to minimize the printing pressure of the pad in order to avoid any mechanical damage.

(iv) The sample was immersed in hot deionized water for 5 min, dissolving the PAA sacrificial layer and releasing the printed membrane. With this technique the membrane release was gradual and gentle on the membrane, avoiding any mechanical damage.

(v) Two released membranes were placed under an equibiaxial prestretch. Several prestretch levels were tested, increasing the surface area by more than 4 times, hence demonstrating the quality of the printed membranes. A low prestretch level was nevertheless preferred in order to limit its impact on the electrodes resistance (The electrodes are applied before prestretch which therefore influence their resistance). The results presented in this work were obtained under a 1.1 equibiaxial prestretch.

(vi) The two membranes were assembled back-to-back to form a DEA. A drop of ethanol was placed between the two membranes to ensure a uniform contact and avoid trapping air bubbles. Due to the presence of a thin layer of alcohol between them, the two layers could slide on top of each other, which enabled precise electrodes alignment. After 5 min at room temperature the alcohol was completely evaporated and surface adhesion held the two membranes together. PMMA rings were fixed on both sides of the actuator using pressure sensitive adhesive (ARclear, Adhesive Research Inc.) to lock the membrane prestretch.

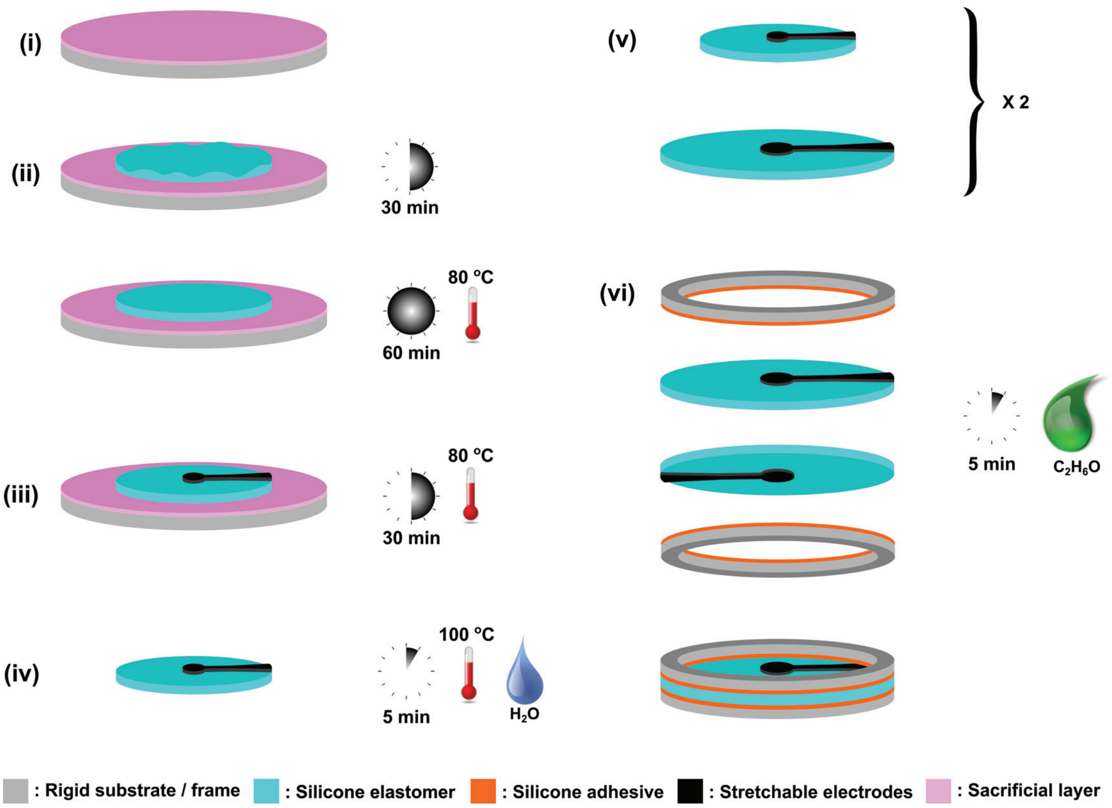

Figure 7.1 – Pad printing was used to produce fully printed DEAs. (i) A water soluble sacrificial layer of PAA was applied on a PET foil. (ii) A silicone layer was then transferred on the substrate using a pad printing machine. The printed silicone layer was allowed time to self-level before it was heat-cured. (iii) Using the same pad printing machine I printed a stretchable electrode on the cured silicone membrane. The carbon-elastomer composite electrode was then heat-cured. (iv) The printed membrane was immersed in hot water to dissolve the sacrificial layer, releasing it from the PET substrate. (v) Two membranes were printed and placed under equibiaxial prestretch. (vi) The two membranes were then assembled back-to-back to form a DEA, using ethanol to ensure a uniform contact between the membranes and avoid trapping air bubbles. PMMA rings were fixed on both sides of the actuator using pressure sensitive to lock the membrane prestretch.

7.4 Actuation performance of printed DEAs

Using the fabrication process presented in the previous section I fabricated a fully printed 3 µm thick DEA and evaluated its performance, comparing it with a typical 30 µm thick DEA that was fabricated following our standard fabrication process [67]. I used expanding circle actuators for this study, a standard for performance evaluation of DEAs [10]. Except for the different membrane thicknesses, the 3 µm and 30 µm devices were identical. They had the same geometry, used the same membrane and electrode materials, and had the same membrane prestretch. Figure 7.2(a) presents a picture of the 3 µm printed DEA where the stretchable electrodes appear in black. The electrodes were 1 µm to 2 µm in thickness, slightly thinner than the printed DEA membrane. The circular active area was 2 mm in diameter and the rigid PMMA rings holding the membrane prestretch had an inner diameter of 20 mm. The membrane was made of Sylgard 184 and placed under a 1.1 equibiaxial prestretch.

Figure 7.2(b) presents the average radial strain of the 3 µm and 30 µm DEAs as a function of the driving voltage. Neglecting the electrodes stiffening impact, the driving voltage of the 3 µm thick DEA is expected to be ten times lower than for the 30 µm thick DEA. The actuation on the thin membrane was limited by dielectric breakdown and a maximum strain of 7.5 % was achieved at only 245 V. For comparison, actuation on the thick membrane required 3.3 kV to reach the same strain level. Limited by loss of mechanical tension, actuation on the thick membrane could reach up to 14.2 % strain at 4.1 kV. Overall, the 3 µm printed DEA was limited to half the strain of its 30 µm thick equivalent. This downside was however easily offset by a more than ten-fold decrease of the driving voltage. In addition, a radial strain of 7.5 % is enough to meet the requirements of various DEA applications [12, 152].

The limited maximum strain of the printed DEA can have two main origins. a) The presence of non-uniformities in the membrane such as thickness variations, air bubbles or inclusion of foreign particles that can lead to premature dielectric breakdown. b) The mechanical stiffening impact of the electrodes which can increase the electric field required to reach a given strain level, effectively decreasing the strain at dielectric breakdown. It is generally difficult to improve membrane uniformities and to reduce electrodes stiffness as those parameters are often already optimized. Further improvement on the electrode stiffness for example would come at the cost of higher resistance. As a result, their relative impact on DEA performance typically increases as the membrane thickness decreases.

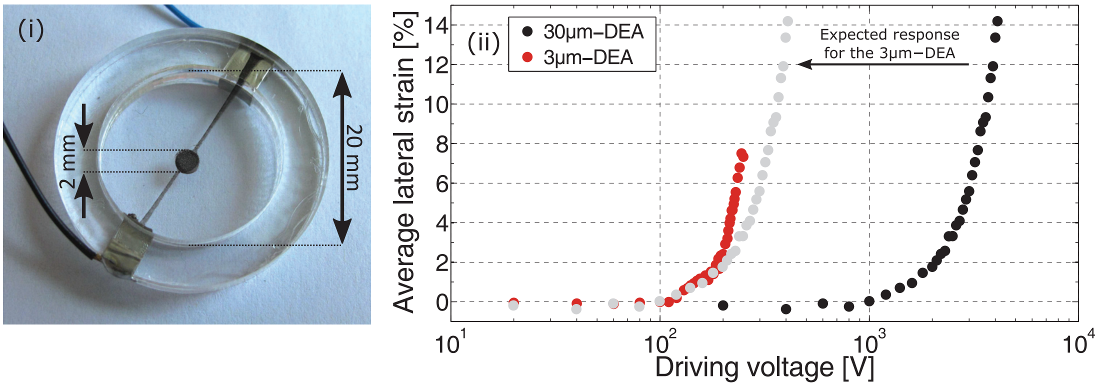

Figure 7.2 – (i) Picture of the printed 3 µm thick DEA with a 3 mm diameter active area on a 20 mm diameter membrane. (ii) The average radial strain was measured on 3 µm and 30 µm thick DEAs. Except for the different membrane thicknesses, both actuators had identical geometry, materials and prestretch. Neglecting the electrodes stiffening impact, the driving voltage of the 3 µm thick DEA is expected to be ten times lower than for the 30 µm thick DEA. The printed 3 µm thick DEA was limited to lower actuation strain but it required more than 10 times lower driving voltage. It exhibited 7.5 % radial strain at only 245 V, which corresponds to a strain-to-voltage squared ratio of 125 %/kV^2.

A comparison metric adapted to this work is the strain-to-voltage-squared ratio (S_x/V^2) which, unlike the more intuitive strain-to-voltage ratio (Sx/V), does not depend on the actuation parameters but solely on the device geometry. Equation 7.1 clearly shows that S_x/V^2 is a device-constant parameter while S_x/V varies linearly with V. Using this metric as a factor of merit the printed DEA improved the actuator performance by more than two orders of magnitude, increasing the S_x/V^2 ratio from 0.7 %kV^{-2} for the 30 µm thick device to 125 %kV^{-2} for the 3 µm thick device. This result is the highest reported value for a DEA, improving by more than one order of magnitude over current state-of-the art devices. While area strain of 488 % [11] and actuation at only 10 Vµm^{-1} [71] have been reported for expanding circle DEAs, the corresponding strain-to-voltage-squared ratios were only 5.7 %kV^{-2} and 7 %kV^{-2} respectively.

7.5 Strain field uniformity of printed DEAs

The actuation strain of DEAs is typically measured by tracking the electrodes boundary and calculating the ratio between their initial and final dimensions. This approach is quick and easy to implement but it can hide some valuable information. The ratio between the initial and final dimensions of the electrodes gives the average strain but it provides no information on how uniform the strain field is. In order to get a better insight on the actuation performance of the printed DEA I characterized the uniformity of its strain field.

In addition to the technical difficulty and complexity of measuring strain over a large array of points (instead of only tracking one or two boundaries for average strain), the main difficulty in mapping strain fields comes from the electrode material. Usually highly absorbent in the visible range, it is challenging to make optical measurements in the electrode-covered regions. The use of periodic metallic microstructures [14] and randomly dispersed fluorescent microbeads [153] can be used to overcome this limitation. Those two techniques however require specialized microfabrication or imaging equipment.

In this work I removed the need for metallic microstructure or fluorescent markers by taking advantage of the electrodes microstructure. Figure 7.3 summarises the mains steps of the strain mapping process.

(i) The DEA was placed under a microscope and pictures of the device were recorded under increasing driving voltages. I adjusted the sample lighting to maximise contrast and avoid saturation of the camera sensor in the electrode-coated regions.

(ii) The unactuated picture was discretized into an array of element (e_x, e_y) each composed of n_x by n_y pixels with a center point located at the pixel coordinate (p_x, p_y). Using normalized cross-correlation, a technique widely used for pattern recognition, I found for each element their new position (p'_x, p'_y) in the actuated picture.

The cross-correlation step requires the element to be scanned over every pixel of the actuated picture, calculating for each position a correlation coefficient C. The coefficient can take any value between -1 and 1 (perfect match), and the final output is a 3D surface with its maximum C_max located at the best match position (p'_x, p'_y). If C_{max} is greater than a predefined confidence threshold, I have found the new element position (p'_x, p'_y). To minimize processing time the cross-correlation can be calculated over a limited region of the actuated picture, for example a region centered on (p_x, p_y) and measuring $n_y + 2\delta_y$ by $n_x + 2\delta_x$ pixels can be used.

Strain levels greater than 5 % are difficult to measure by normalized cross-correlation. One solution is to digitally stretch the elements before the cross-correlation step, but this approach requires guessing the expected strain and can therefore require long iteration loops. A second approach is to simply process a series of pictures recorded at intermediate steps, adding up the strain maps to obtain the total strain field.

(iii) Finally, from the initial (p_x, p_y) and final positions (p'_x, p'_y) I calculated the displacement and strain fields. The displacement field was simply obtained by calculating the distance separating the two positions. The overlaid black arrows in Fig. 7.3(iii) correspond to the displacement direction. The amplitude of the displacement is given by the arrows length and by the color coded contour lines. The strain field was obtained by calculating the derivative of the displacement field. The overlaid black lines in Fig. 7.3(iii) correspond to the vertical/horizontal strain ratio i.e. 45° lines indicates an equibiaxial strain, horizontal lines correspond to a uniaxial horizontal strain, and vertical lines correspond to a uniaxial vertical strain. The strain amplitude is given by the lines length and by the color coded contour lines.

Measurements of strain-distribution on the 3µm-DEA and the 30µm-DEA are presented in Fig. 7.4. The devices were respectively actuated at 245 V and 3.3 kV which corresponds to an average lateral strain of 7.5% (Fig.7.2). While the 30µm-DEA exhibits excellent strain uniformity, the 3µm-DEA shows variations over the device area, with local strain values greater than 10 % for a 7.5 % average lateral strain. This result gives an important insight on the actuation performance of the printed DEA i.e. Regions under higher strain are exposed to higher electric field and are consequently prone to induce early dielectric breakdown. Actuation strain of the printed DEA was therefore partially limited by its non-uniform strain profile.

The non-uniform strain profile measured on the 3 µm thick DEA can origin from thickness variations over the membrane and from the electrodes stiffening impact (i.e. the effects of electrodes thickness variations and the presence of leads connecting the circular active area). While both effects must have influenced the device performance, believe that the electrodes mechanical impact was dominating. White light interferometry measurements showed membrane thickness uniformity with less than 10 % variations, which according to our simulation is not enough to explain the variations measured in the strain profile. In addition, the same strain distribution presented in Fig. 7.4(a) was observed on all printed DEAs i.e. a high strain region located in the center of the device, and elongated in the direction perpendicular to the feedlines. This regular strain profile can be explained by the electrodes mechanical impact but not by random thickness variations over the membrane.

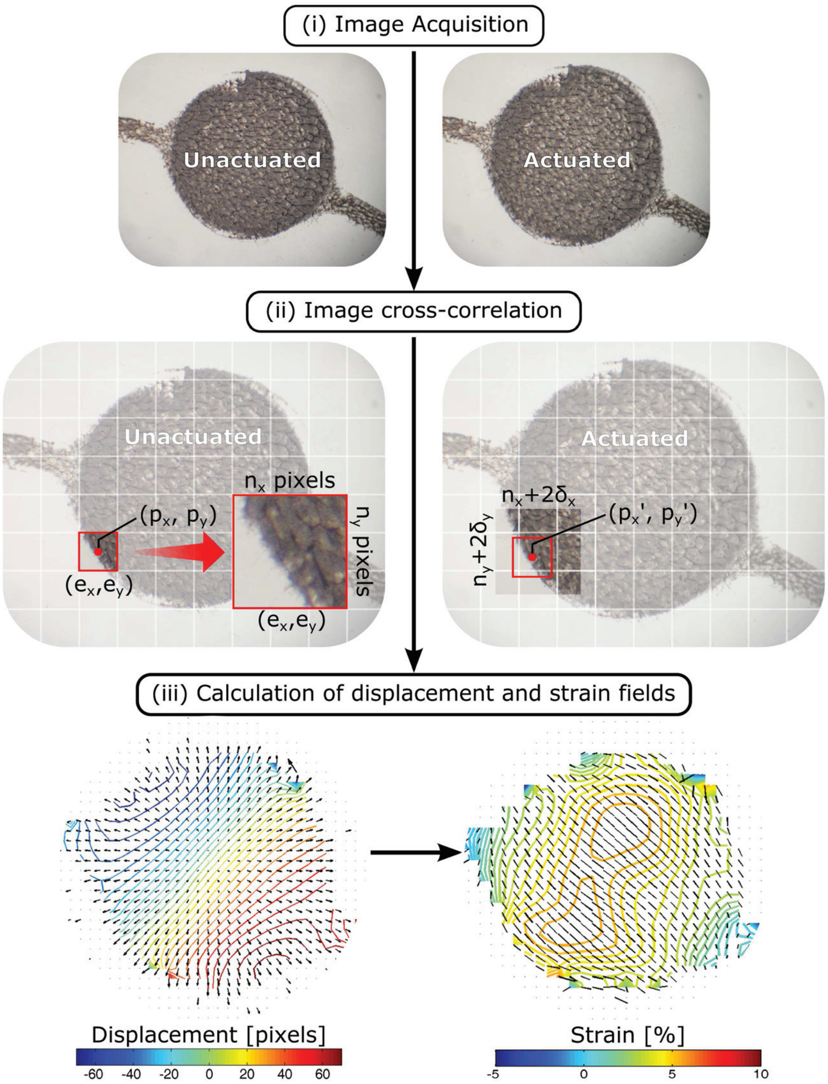
(i) Image Acquisition
Unactuated
Actuated
(ii) Image cross-correlation
Unactuated
n_x pixels
(p_x, p_y)
(e_x,e_y)
n_y pixels
(e_x,e_y)
Actuated
n_x+2δ_x
n_y+2δ_y
(p_x', p_y')
(iii) Calculation of displacement and strain fields
Displacement [pixels]
-60 -40 -20 0 20 40 60
Strain [%]
-5 0 5 10

Figure 7.3 – Digital Image Correlation (DIC) was used to measure the strain field of the actuator. Taking advantage of the electrodes topography I achieve this measurement without the need for additional markers as typically required for DIC. (i) The fully printed DEA was actuated while pictures of the active area were recorded at increasing voltages. (ii) The unactuated picture was first discretized into an array of elements (ex, ey), each composed of n_x by n_y pixels and with their center points located at the pixels coordinates (p_x, p_y). Using normalized cross-correlation, a technique widely used for pattern recognition, I found for each element its new position (p'_x, p'_y) in the actuated picture. To minimize processing time I calculated correlation only over a sub-region centered on (p_x, p_y) and measuring $n_y + 2\delta_y$ by $n_x + 2\delta_x$ pixels. (iii) From the position of each element in the unactuated and actuated states I calculated the displacement and strain fields. The overlaid black arrows give the displacement directions while the black line corresponds to the vertical/horizontal strains ratio i.e. a 45° line indicates equibiaxial strain.

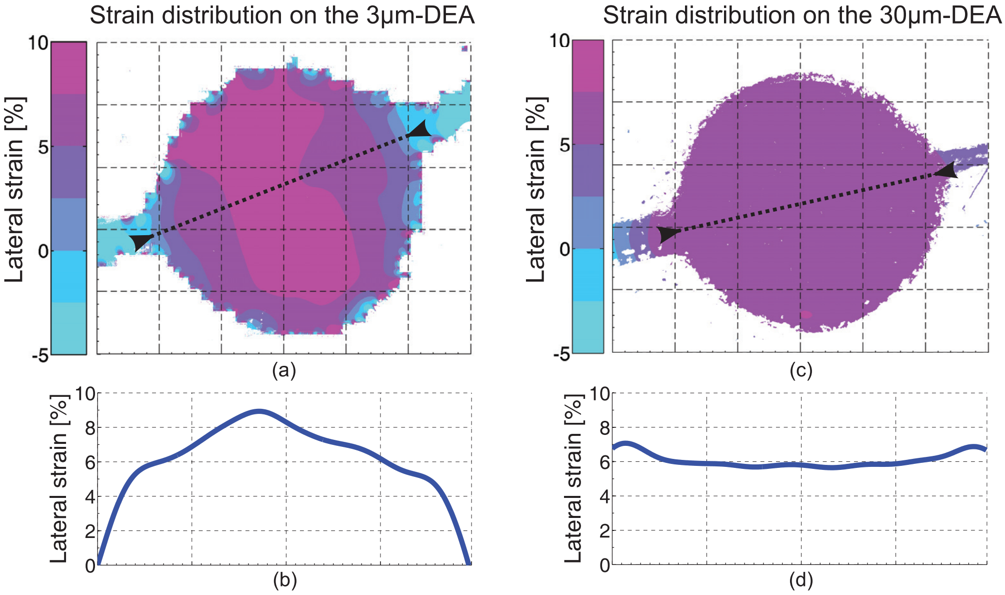

Figure 7.4 – (a) Lateral strain distribution and (b) cross-section along the black dotted line for the 3 µm-DEA . (c) Lateral strain distribution and (d) cross-section along the black dotted line for the 30 µm-DEA . The stiffening impact of the electrodes induces high-strain regions on the 3 µm-DEA. Those regions experience higher electric field and can therefore induce premature dielectric breakdown.

7.6 Modelling the electrodes stiffening impact

Significant work has already been done to develop theoretical models describing the actuation mechanism of DEAs. These models helped identifying and predicting the main failure mechanisms [46], and were used to maximize DEAs actuation strain [11, 29] and displacement [30]. While the mechanical forces acting in the membrane are usually well described with those models, taking into account the hyperelastic properties and the incompressibility of the material, the mechanics of the electrodes is typically neglected. This approximation is valid for soft electrodes on thick membranes, but our experimental results on the 3 µm DEA suggest that it is not valid anymore for thin DEAs.

I developed a simple energy-based model that predicts the actuation strain of an expanding circle DEA as a function of the applied voltage. The boundary effect on the membrane is neglected (a valid approximation if the radius of the active area is much larger than the radius of the passive area) and the prestretch is modeled as a constant force. Figure 7.5 presents the actuator geometry and lists the input parameters (in red), variables (in blue) and assumptions (in green) of the model. Using an energy minimization approach I calculated the voltage V as a function of the actuation stretch λ_{act}. I first wrote the equations of the different energy contributions, as well as their first derivatives. Using those equations I calculated the total energy of the system and minimized it to find a stable solution. I expressed the analytical solution as a function of the form $V(\lambda_{act})$ which can be used to predict the voltage required to reach any stretch level for a given actuator design.

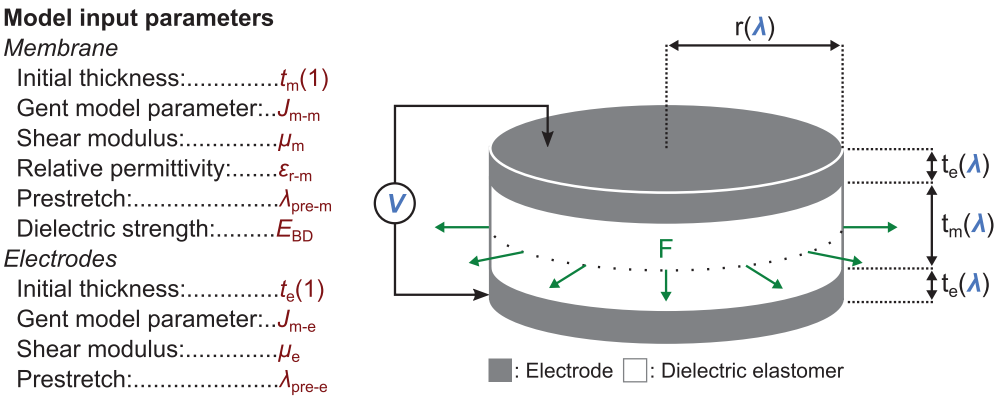
Model input parameters
Membrane
Initial thickness:..............t_m(1)
Gent model parameter:..J_m-m
Shear modulus:..............μ_m
Relative permittivity:.......ε_r-m
Prestretch:.....................λ_pre-m
Dielectric strength:.........E_BD
Electrodes
Initial thickness:..............t_e(1)
Gent model parameter:..J_m-e
Shear modulus:..............μ_e
Prestretch:.....................λ_pre-e
r(λ)
V
F
t_e(λ)
t_m(λ)
t_e(λ)
▮: Electrode ☐: Dielectric elastomer

Figure 7.5 – I developed an energy based model to predict the strain of an expanding circle DEA as a function of the applied voltage. It has the particularity of including the electrodes mechanical properties, a critical element in the development of thin DEAs. The model describes prestretch as a constant force acting at the boundary of the device active area. The mechanical energy stored in the membrane and the electrodes is calculated using the strain energy density function of the Gent model. The figure lists the model assumptions (green), input parameters (red) and variables (blue).

The prestretch λ_{pre} was modeled a constant force F acting on the periphery of the stretched layer. The stored mechanical energy can be expressed as

$$\begin{aligned} U_{pre} &= F\delta_r \\ &= 2\pi r(\lambda_{pre})t(\lambda_{pre})\sigma(\lambda_{pre})(r(\lambda)-r_0)) \\ &= 2\pi r_0^2 t_0 \lambda_{pre}^{-1}\sigma(\lambda_{pre})(\lambda-1) \end{aligned} \tag{7.2}$$

where $\lambda = \lambda_{pre}\lambda_{act}$ is the total stretch, $r(\lambda)$ is the actuator radius, $t(\lambda)$ is the layer thickness, and $\sigma(\lambda)$ is the mechanical stress in the layer. Using the Gent model equation for equibiaxial stress

$$\sigma(\lambda) = \left(\lambda^2 - \frac{1}{\lambda^4}\right)\left(\frac{\mu J_m}{J_m - I_1 + 3}\right) \text{ [49]}, \tag{7.3}$$

where μ is the layer shear modulus, J_m is a model parameter and I_1 is the first invariant of the Cauchy-Green tensor, I replaced $\sigma(\lambda)$ in Eq.7.2 and obtained

$$U_{pre} = \left[2\pi r_0^2 t_0 \lambda_{pre}^{-1}\left(\lambda_{pre} - \frac{1}{\lambda_{pre}^4}\right)\left(\frac{\mu J_m}{J_m - I_1(\lambda_{pre}) + 1}\right)\right](\lambda - 1)$$

and

$$\frac{dU_{pre}}{d\lambda_{act}} = \left[2\pi r_0^2 t_0 \left(\lambda_{pre} - \frac{1}{\lambda_{pre}^4}\right)\left(\frac{\mu J_m}{J_m - I_1(\lambda_{pre}) + 1}\right)\right]. \tag{7.4}$$

This equation was used to separately calculate the membrane and electrodes prestretch energy.

For the actuation stretch contribution I used the strain energy density function W of the Gent model and obtained

$$U_{act} = -\frac{\mu J_m}{2} ln\left(1 - \frac{I_1(\lambda) - 3}{J_m}\right)\pi r_0^2 t_0$$

and

$$\frac{dU_{act}}{d\lambda_{act}} = \frac{2\mu J_m \pi r_0^2 t_0}{(J_m - I_1(\lambda) + 3)}\left(\frac{\lambda^6 - 1}{\lambda_{act}\lambda^4}\right). \tag{7.5}$$

This equation was used to separately compute the membrane and electrodes actuation stretch energy. For the electrostatic contribution to the total energy I considered a parallel plate capacitor and neglected the edge effect. I obtained

$$U_{elec} = \frac{\epsilon\pi r_0 \lambda^4 V^2}{2 t_0}$$

and

$$\frac{dU_{elec}}{d\lambda_{act}} = \frac{2\epsilon\pi r_0 \lambda^3 V^2}{t_0} \tag{7.6}$$

where ϵ is the membrane dielectric permittivity and V is the voltage. The total system energy was expressed as

$$U_{tot} = 2U_{pre-e} + U_{pre-m} + 2U_{act-e} + U_{act-m} + U_{elec}$$

and setting its first derivative equal to zero (to minimize the system energy) I obtained

$$-\frac{dU_{elec}}{d\lambda_{act}} = 2\frac{dU_{pre-e}}{d\lambda_{act}} + \frac{dU_{pre-m}}{d\lambda_{act}} + 2\frac{dU_{act-2}}{d\lambda_{act}} + \frac{U_{act-m}}{d\lambda_{act}} \tag{7.7}$$

where U_{pre-e} is the prestretch energy of the electrode (In our fabrication process the electrodes were printed before applying prestretch to the membrane), U_{pre-m} the prestretch energy of the membrane, U_{act-e} the actuation stretch energy of the electrode, U_{act-m} the actuation stretch energy of the membrane, and U_{elec} the electrostatic energy of the system. Combining Equations 7.4 – 7.7 I isolated the voltage V as a function of the actuation stretch λ_{act} and used this analytical solution to predict the strain-voltage curves for different DEA geometries.

Figure 7.6 compares the strain-voltage curves of actuators with membrane thicknesses ranging from 5 µm to 60 µm. The solid lines correspond to the results obtained for realistic electrodes of finite stiffness, whereas doted lines correspond to the results obtained for ideal electrodes of zero stiffness. The red crosses indicate where the electric field in the membrane exceeds the dielectric breakdown strength that was set to 160 Vµm^{-1}. I considered 1 µm thick electrodes that had the same shear modulus as the membrane. The complete list of model parameters is detailed on the right hand side of the figure. As expected, I observed for ideal and realistic electrodes that the driving voltage decreases with the membrane thickness. The strain at dielectric breakdown however evolved differently for the two configurations. It remained constant for the ideal electrodes, but decreased with the membrane thickness for the realistic electrodes.

The offset observed between the two set of curves on Figure 7.6 comes from the stiffening impact of the electrodes which slightly increases the driving voltage. I observed that the relative stiffening impact of the electrodes is not constant, but that it rather increases as the membrane thickness decreases. This effect is clearly visible in Figure 7.7 which presents the driving voltage at 5 % radial strain as a function of the membrane thickness. I considered 1 µm thick electrodes (constant parameter that was not scaled with the membrane thickness) that had the same shear modulus as the membrane. The complete list of model parameters is detailed on the right hand side of the figure. I observed that the realistic and ideal electrodes models diverge below 15 µm thick membranes. As the membrane thickness decreases, the actuator mechanics is gradually dominated by the electrodes rather than the membrane.

The results presented in this section showed that the development of thin DEAs is not bounded to simply reducing the membrane thickness. I identified the electrodes stiffness as a critical parameter that can lead to premature dielectric breakdown if not carefully considered in the design of the actuator. The simulations results showed that the ideal electrode assumption is not valid anymore for thin DEAs, or more precisely when the actuator stiffness is not anymore dominated by the mechanical properties of the membrane. Based on those results and on the strain fields measurements presented in the previous section, I believe that the actuation performance of the 3 µm DEA was mainly limited by the stiffening impact of the electrodes. One approach to further improve its performance would therefore be to develop a softer and more conductive electrode material that could be applied in thinner layers.

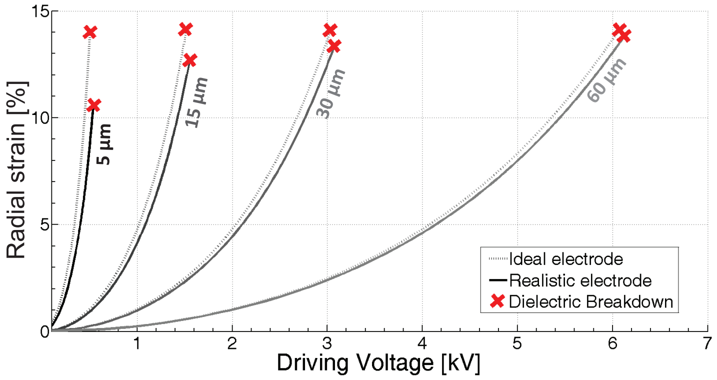

Model input parameters

Membrane

Initial thickness:..............$t_m(1)$=5-60 um
Gent model parameter:...$J_{m\text{-}m}$=3
Shear modulus:..............μ_m=0.75 Mpa
Relative permittivity:.......$\varepsilon_{r\text{-}m}$=2.72
Prestretch:.....................$\lambda_{pre\text{-}m}$=1.1
Dielectric strength:.........E_{BD}=160 V/um

Electrodes

Initial thickness:..............$t_e(1)$=1 um
Gent model parameter:...$J_{m\text{-}e}$=3
Shear modulus:..............μ_e=0-0.75 Mpa
Prestretch:.....................$\lambda_{pre\text{-}e}$=1.1

Figure 7.6 – Simulation results for a circular DEA with membrane thicknesses ranging from 5 µm to 60 µm. The solid lines correspond to the results obtained for realistic electrodes of finite stiffness, whereas doted lines correspond to the results obtained for ideal electrodes of zero stiffness. The red crosses indicate where the electric field in the membrane exceeds the dielectric breakdown strength of the material. The model parameters are listed on the right hand side of the figure. I observed that the realistic electrode model predicts higher actuation voltage due to the mechanical stiffening impact of the electrodes. This effect leads to lower strain at dielectric breakdown, demonstrating that there is an optimal membrane thickness that depends on the DEA voltage and strain requirements.

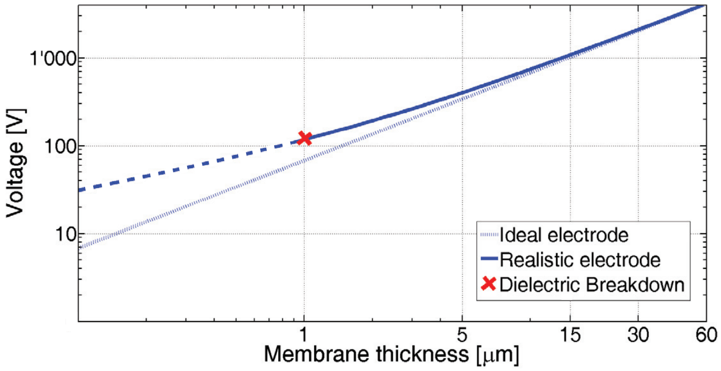

Model input parameters

Membrane

Initial thickness:..............$t_m(1)$=5-60 um
Gent model parameter:..$J_{m\text{-}m}$=3
Shear modulus:..............μ_m=0.75 Mpa
Relative permittivity:.......$\varepsilon_{r\text{-}m}$=2.72
Prestretch:......................$\lambda_{pre\text{-}m}$=1.1
Dielectric strength:.........E_{BD}=160 V/um

Electrodes

Initial thickness:..............$t_e(1)$=1 um
Gent model parameter:..$J_{m\text{-}e}$=3
Shear modulus:..............μ_e=0-0.75 Mpa
Prestretch:......................$\lambda_{pre\text{-}e}$=1.1

Figure 7.7 – The driving voltage required to reach 5 % radial strain on a circular DEA was calculated and presented here as a function of the membrane thickness. The solid lines correspond to the results obtained for realistic electrodes of finite stiffness, whereas doted lines correspond to the results obtained for ideal electrodes of zero stiffness. The red crosses indicate where the electric field in the membrane exceeds the dielectric breakdown strength of the material. The model parameters are detailed on the right hand side of the figure. As I decreased the membrane thickness, the actuator stiffness was slowly dominated by the electrodes. As a result I observed that the realistic model slowly diverged from the ideal case, demonstrating that the ideal electrode assumption is not valid for thin DEAs.

7.7 Conclusion

In this chapter, I presented a fully printed 3 μm thick DEA, and demonstrated that decreasing the membrane thickness to only a few microns significantly reduces the driving voltage. A radial actuation strain of 7.5 % was reported at only 245 V. This result corresponds to an actuation of 125 % kV^{-2} which is the highest reported value to date for a DEA. In order to investigate the stiffening impact of the electrodes I developed a simple DEA model that includes their mechanical properties. I also developed a strain-mapping algorithm based on optical correlation. The simulation results and the strain-mapping measurements identify the electrodes as an important parameter that should not be neglected in the design and optimization of thin DEAs.

This work presents a practical approach toward low-voltage DEAs, a critical step in the development of real-world application. With driving voltage below 300 V, a range covered by commercially available CMOS circuitry, consumer market applications are already possible. Combined with progress in material engineering of elastomers, this work could decrease the driving voltage by and additional order of magnitude, and open the door to a variety of new opportunities for DEA-based technologies.

8 Conclusion

In this chapter, I summarize the contributions of this thesis to the field of DEAs, and present an outlook on future work.

8.1 Summary

8.1.1 DEA-based deformable bioreactor

DEAs find promising applications in the field of cellular mechanobiology. There is for example great interests in miniaturized deformable bioreactors, devices which are designed to apply precise and controlled mechanical stain on cell *in vitro*. Interfacing DEAs with living cells is however challenging, and advances in this area require the development of novel designs, fabrication, and characterization techniques.

Main results

In this thesis, I successfully developed a DEA-based deformable bioreator, capable of generating uniform strain on a 0.5 mm x 1.5 mm transparent area of a larger cytocompatible membrane. Its versatile design achieved up to 35 % uniaxial tensile strain, or 10 % uniaxial compressive strain. The stability and lifetime of the device was demonstrated in culture conditions, with less than 2 % strain variation over more than 12 h and 50 000 actuation cycles (0-10 % strain). In addition, it demonstrated strain rate higher than 700 s^{-1}, approximately 100 times faster than common pneumatic systems, thus enabling the *in vivo* mechanical environment to be replicated with unprecedented precision. The overall performance of the DEA-based deformable bioreactor was found to be comparable to alternative technologies in terms of strain, but significantly better in terms of response time.

I demonstrated the biocompatibility of the system, which supported the growth of several cell types, including lymphatic endothelial cells, osteoblasts, fribroblasts, and cardiomyocites. I demonstrated the system compatibility with standard cell culture protocols and equipment, such as ethanol sterilization, surface functionalization (i.e. fibronectin and collagen to promote cell adhesion), incubation (37 °C and 95 % relative humidity), immersion in culture medium, cell fixation, cell permeabilization, and different types of staining. I also demonstrated the system compatibility with inverted microscopes, where cells could be imaged in real-time during stretching (at up to 20X magnification).

In collaboration with our partners from the Vascular and Tumor Biology Laboratory (UNIL, Switzerland), I designed an experiment to demonstrate the application of the DEA-based deformable bioreactor. In this experiment, I cycled a small population (~100 cells) of LECs between 0 % and 10 % strain, at a 0.1 Hz frequency for 24 h. The results showed that the stimulated cells aligned perpendicular to strain, while cells in the static control population maintained a random orientation. In addition, a second control experiment demonstrated that the device fringing electric field has no effect on LECs morphology, hence confirming that the alignment observed in the test experiment was stretch-induced.

Impact statement

The work that I accomplished on the DEA-based deformable bioreactor provides the first demonstration that DEAs can be interfaced with living cells, and used to control their mechanical environment. It opens the door to a promising field of research, where real-world applications are possible for DEAs, a critical step for the development of this emerging technology.

8.1.2 Printing low-voltage DEAs

DEAs are capable of strains greater than 100 %, and response time below 1 ms, but require driving voltage in the kV range, which limits the possible applications. There is therefore great interests in reducing the actuation voltage of DEAs. One approach is to decrease the membrane thickness, typically in the 20-100 µm range, as reliable fabrication becomes challenging below this thickness.

Main results

In this thesis, I showed for the first time that pad-printing (a soft-contact printing technique used in many industries) can be used to manufacture thin dielectric elastomer membranes for DEA applications. Using this technique, I fabricated a fully-printed 3 µm thick DEA, and successfully demonstrated that decreasing the membrane thickness to only a few microns significantly reduces the driving voltage. The device achieved a radial actuation strain of 7.5 % at only 245 V. This result corresponds to an actuation of 125 % kV^{-2}, which is to my knowledge the highest reported value to date for a DEA.

I aslso investigated the electrodes stiffening impact on DEA performance as the membrane thickness decreases. I developed a simple DEA model (based on the Gent model) that includes realistic electrodes of finite stiffness, rather than neglecting their mechanical impact as is commonly done. I also developed a strain-mapping algorithm based on optical correlation, and compared the strain uniformity of 3 µm- and 30 µm-thick DEAs. The simulation results and the strain-mapping measurements identified the electrodes as an important parameter that should not be neglected in the design and optimization of thin DEAs.

Impact statement

The work that I accomplished in this section of the thesis provides a practical approach toward low-voltage DEAs, a critical step in the development of real-world applications. With driving voltage below 300 V, a range covered by commercially available CMOS circuitry, this work opens the door to a variety of new opportunities for DEA-based technologies.

8.2 Future work

8.2.1 DEA-based deformable bioreactor

Now that the application of the DEA-based deformable bioreactor has been demonstrated, the next important step is to have biologist partners using this technology for their research in cell mechanotransduction. In its current state, the device can already serve its purpose, and meet the performance requirements of most mechanotransduction experiments. The device could however benefits from some additions or improvements, which I discuss here.

Integrating tensile and compressive strain on a single device

In this thesis, I presented a DEA design which can generate compressive or tensile uniaxial strain depending on the orientation of the high-prestretch axis (see Section 4.3). Both strain types are however often present *in vivo*, like in the vascular system for example, which can exhibit episodes of tensile and compressive strain over a full cardiac cycle. The DEA design presented in Fig. 8.1 can overcome this limitation, providing compressive and tensile uniaxial strain on the same device. With two sets of independent electrodes, it is important to avoid dielectric dielectric breakdown between the tensile and compressive high-voltage electrodes. However, because of the oil backing which covers the high-voltage side of the DEA-based deformable bioreactor, the spacing between the tensile and compressive electrodes can be as small as 0.5 mm. This is considering a maximum voltage of 5 kV and a dielectric strength of 10 MV m^{-1} for the oil.

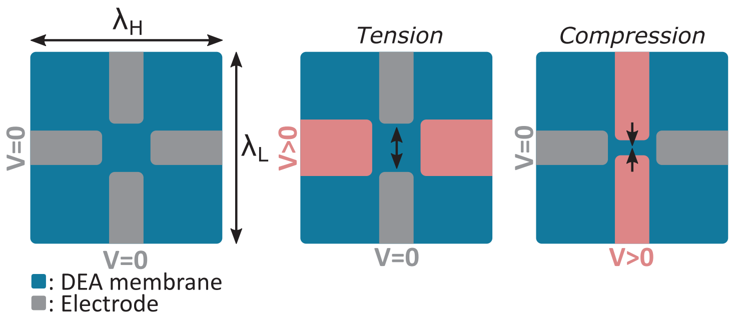

Figure 8.1 – TheDEA-based deformable bioreactor I developed in this thesis is limited to tensile or compressive uniaxial strain, depending on the orientation of the high prestretch λ_H. This new design can generate tensile and compressive strain on the same device.

Improved stability

Precise mechanical stimulation is essential for cell mechanotransduction experiments, and I showed that the DEA-based deformable bioreactor exhibits small strain drift over time. Drifts were observed at small time scale when actuated with a step function (∼3 % over 5 min), and at larger time scale when actuated for 50 000 cycles (∼2 % over 12 h). Those small variations are mainly caused by viscoelasticity and mechanical degradation of the actuator. They are difficult to suppress, but can be actively compensated by monitoring the actuation strain in real-time, and correct the driving signal accordingly. Future work could implement capacitive strain sensing, a challenging task due to the extremely small capacitance (∼10 pF) of the miniaturized DEA, the high resistance of the electrodes (∼100 kΩ), and the difficult environment (device immersed in water and coated with living cells).

Instead of using the capacitance of the actuator, an interesting alternative is to add a sensing element on top of the ground electrode as presented in in Fig. 8.2. The sensing element is composed of a thin dielectric elastomer membrane, a sensing electrode (in green), and shares its ground electrode (in grey) with the actuator. The sensing dielectric elastomer layer can be made only a few µm thick using pad-printing, hence providing a sensing capacitance (∼100 pF) ten times larger than the DEA capacitance. The strain can be calculated from the capacitive readout, and monitored in real-time. With an external control system, this information can be used to compensate strain drift observed during static or cyclic actuation, by adjusting the driving voltage accordingly. This capability becomes key for array configurations, where distributed sensing makes it possible to monitor many actuators in parallel.

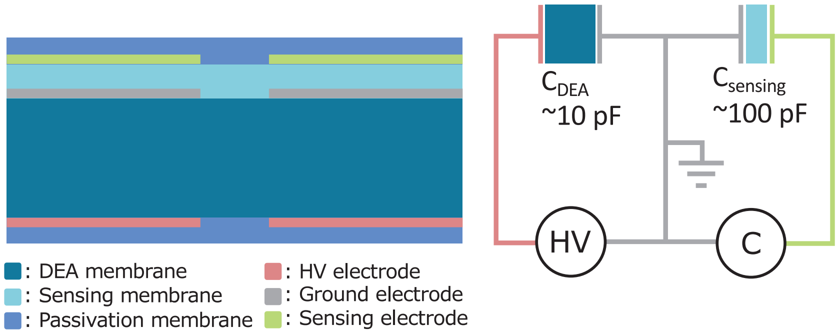

Figure 8.2 – A capacitive sensing element composed of a thin dielectric elastomer membrane, a sensing electrode, and a shared (with the actuator) ground electrode can be added on the device. The capacitive readout can be used to monitor strain in real-time, and correct for any drift by adjusting the driving voltage accordingly.

Arrays for high-throughput experiments

Statistical studies are essential to the field of cell biology, and are greatly facilitated by high-throughput experiments. The DEA-based deformable bioreactor that I developed is designed for single experiments, but it can be integrated into arrays for statistical or parametric studies. Future work could investigate two main configurations: The first is to assemble an array of single deformable bioreactors, as presented in Fig. 8.3(a). The second is to build a single deformable bioreactor, comprised of an array of DEAs as presented in Fig. 8.3(b). The first approach is more robust, as it provides individual addressing and avoid mechanical cross-talk between the actuators. However, the second approach can be particularly interesting for biologists. It is typically difficult to reproduce the exact same experimental conditions between different cell culture, and this approach greatly minimizes variability by enabling multiple experiments to be done in parallel on a single cell culture.

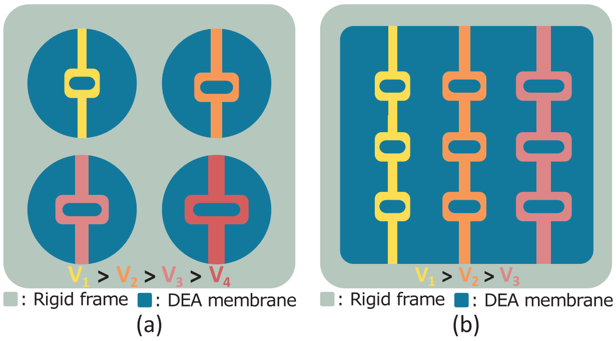

Figure 8.3 – There is a need in cell biology for high-throughput experiments, and the DEA-based deformable bioreactor can be integrated into an array configuration to provide this capability. Two approaches are possible: (a)an array of deformable bioreactors or (b)a single deformable bioreactor, comprised of an array of DEAs.

Improved lifetime

Future work could also improve the device lifetime, a challenging task as the exact failure mechanism isn't identified. My hypothesis is that the presence of defects (i.e. air bubbles, dust particles and silica aggregates) in the membrane is currently the main limiting factor. I also believe that the membrane high prestretch ($\lambda_H = 2.7$) might accelerate failure by adding stress on those defects. Another plausible hypothesis is that the failure could be induced by a gradual polarisation of the material over cyclic actuation. A solution to material polarization would be to periodically switch polarity on the high-voltage electrode. If future work aim at improving the device lifetime, those hypothesis should be investigated first.

Additional types of stimuli

To expand the possible applications of the DEA-based deformable bioreactor, future work could integrate additional capabilities to the system. For example, electrodes for electrical stimulation and sensing can be patterned on the membrane. Combined with the DEA element, they can be used to study how stretch affect the action potential propagation velocity of different cell types, including cardiomyocytes, nerve cells, and neurones. The rigid frame supporting the device, which is now purely structural, can also be given a functional purpose. It can be made of PDMS, and designed to integrate microfluidics for circulation of culture medium, temperature control of the culture bath, or injection of soluble factors (i.e. biochemical stimuli).

8.2.2 Pad-printing dielectric elastomer transducers

In this thesis, I demonstrated that pad-printing can be used to manufacture thin dielectric elastomer membranes for DEA applications. In addition to produce µm-thick films, this technique enables direct in-plane patterning, with a lateral resolution of approximately 100 µm. Future work could make use of the the design flexibility provided by this unique feature. For example, an array of soft suspended microbeams with integrated capacitive strain sensors could be fabricated as presented in Fig. 8.4(a). This type of structure could find applications in cell biology, where it could be used to measure traction force generated by small groups of cells located on the suspended beams. In-plane patterning can also be used to enable vertical integration. With the ability to pattern the dielectric film and the electrodes, pad-printing can be used to print electrical vias as presented in Fig. 8.4(b). Vertical integration can be used for multi-stack dielectric elastomer transducers, where reliable interconnection is often challenging. It can also enable high-density arrays of individually addressable electrodes, by having the electrodes on one side of the membrane, and the leads on the opposite side. Future work could also investigate the printing of other materials. For example, it could be interesting to print stiffer elements with structural purposes, to either simply support a soft membrane, or guide its deformation.

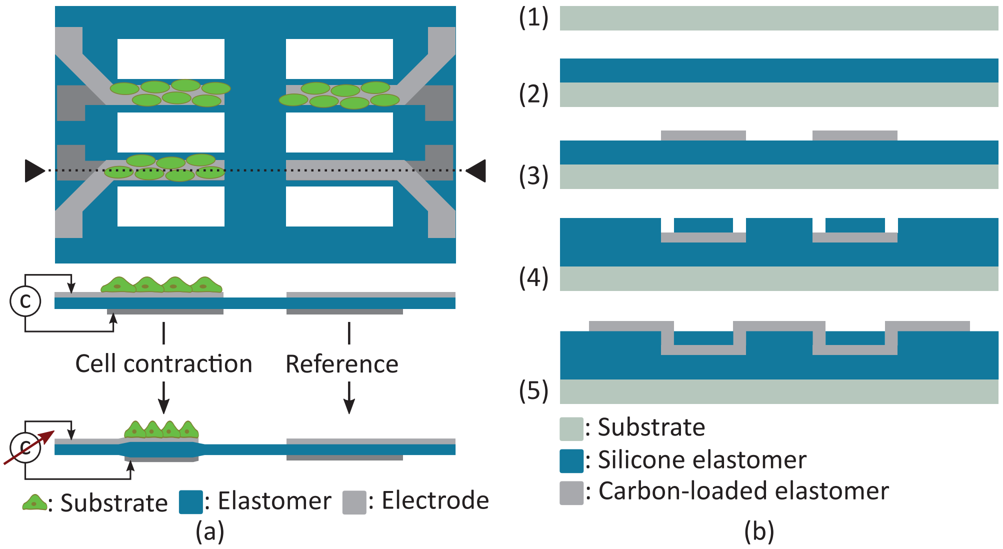

Figure 8.4 – Pad-printing of silicone elastomer films enables in-plane patterning with a lateral resolution of approximately 100 µm. This can be used to fabricate (a)an array of suspended microbeams for cell force measurements, or (b)electrical vias which enable vertical integration of dielectric elastomer transducers.

8.3 Concluding remark

The field of DEAs has progressed significantly in the 17 years since its birth. Advances in modelling provided insights into the complex interplay of non-linear processes, which helped guide the development and optimization of new generations of DEAs with vastly improved performance. The development of new dielectrics and materials for stretchable electrodes also greatly improved the performance and reliability of DEAs. Limitations are now much better understood, and fabrication methods are much more mature. This is an exciting time in DEAs, with increasing industrial research and development towards real-world applications where the intrinsic advantages of DEAs can be harnessed to provide unique advantages.

Bibliography

[1] D.-H. Kim, P. K. Wong, J. Park, A. Levchenko, and Y. Sun, “Microengineered platforms for cell mechanobiology.” *Annual review of biomedical engineering*, vol. 11, pp. 203–33, jan 2009.

[2] G. Bao and S. Suresh, “Cell and molecular mechanics of biological materials.” *Nature materials*, vol. 2, no. 11, pp. 715–25, nov 2003.

[3] D. E. Jaalouk and J. Lammerding, “Mechanotransduction gone awry,” *Nature Reviews Molecular Cell Biology*, vol. 10, no. 1, pp. 63–73, 2009.

[4] J. H.-C. Wang and B. P. Thampatty, “An introductory review of cell mechanobiology.” *Biomechanics and modeling in mechanobiology*, vol. 5, no. 1, pp. 1–16, mar 2006.

[5] Flexcell International Corporation. [Online] http://www.flexcellint.com (Accessed on 2016-08-25).

[6] CellScale Biomaterial Testing. [Online] http://cellscale.com (Accessed on 2016-08-25).

[7] Strex USA. [Online] https://strexcell.com (Accessed on 2016-09-25).

[8] S. Giulitti, A. Zambon, F. Michielin, and N. Elvassore, “Mechanotransduction through substrates engineering and microfluidic devices,” no. Figure 1, 2016.

[9] C. a. Davis, S. Zambrano, P. Anumolu, A. C. B. Allen, L. Sonoqui, and M. R. Moreno, “Device-based in vitro techniques for mechanical stimulation of vascular cells: A review,” *Journal of Biomechanical Engineering*, vol. 137, no. 4, p. 040801, 2015.

[10] R. Pelrine, R. Kornbluh, and J. Joseph, “High-Speed electrically actuated elastomers with strain greater than 100%,” *Science*, vol. 287, no. 5454, pp. 836–839, 2000.

[11] J. Huang, T. Li, C. Chiang Foo, J. Zhu, D. R. Clarke, and Z. Suo, “Giant, voltage-actuated deformation of a dielectric elastomer under dead load,” *Applied Physics Letters*, vol. 100, no. 4, 2012.

[12] L. Maffli, S. Rosset, M. Ghilardi, F. Carpi, and H. Shea, “Ultrafast all-polymer electrically tunable silicone lenses,” *Advanced Functional Materials*, vol. 25, no. 11, pp. 1656–1665, 2015.

[13] Y. Huang and N. T. Nguyen, “A polymeric cell stretching device for real-time imaging with optical microscopy,” *Biomedical Microdevices*, vol. 15, no. 6, pp. 1043–1054, 2013.

[14] S. Akbari and H. R. Shea, “An array of 100μm×100μm dielectric elastomer actuators with 80% strain for tissue engineering applications,” *Sensors and Actuators A: Physical*, vol. 186, pp. 236–241, oct 2012.

[15] D. Rus and M. T. Tolley, “Design, fabrication and control of soft robots,” *Nature*, vol. 521, no. 7553, pp. 467–475, 2015.

[16] J. Mohd Jani, M. Leary, A. Subic, and M. A. Gibson, “A review of shape memory alloy research, applications and opportunities,” *Materials and Design*, vol. 56, pp. 1078–1113, 2014.

[17] I. A. Anderson, T. Hale, T. Gisby, T. Inamura, T. McKay, B. O’Brien, S. Walbran, and E. P. Calius, “A thin membrane artificial muscle rotary motor,” *Applied Physics A: Materials Science and Processing*, vol. 98, no. 1, pp. 75–83, 2010.

[18] P. Romano, O. Araromi, S. Rosset, H. Shea, and J. Perruisseau-Carrier, “Tunable millimeter-wave phase shifter based on dielectric elastomer actuation,” *Applied Physics Letters*, vol. 104, no. 2, 2014.

[19] G. Kofod, M. Paajanen, and S. Bauer, “Self-organized minimum-energy structures for dielectric elastomer actuators,” *Applied Physics A*, vol. 85, no. 2, pp. 141–143, sep 2006.

[20] M. Duduta, R. J. Wood, and D. R. Clarke, “Multilayer dielectric elastomers for fast, programmable actuation without prestretch,” *Advanced Materials*, vol. 28, no. 36, pp. 8058–8063, 2016.

[21] X. Niu, X. Yang, P. Brochu, H. Stoyanov, S. Yun, Z. Yu, and Q. Pei, “Bistable large-strain actuation of interpenetrating polymer networks.” *Advanced Materials*, vol. 24, no. 48, pp. 6513–6519, sep 2012.

[22] Z. Yu, W. Yuan, P. Brochu, B. Chen, Z. Liu, and Q. Pei, “Large-strain, rigid-to-rigid deformation of bistable electroactive polymers,” *Applied Physics Letters*, vol. 95, no. 19, p. 192904, 2009.

[23] S. Yun, X. Niu, Z. Yu, W. Hu, P. Brochu, and Q. Pei, “Compliant silver nanowire-polymer composite electrodes for bistable large strain actuation.” *Advanced materials*, vol. 24, no. 10, pp. 1321–7, mar 2012.

[24] D. R. Shian, Samuel and Bertoldi, Katia and Clarke, “Dielectric elastomer based “grippers” for soft robotics,” vol. 27, no. 43, pp. 6814–6819, 2015.

[25] O. a. Araromi, I. Gavrilovich, J. Shintake, S. Rosset, M. Richard, V. Gass, and H. R. Shea, “Rollable multisegment dielectric elastomer minimum energy structures for a deployable microsatellite gripper,” *IEEE/ASME Transactions on Mechatronics*, vol. 20, no. 1, pp. 438–446, 2014.

[26] J. Shintake, S. Rosset, B. Schubert, D. Floreano, and H. Shea, “Versatile soft grippers with intrinsic electroadhesion based on multifunctional polymer actuators,” *Advanced Materials*, vol. 28, no. 2, pp. 1–8, 2016.

[27] G. Kofod, W. Wirges, M. Paajanen, and S. Bauer, “Energy minimization for self-organized structure formation and actuation,” *Applied Physics Letters*, vol. 90, no. 8, pp. 9–12, 2007.

[28] S. Rosset and H. Shea, “Small, fast and tough: shrinking down integrated elastomer transducers,” vol. 3, p. 031105, 2016.

[29] C. Keplinger, T. Li, R. Baumgartner, Z. Suo, and S. Bauer, “Harnessing snap-through instability in soft dielectrics to achieve giant voltage-triggered deformation,” *Soft Matter*, vol. 8, no. 2, p. 285, 2012.

[30] S. Rosset and H. R. Shea, “Towards fast, reliable, and manufacturable DEAs: miniaturized motor and Rupert the rolling robot,” in *Electroactive Polymer Actuators and Devices (EAPAD)*, vol. 9430, San Diego, 2015, p. 943009.

[31] S. Rosset, P. Gebbers, B. M. O’Brien, and H. R. Shea, “The need for speed,” in *Electroactive Polymer Actuators and Devices (EAPAD)*, vol. 8340, apr 2012, pp. 834 004–834 004–12.

[32] M. Hodgins and S. Seelecke, “Systematic experimental study of pure shear type dielectric elastomer membranes with different electrode and film thicknesses,” *Smart Materials and Structures*, vol. 25, no. 9, p. 095001, 2016.

[33] M. Bozlar, C. Punckt, S. Korkut, J. Zhu, C. Chiang Foo, Z. Suo, and I. A. Aksay, “Dielectric elastomer actuators with elastomeric electrodes,” *Applied Physics Letters*, vol. 101, no. 9, 2012.

[34] K. Min, J. Y. Jung, T. H. Han, Y. Park, C. Jung, S. M. Hong, and C. M. Koo, “Graphene electrodes for artificial muscles,” *Molecular Crystals and Liquid Crystals*, vol. 539, no. 1, pp. 260/[600]–265/[605], 2011.

[35] R. Sarban and R. W. Jones, “Electromechanical model-based vibration isolation using a dielectric elastomer actuator,” *2011 IEEE International Conference on Mechatronics*, vol. 23, no. 4, pp. 603–608, 2011.

[36] C. Keplinger, M. Kaltenbrunner, N. Arnold, and S. Bauer, “Rontgen’s electrode-free elastomer actuators without electromechanical pull-in instability.” *Proceedings of the National Academy of Sciences of the United States of America*, vol. 107, no. 10, pp. 4505–10, mar 2010.

[37] B. Chen, J. J. Lu, C. H. Yang, J. H. Yang, J. Zhou, Y. M. Chen, and Z. Suo, “Highly stretchable and transparent ionogels as nonvolatile conductors for dielectric elastomer transducers,” *ACS Applied Materials and Interfaces*, vol. 6, no. 10, pp. 7840–7845, 2014.

[38] L. Hu, W. Yuan, P. Brochu, G. Gruner, and Q. Pei, “Highly stretchable, conductive, and transparent nanotube thin films,” *Applied Physics Letters*, vol. 94, no. 16, p. 161108, 2009.

[39] S. Rosset, M. Niklaus, P. Dubois, and H. R. Shea, “Metal ion implantation for the fabrication of stretchable electrodes on elastomers,” *Advanced Functional Materials*, vol. 19, no. 3, pp. 470–478, feb 2009.

[40] P. Carpi, Federico and De Rossi, Danilo and Kornbluh, Roy and Pelrine, Ronald Edward and Sommer-Larsen, *Dielectric elastomers as electromechanical transducers: Fundamentals, materials, devices, models and applications of an emerging electroactive polymer technology*. Elsevier, 2011.

[41] S. Shian, R. M. Diebold, and D. R. Clarke, “Tunable lenses using transparent dielectric elastomer actuators.” *Optics express*, vol. 21, no. 7, pp. 8669–76, apr 2013.

[42] C. Graetzel, M. Suter, and M. Aschwanden, “Reducing laser speckle with electroactive polymer actuators,” *Electroactive Polymer Actuators and Devices (EAPAD)*, vol. 9430, no. 943004, pp. 943 004–8, 2015.

[43] M. Kollosche, S. Döring, J. Stumpe, and G. Kofod, “Voltage-controlled compression for period tuning of optical surface relief gratings.” *Optics letters*, vol. 36, no. 8, pp. 1389–91, apr 2011.

[44] M. B. Krishnan, S. Rosset, S. Bhattacharya, and H. R. Shea, “Fabrication of transmissive dielectric elastomer actuator driven tunable optical gratings with improved tunability,” *Optical Engineering*, vol. 55, no. 4, p. 047104, 2016.

[45] M. Aschwanden and A. Stemmer, “Polymeric, electrically tunable diffraction grating based on artificial muscles,” *Optics letters*, vol. 31, no. 17, pp. 2610–2612, 2006.

[46] S. J. A. Koh, T. Li, J. Zhou, X. Zhao, W. Hong, J. Zhu, and Z. Suo, “Mechanisms of large actuation strain in dielectric elastomers,” *Journal of Polymer Science Part B: Polymer Physics*, vol. 49, no. 7, pp. 504–515, apr 2011.

[47] X. Zhao and Z. Suo, “Theory of dielectric elastomers capable of giant deformation of actuation,” *Physical Review Letters*, vol. 104, no. 17, pp. 1–4, apr 2010.

[48] X. Zhao and Q. Wang, “Harnessing large deformation and instabilities of soft dielectrics: Theory, experiment, and application,” *Applied Physics Reviews*, vol. 1, no. 2, 2014.

[49] A. Gent, “A new constitutive relation for rubber,” *Rubber chemistry and technology*, vol. 69, no. 1, pp. 59–61, 1996.

[50] R. E. Pelrine, R. D. Kornbluh, J. P. Joseph, S. R. I. International, R. Ave, and M. Park, “Electrostriction of polymer dielectrics with compliant electrodes as a means of actuation,” vol. 64, no. 97, pp. 77–85, 1998.

[51] W. M. Zhang, H. Yan, Z. K. Peng, and G. Meng, “Electrostatic pull-in instability in MEMS/NEMS: A review,” *Sensors and Actuators, A: Physical*, vol. 214, pp. 187–218, 2014.

[52] P. Sommer-Larsen, J. Hooker, G. Kofod, K. West, M. Benslimane, and P. Gravesen, "Response of dielectric elastomer actuators," *Structures and Materials*, vol. 4329, pp. 157–163, 2001.

[53] W. Yuan, L. Hu, S. Ha, T. Lam, G. Gr, and Q. Pei, "Self-clearable carbon nanotube electrodes for improved performance of dielectric elastomer actuators," vol. 6927, pp. 1–12, 2008.

[54] G. K. Lau, S. C. K. Goh, and L. L. Shiau, "Dielectric elastomer unimorph using flexible electrodes of electrolessly deposited (ELD) silver," *Sensors and Actuators, A: Physical*, vol. 169, no. 1, pp. 234–241, 2011.

[55] X. Niu, H. Stoyanov, W. Hu, R. Leo, P. Brochu, and Q. Pei, "Synthesizing a new dielectric elastomer exhibiting large actuation strain and suppressed electromechanical instability without prestretching," *Journal of Polymer Science, Part B: Polymer Physics*, vol. 51, no. 3, pp. 197–206, 2013.

[56] J. S. Plante and S. Dubowsky, "Large-scale failure modes of dielectric elastomer actuators," *International Journal of Solids and Structures*, vol. 43, no. 25-26, pp. 7727–7751, 2006.

[57] J. Zhu, M. Kollosche, T. Lu, G. Kofod, and Z. Suo, "Two types of transitions to wrinkles in dielectric elastomers," *Soft Matter*, vol. 8, no. 34, pp. 8840–8846, 2012.

[58] T. Lu, J. Huang, C. Jordi, G. Kovacs, R. Huang, D. R. Clarke, and Z. Suo, "Dielectric elastomer actuators under equal-biaxial forces, uniaxial forces, and uniaxial constraint of stiff fibers," *Soft Matter*, vol. 8, no. 22, p. 6167, 2012.

[59] M. Kollosche, J. Zhu, Z. Suo, and G. Kofod, "Complex interplay of nonlinear processes in dielectric elastomers," *Physical Review E*, vol. 85, no. 5, pp. 2–5, may 2012.

[60] J. Rossiter, B. Yap, and A. Conn, "Biomimetic chromatophores for camouflage and soft active surfaces," *Bioinspir Biomim*, vol. 7, no. 3, p. 36009, 2012.

[61] P. Brochu and Q. Pei, "Advances in dielectric elastomers for actuators and artificial muscles." *Macromolecular rapid communications*, vol. 31, no. 1, pp. 10–36, jan 2010.

[62] W. C. Röntgen, "Ueber die durch Electricität bewirkten Form- und Volumenänderungen von dielectrischen Körpern," *Annalen der Physik und Chemie*, vol. 247, no. 13, pp. 771–786, 1880.

[63] M. Wissler and E. Mazza, "Mechanical behavior of an acrylic elastomer used in dielectric elastomer actuators," *Sensors and Actuators, A: Physical*, vol. 134, no. 2, pp. 494–504, 2007.

[64] F. B. Madsen, A. E. Daugaard, S. Hvilsted, and A. L. Skov, "The current state of silicone-based dielectric elastomer transducers," *Macromolecular Rapid communications*, vol. 37, no. 5, pp. 378–413, 2016.

[65] G. Gallone, F. Carpi, F. Galantini, D. De Rossi, and G. Levita, "Enhancing the electromechanical response of maxwell stress actuators," *Advances in Science and Technology*, vol. 61, no. 1, pp. 46–53, 2008.

[66] R. Shankar, T. K. Ghosh, and R. J. Spontak, "Electroactive nanostructured polymers as tunable actuators," *Advanced Materials*, vol. 19, no. 17, pp. 2218–2223, 2007.

[67] S. Rosset, S. Araromi, S. Schlatter, and H. Shea, "Fabrication process of silicone-based dielectric elastomer actuators," *Journal of Visualized Experiments (JoVE)*, vol. 108, pp. 231–238, 2016.

[68] O. A. Araromi, A. T. Conn, C. S. Ling, J. M. Rossiter, R. Vaidyanathan, and S. C. Burgess, "Spray deposited multilayered dielectric elastomer actuators," *Sensors and Actuators, A: Physical*, vol. 167, no. 2, pp. 459–467, 2011.

[69] T. Töpper, F. Weiss, B. Osmani, C. Bippes, V. Leung, and B. Müller, "Siloxane-based thin films for biomimetic low-voltage dielectric actuators," *Sensors and Actuators A: Physical*, vol. 233, pp. 32–41, 2015.

[70] D. M. Opris, M. Molberg, C. Walder, Y. S. Ko, B. Fischer, and F. A. Nüesch, "New silicone composites for dielectric elastomer actuator applications in competition with acrylic foil," *Advanced Functional Materials*, vol. 21, no. 18, pp. 3531–3539, 2011.

[71] S. J. Dünki, Y. S. Ko, F. a. Nüesch, and D. M. Opris, "Self-repairable, high permittivity dielectric elastomers with large actuation strains at low electric fields," *Advanced Functional Materials*, vol. 25, no. 16, pp. 2467–2475, 2015.

[72] S. Rosset and H. R. Shea, "Flexible and stretchable electrodes for dielectric elastomer actuators," *Applied Physics A: Materials Science and Processing*, vol. 110, no. 2, pp. 281–307, 2013.

[73] D. McCoul, W. Hu, M. Gao, V. Mehta, and Q. Pei, "Recent advances in stretchable and transparent electronic materials," *Advanced Electronic Materials*, vol. 2, no. 5, 2016.

[74] H. Stoyanov, M. Kollosche, S. Risse, R. Waché, and G. Kofod, "Soft conductive elastomer materials for stretchable electronics and voltage controlled artificial muscles." *Advanced materials (Deerfield Beach, Fla.)*, pp. 1–6, oct 2012.

[75] S. Shian, R. M. Diebold, A. McNamara, and D. R. Clarke, "Highly compliant transparent electrodes," *Applied Physics Letters*, vol. 101, no. 6, 2012.

[76] P. Lochmatter, G. Kovacs, and P. Ermanni, "Design and characterization of shell-like actuators based on soft dielectric electroactive polymers," *Smart Materials and Structures*, vol. 16, no. 4, pp. 1415–1422, 2007.

[77] B. Fasolt, M. Hodgins, and S. Seelecke, "Characterization of screen-printed electrodes for Dieletric Elastomer (DE) membranes: influence of screen dimensions and electrode

thickness on actuator performance," *Proc. SPIE 9798, Electroactive Polymer Actuators and Devices (EAPAD)*, vol. 9798, p. 97983E, 2016.

[78] M. Aschwanden and A. Stemmer, "Low voltage, highly tunable diffraction grating based on dielectric elastomer actuators," *Proceedings of SPIE*, p. 65241N, 2007.

[79] O. A. Araromi, S. Rosset, and H. R. Shea, "High-resolution, large-area fabrication of compliant electrodes via laser ablation for robust, stretchable dielectric elastomer actuators and sensors," *ACS Applied Materials & Interfaces*, vol. 7, no. 32, pp. 18 046–18 053, 2015.

[80] S. Rosset, M. Niklaus, P. Dubois, M. Dadras, and H. R. Shea, "Mechanical properties of electroactive polymer microactuators with ion implanted electrodes," *Spie*, vol. 6524, pp. 652 410–652 410–11, 2007.

[81] R. Pelrine, R. Kornbluh, J. Joseph, R. Heydt, Q. Pei, and S. Chiba, "High-field deformation of elastomeric dielectrics for actuators," *Materials Science and Engineering C*, vol. 11, no. 2, pp. 89–100, 2000.

[82] A. Pimpin, Y. Suzuki, and N. Kasagi, "Microelectrostrictive actuator with large out-of-plane deformation for flow-control application," *Journal of Microelectromechanical Systems*, vol. 16, no. 3, pp. 753–764, 2007.

[83] R. W. Jones and R. Sarban, "Inverse grey-box model-based control of a dielectric elastomer actuator," *Smart Materials and Structures*, vol. 21, no. 7, p. 075019, 2012.

[84] S. P. Lacour, J. Jones, Z. Suo, and S. Wagner, "Design and performance of thin metal film interconnects for skin-like electronic circuits," *IEEE Electron Device Letters*, vol. 25, no. 4, pp. 179–181, 2004.

[85] J. Shintake, B. Schubert, S. Rosset, H. Shea, and D. Floreano, "Variable stiffness actuator for soft robotics using dielectric elastomer and low-melting-point alloy," *IEEE International Conference on Intelligent Robots and Systems*, vol. 2015-Decem, pp. 1097–1102, 2015.

[86] M. Urdaneta, R. Delille, and E. Smela, "Stretchable electrodes with high conductivity and photo-patternability," *Advanced Materials*, vol. 19, no. 18, pp. 2629–2633, sep 2007.

[87] S. Li, N. F. Huang, and S. Hsu, "Mechanotransduction in endothelial cell migration," *Journal of Cellular Biochemistry*, vol. 96, no. 6, pp. 1110–1126, 2005.

[88] T. M. Maul, D. W. Chew, A. Nieponice, and D. A. Vorp, "Mechanical stimuli differentially control stem cell behavior : morphology , proliferation , and differentiation," *Biomech Model Mechanobiol*, vol. 10, pp. 939–953, 2011.

[89] A. Aryaei and A. C. Jayasuriya, "The effect of oscillatory mechanical stimulation on osteoblast attachment and proliferation," *Materials Science and Engineering: C*, vol. 52, pp. 129–134, 2015.

[90] Y. Gao, B. Zhou, X. Wu, X. Gao, X. Zeng, J. Xie, C. Wang, Z. Ye, J. Wan, and W. Wen, "Three dimensional and homogenous single cell cyclic stretch within a magnetic micropillar array (mMPA) for a cell proliferation study," *ACS Biomaterials Science & Engineering*, vol. 2, pp. 65–72, 2015.

[91] J. Lammerding, J. Hsiao, P. C. Schulze, S. Kozlov, C. L. Stewart, and R. T. Lee, "Abnormal nuclear shape and impaired mechanotransduction in emerin-deficient cells," *Journal of Cell Biology*, vol. 170, no. 5, pp. 781–791, 2005.

[92] J. S. Park, J. S. F. Chu, C. Cheng, F. Chen, D. Chen, and S. Li, "Differential effects of equiaxial and uniaxial strain on mesenchymal stem cells," *Biotechnology and Bioengineering*, vol. 88, no. 3, pp. 359–368, 2004.

[93] D. M. Wootton and D. N. Ku, "Fluid mechanics of vascular systems, diseases, and thrombosis." *Annual review of biomedical engineering*, vol. 1, pp. 299–329, 1999.

[94] K. R. Levental, H. Yu, L. Kass, J. N. Lakins, M. Egeblad, J. T. Erler, S. F. T. Fong, K. Csiszar, A. Giaccia, W. Weninger, M. Yamauchi, D. L. Gasser, and V. M. Weaver, "Matrix crosslinking forces tumor progression by enhancing integrin signaling," *Cell*, vol. 139, no. 5, pp. 891–906, 2009.

[95] B. Katz, "Depolarization of sensory terminals and the initiation of impulses in the muscle spindle," *The Journal of physiology*, vol. 111, pp. 261–282, 1950.

[96] F. Guharay and F. Sachs, "Stretch-activated single ion channel currents in tissue-cultured embryonic chick skeletal muscle." *The Journal of physiology*, vol. 352, pp. 685–701, 1984.

[97] W. J. Polacheck, R. Li, S. G. M. Uzel, and R. D. Kamm, "Microfluidic platforms for mechanobiology." *Lab on a chip*, vol. 13, no. 12, pp. 2252–67, 2013.

[98] J. G. McGarry, P. Maguire, V. A. Campbell, B. C. O'Connell, P. J. Prendergast, and S. P. Jarvis, "Stimulation of nitric oxide mechanotransduction in single osteoblasts using atomic force microscopy," *Journal of Orthopaedic Research*, vol. 26, no. 4, pp. 513–521, 2008.

[99] G. T. Charras and M. a. Horton, "Single cell mechanotransduction and its modulation analyzed by atomic force microscope indentation." *Biophysical journal*, vol. 82, no. 6, pp. 2970–2981, 2002.

[100] J. Chen, B. Fabry, E. L. Schiffrin, N. Wang, Y. Wang, Z. Huang, P. S. Nayak, B. D. Matthews, D. Warburton, J. Sanchez-esteban, B. D. Johnson, K. J. Mather, J. P. Wallace, H. Huang, J. Sylvan, M. Jonas, R. Barresi, P. T. C. So, K. P. Campbell, R. T. Lee, M. Hughes-fulford, and B. E. N. Fabry, "Twisting integrin receptors increases endothelin-1 gene expression in endothelial cells Twisting integrin receptors increases endothelin-1 gene expression in endothelial cells," 2013.

[101] V. Lulevich, T. Zink, H.-Y. Chen, F.-T. Liu, and G.-Y. Liu, “Cell mechanics using atomic force microscopy-based single-cell compression.” *Langmuir : the ACS journal of surfaces and colloids*, vol. 22, no. 19, pp. 8151–5, sep 2006.

[102] a. R. Bausch, W. Möller, and E. Sackmann, “Measurement of local viscoelasticity and forces in living cells by magnetic tweezers.” *Biophysical journal*, vol. 76, no. 1 Pt 1, pp. 573–579, 1999.

[103] T. Ohashi, M. Hagiwara, D. L. Bader, and M. M. Knight, “Intracellular mechanics and mechanotransduction associated with chondrocyte deformation during pipette aspiration.” *Biorheology*, vol. 43, no. 3-4, pp. 201–14, 2006.

[104] P. Honarmandi, H. Lee, M. J. Lang, and R. D. Kamm, “A microfluidic system with optical laser tweezers to study mechanotransduction and focal adhesion recruitment.” *Lab on a chip*, vol. 11, no. 4, pp. 684–694, 2011.

[105] R. M. Hochmuth, “Micropipette aspiration of living cells.” *Journal of biomechanics*, vol. 33, no. 1, pp. 15–22, jan 2000.

[106] G. Lenormand and A. Richert, “A new determination of the shear modulus of the human erythrocyte membrane using optical tweezers,” *Biophysical Journal*, vol. 76, no. February, pp. 1145–1151, 1999.

[107] M. Morioka, H. Parameswaran, K. Naruse, M. Kondo, M. Sokabe, Y. Hasegawa, B. Suki, and S. Ito, “Microtubule dynamics regulate cyclic stretch-induced cell alignment in human airway smooth muscle cells,” *PLoS ONE*, vol. 6, no. 10, pp. 1–9, 2011.

[108] C. Moraes, G. Wang, Y. Sun, and C. a. Simmons, “A microfabricated platform for high-throughput unconfined compression of micropatterned biomaterial arrays.” *Biomaterials*, vol. 31, no. 3, pp. 577–84, jan 2010.

[109] A. Gelmi, A. Cieslar-Pobuda, E. de Muinck, M. Los, M. Rafat, and E. W. H. Jager, “Direct mechanical stimulation of stem cells: a beating electromechanically active scaffold for cardiac tissue engineering.” *Advanced healthcare materials*, pp. 1–10, 2016.

[110] E. Zamir and B. Geiger, “Molecular complexity and dynamics of cell-matrix adhesions.” *Journal of cell science*, vol. 114, no. Pt 20, pp. 3583–3590, 2001.

[111] J. Kim and R. C. Hayward, “Mimicking dynamic in vivo environments with stimuli-responsive materials for cell culture,” *Trends in Biotechnology*, vol. 30, no. 8, pp. 426–439, 2012.

[112] D. Desmaële, M. Boukallel, and S. Régnier, “Actuation means for the mechanical stimulation of living cells via microelectromechanical systems: A critical review.” *Journal of biomechanics*, vol. 44, no. 8, pp. 1433–46, may 2011.

[113] A. Gerstmair, G. Fois, S. Innerbichler, P. Dietl, and E. Felder, "A device for simultaneous live cell imaging during uni-axial mechanical strain or compression." *Journal of applied physiology*, vol. 107, no. 2, pp. 613–620, 2009.

[114] B. J. Bell, E. Nauman, and S. L. Voytik-Harbin, "Multiscale strain analysis of tissue equivalents using a custom-designed biaxial testing device," *Biophysical Journal*, vol. 102, no. 6, pp. 1303–1312, 2012.

[115] K. Shimizu, A. Shunori, K. Morimoto, M. Hashida, and S. Konishi, "Development of a biochip with serially connected pneumatic balloons for cell-stretching culture," *Sensors and Actuators, B: Chemical*, vol. 156, no. 1, pp. 486–493, 2011.

[116] D. Tremblay, S. Chagnon-Lessard, M. Mirzaei, A. E. Pelling, and M. Godin, "A microscale anisotropic biaxial cell stretching device for applications in mechanobiology," *Biotechnology Letters*, vol. 36, no. 3, pp. 657–665, 2014.

[117] D. Huh, B. D. Matthews, A. Mammoto, H. Y. Hsin, and D. E. Ingber, "Reconstituting organ-level lung functions on a chip," *Science*, vol. 328, no. 5986, pp. 1662–1668, 2010.

[118] H. J. Kim, D. Huh, G. Hamilton, and D. E. Ingber, "Human gut-on-a-chip inhabited by microbial flora that experiences intestinal peristalsis-like motions and flow." *Lab on a chip*, vol. 12, no. 12, pp. 2165–74, 2012.

[119] A. Pavesi, G. Adriani, M. Rasponi, I. K. Zervantonakis, G. B. Fiore, and R. D. Kamm, "Controlled electromechanical cell stimulation on-a-chip," *Scientific Reports*, vol. 5, p. 11800, 2015.

[120] C. S. Simmons, J. Y. Sim, P. Baechtold, a. Gonzalez, C. Chung, N. Borghi, and B. L. Pruitt, "Integrated strain array for cellular mechanobiology studies." *Journal of micromechanics and microengineering : structures, devices, and systems*, vol. 21, no. 5, pp. 54 016–54 025, may 2011.

[121] Q. Wang, X. Zhang, and Y. Zhao, "Micromechanical stimulator for localized cell loading: fabrication and strain analysis," *Journal of Micromechanics and Microengineering*, vol. 23, no. 1, p. 015002, 2013.

[122] F. Michielin, E. Serena, P. Pavan, and N. Elvassore, "Micro fluidic-assisted cyclic mechanical stimulation affects cellular membrane integrity in a human muscular dystrophy in vitro model," *RSC Advances*, vol. 5, pp. 98 429–98 439, 2015.

[123] Y. Kamotani, T. Bersano-Begey, N. Kato, Y. C. Tung, D. Huh, J. W. Song, and S. Takayama, "Individually programmable cell stretching microwell arrays actuated by a Braille display," *Biomaterials*, vol. 29, no. 17, pp. 2646–2655, 2008.

[124] D. Chen, R. D. Hyldahl, and R. C. Hayward, "Creased hydrogels as active platforms for mechanical deformation of cultured cells." *Lab on a chip*, vol. 15, no. 4, pp. 1160–7, 2015.

[125] F. Khademolhosseini, “Magnetically actuated microstructured surfaces can actively modify cell migration behaviour,” *Biomedical Microdevices*, pp. 1–11, 2016.

[126] A. Agrawal, O. Adetiba, H. Kim, H. Chen, J. G. Jacot, and R. Verduzco, “Stimuli-responsive liquid crystal elastomers for dynamic cell culture,” *Journal of Materials Research*, vol. 30, no. 04, pp. 453–462, 2015.

[127] F. Khademolhosseini and M. Chiao, “Fabrication and patterning of magnetic polymer micropillar structures using a dry-nanoparticle embedding technique,” *Journal of Microelectromechanical Systems*, vol. 22, no. 1, pp. 131–139, 2013.

[128] A. Stemmer, M. Aschwander, A. Franco-Obregon, A. G. Rey, A. Vonderheit, R. Enning, and M. Sakai, “Bioreactor to apply mechanical forces as an anabolic stimulus,” Patent, 2007.

[129] S. Akbari and H. R. Shea, “Microfabrication and characterization of an array of dielectric elastomer actuators generating uniaxial strain to stretch individual cells,” *Journal of Micromechanics and Microengineering*, vol. 22, no. 4, p. 045020, apr 2012.

[130] R. Sinha, S. Le Gac, N. Verdonschot, A. Van Den Berg, B. Koopman, and J. Rouwkema, “Endothelial cell alignment as a result of anisotropic strain and flow induced shear stress combinations,” *Nature Publishing Group*, no. April, pp. 1–12, 2016.

[131] M. Imboden, A. Poulin, E. de Coulon, S. Rosset, and H. Shea, “Electrically shielded dielectric elastomer actuators for the study of the mechanical perturbation of cardiomyocytes,” in *EuroEAP 2016 - Sixth international conference on Electromechanically Active Polymer (EAP) transducers & artificial muscles*, Copenhagen, 2016.

[132] K. B. Subramani, E. Cakmak, R. J. Spontak, and T. K. Ghosh, “Enhanced electroactive response of unidirectional elastomeric composites with high-dielectric-constant fibers,” *Advanced Materials*, vol. 26, no. 18, pp. 2949–2953, 2014.

[133] S. Akbari, S. Rosset, and H. R. Shea, “Improved electromechanical behavior in castable dielectric elastomer actuators,” *Applied Physics Letters*, vol. 102, no. 7, p. 071906, 2013.

[134] A. Poulin, S. Rosset, and H. Shea, “Fully printed 3 microns thick dielectric elastomer actuator,” in *Proc. SPIE 9798, Electroactive Polymer Actuators and Devices (EAPAD) 2016*, vol. 9798, 2016, p. 97980L.

[135] D. A. Serban, L. Marsavina, and N. Modler, “Low-cycle fatigue behaviour of polyamides,” *Fatigue & Fracture of Engineering Materials & Structures*, vol. 38, no. 11, pp. 1383–1394, 2015.

[136] S. Rosset, B. M. O’Brien, T. Gisby, D. Xu, H. R. Shea, and I. a. Anderson, “Tunable grating with active feedback,” *Proceedings of SPIE*, vol. 8687, p. 86872F, 2013.

[137] K. N. Margaris and R. a. Black, “Modelling the lymphatic system : challenges and opportunities,” *J R Soc Interface*, vol. 9, no. 69, pp. 601–612, 2012.

[138] J. E. P. Waktare, “Atrial fibrillation,” *Circulation*, vol. 106, no. 1, pp. 14–16, 2002.

[139] G. P. Aurigemma, M. R. Zile, and W. H. Gaasch, “Contractile behavior of the left ventricle in diastolic heart failure: With emphasis on regional systolic function,” *Circulation*, vol. 113, no. 2, pp. 296–304, 2006.

[140] C. Norrmen, W. Vandevelde, A. Ny, P. Saharinen, M. Gentile, G. Haraldsen, P. Puolakkainen, E. Lukanidin, M. Dewerchin, K. Alitalo, and T. V. Petrova, “Liprin B1 is highly expressed in lymphatic vasculature and is important for lymphatic vessel integrity,” *Blood*, vol. 115, no. 4, pp. 906–909, 2010.

[141] L. Wang, B. Sun, K. S. Ziemer, G. A. Barabino, and R. L. Carrier, “Chemical and physical modifications to poly(dimethylsiloxane) surfaces affect adhesion of Caco-2 cells,” *Journal of Biomedical Materials Research - Part A*, vol. 93, no. 4, pp. 1260–1271, 2010.

[142] A. Poulin, S. Rosset, and H. R. Shea, “Printing low-voltage dielectric elastomer actuators,” *Applied Physics Letters*, vol. 107, no. 24, p. 244104, 2015.

[143] F. Xia, S. Tadigadapa, and Q. M. Zhang, “Electroactive polymer based microfluidic pump,” *Sensors and Actuators, A: Physical*, vol. 125, no. 2, pp. 346–352, 2006.

[144] C. Murray, D. McCoul, E. Sollier, T. Ruggiero, X. Niu, Q. Pei, and D. D. Carlo, “Electro-adaptive microfluidics for active tuning of channel geometry using polymer actuators,” *Microfluidics and Nanofluidics*, vol. 14, no. 1-2, pp. 345–358, 2013.

[145] I. a. Anderson, T. a. Gisby, T. G. McKay, B. M. O’Brien, and E. P. Calius, “Multi-functional dielectric elastomer artificial muscles for soft and smart machines,” *Journal of Applied Physics*, vol. 112, no. 4, 2012.

[146] S. Risse, B. Kussmaul, H. Krüger, and G. Kofod, “Synergistic improvement of actuation properties with compatibilized high permittivity filler,” *Advanced Functional Materials*, vol. 22, no. 18, pp. 3958–3962, 2012.

[147] L. J. Romasanta, P. Leret, L. Casaban, M. Hernández, M. a. de la Rubia, J. F. Fernández, J. M. Kenny, M. a. Lopez-Manchado, and R. Verdejo, “Towards materials with enhanced electro-mechanical response: CaCu3Ti4O12–polydimethylsiloxane composites,” *Journal of Materials Chemistry*, pp. 24 705–24 712, 2012.

[148] A. L. Thangawng, R. S. Ruoff, M. a. Swartz, and M. R. Glucksberg, “An ultra-thin PDMS membrane as a bio/micro-nano interface: fabrication and characterization.” *Biomedical microdevices*, vol. 9, no. 4, pp. 587–95, aug 2007.

[149] F. M. Weiss, T. Töpper, B. Osmani, S. Peters, G. Kovacs, and B. Müller, “Electrospraying nanometer-thin elastomer films for low-voltage dielectric actuators,” *Advanced Electronic Materials*, vol. 2, no. 5, 2016.

[150] J. H. Kim, Y. W. Choi, M. S. Kim, H. S. Um, S. H. Lee, P. Kim, and K.-Y. Suh, “Repetitive cleavage of elastomeric membrane via controlled interfacial fracture.” *ACS applied materials & interfaces*, vol. 6, no. 14, pp. 11 734–40, jul 2014.

[151] E. Kang, J. Ryoo, G. S. Jeong, Y. Y. Choi, S. M. Jeong, J. Ju, S. Chung, S. Takayama, and S. H. Lee, “Large-scale, ultrapliable, and free-standing nanomembranes,” *Advanced Materials*, vol. 25, no. 15, pp. 2167–2173, 2013.

[152] P. Lotz, M. Matysek, and H. F. Schlaak, “Fabrication and application of miniaturized dielectric elastomer stack Actuators,” *IEEE/ASME Transactions on Mechatronics*, vol. 16, no. 1, pp. 58–66, feb 2011.

[153] J. P. Butler, I. V. A. M. Tolic, B. E. N. Fabry, and J. J. Fredberg, “Traction fields, moments, and strain energy that cells exert on their surroundings,” *American Journal of Cell Physiology*, vol. 282, no. 3, pp. 595–605, 2002.

List of Abbreviations

2D	bi-dimensional
3D	three-dimensional
AFM	atomic force microscopy
CMOS	complementary Metal Oxide Semiconductor
CNT	carbon nanotube
DAQ	data acquisition
DE	dielectric elastomer
DEA	dielectric elastomer actuators
DIC	digital image correlation
DNA	deoxyribonucleic Acid
EMI	electromechanical instability
IPA	isopropyl alcohol
LEC	lymphatic endothelial cell
PAA	poly(acrylic) acrid
PBS	phosphate buffered saline
PET	polyethylene terephthalate
PMMA	poly(methyl methacrylate)

List of publications

Journal articles

- **A. Poulin**, C.S. Demin, S. Rosset, T.V. Petrova, and H. Shea, Dielectric Elastomer Actuator for Mechanical Loading of 2D cell Cultures, in Lab on a Chip, vol. 16, num. 19, p. 3788-3794, 2016. doi:10.1039/C6LC00903D

- O. Araromi, **A. Poulin**, M. Imoboden, S. Rosset, and H. Shea, Optimization of thin-film highly-compliant elastomer sensors for contractility measurement of muscle cells, in Extreme Mechanics Letters, (in press), 2016. doi:10.1016/j.eml.2016.03.017

- **A. Poulin**, S. Rosset, and H. Shea, Printing low-voltage dielectric elastomer actuators, in Applied Physics Letters, vol. 107, num. 24, p. 244101-3794, 2015. doi:10.1063/1.4937735

In preparation

- **A. Poulin**, M. Imobden, F. Sorba, S. Rosset, and H. Shea, Electrostatically actuated transparent deformable bioreactor capable of ultra-fast uniaxial mechanical loading of cells in vitro (Manuscript in preparation).

- A. Marette, **A. Poulin**, N. Besse, S. Rosset, D. Briand, and H. Shea, Enabling addressing and complex motion in soft machines by using flexible high-voltage TFTs to drive arrays of DEAs (Manuscript in preparation).

Conference proceedings

- **A. Poulin**, S. Rosset, and H. Shea, Fully printed 3 microns thick dielectric elastomer actuator, In Proceedings of the Electroative Polymer Actuators and Devices conference, Las Vegas, USA, 2016. **(Received Best Student Presentation Award)**

- **A. Poulin**, L. Maffli, S. Rosset, and H. Shea, Interfacing dielectric elastomer actuators with liquids. Electroactive Polymer Actuators and Devices, In Proceedings of the Electroative Polymer Actuators and Devices conference, San Diego, USA, 2015.

- O. Araromi, **A. Poulin**, S. Rosset, M. Favre and M. Giazzon, C. Martin-Olmos, M. Liley, and H. Shea. Thin-film dielectric elastomer sensors to measure the contraction force of smooth muscle cells. In Proceedings of the Electroactive Polymer Actuators and Devices (EAPAD)conference, San Diego, USA, 2015.

- **A. Poulin**, S. Rosset, and H. Shea, Toward compression of small cell population: Harnessing stress in passive regions of dielectric elastomer actuators, In Proceedings of the Electroative Polymer Actuators and Devices conference, San Diego, USA, 2014.

Submitted

- S. Rosset, **A. Poulin**, A. Zollinger, M. Smith, and H. Shea, Dielectric Elastomer Actuator for the measurement of cell traction forces with sub-cellular resolution (Submitted to Electroative Polymer Actuators and Devices 2017 conference).

Poster Presentations

- **A. Poulin**, M. Imboden and H. Shea. Smart bioreactor for Mechanical Loading of Monolayer Cell Cultures. Biointerfaces International, Zurich, Switzerland, 2016.

- **A. Poulin**, S. Rosset and H. Shea. Pad printing 1-10 mm thick elastomer membranes for DEAs. EuroEAP 2015 - Fifth international conference on Electromechanically Active Polymer (EAP) transducers and artificial muscles, Tallinn, Estonia, 2015.

- **A. Poulin**, C. Martin-Olmos, S. Rosset, M. Liley and H. Shea. DEA-based deformable cell culture system. EuroEAP 2014 - Fourth international conference on Electromechanically Active Polymer (EAP) transducers and artificial muscles, Linköping, Sweden, 2014.

- **A. Poulin**, S. Akbari, S. Rosset and H. Shea. Chip-scale array of artificial muscles for investigation of cell mechanotransduction properties. EuroEAP 2013 - Third international conference on Electromechanically Active Polymer (EAP) transducers and artificial muscles, Dübendorf (Zürich), Switzerland, 2013.

Provisional patent application

- H. Shea, **A. Poulin**, M. Imboden, S. Rosset, Bioreactor Device and System for In-Vitro Cell Strain, US Provisional Patent Application No. 62/397,429 filed on September 21, 2016.

Alexandre Poulin
Sablons 12
CH-2000 Neuchâtel
Switzerland

Phone : +41 21 6954403
Website: `http://lmts.epfl.ch/`
`http://people.epfl.ch/alexandre.poulin`
E-mail : `alexandre.poulin@epfl.ch`

Education

2012–2016	**PhD in Microsystems and Microelectronics** Ecole Polytechnique Fédérale de Lausanne, Switzerland *Title : Miniaturized Dielectric Elastomer actuators for Mechanical Stimulation of Monolayer Cell Cultures.*
2005–2012	**Integrated Bachelor-Master (research) in Engineering Physics** Ecole Polytechnique de Montréal, Canada *Title : Réseaux de Bragg Verticaux Accordables en Silicium pour le Developpement de Microsystèmes Optiques Appliqués.*

Languages

French: Fluent (Native), written and spoken
English: Fluent, written and spoken

Computer skills

Programming languages: Matlab
Design and simulation: SolidWorks, CoventorWare, L-Edit
Others: LabView, ImageJ

Selected publications

Papers in international journal

A. Poulin, C.S. Demin, S. Rosset, T.V. Petrova, and H. Shea, Dielectric Elastomer Actuator for Mechanical Loading of 2D cell Cultures, in Lab on a Chip, vol. 16, num. 19, p. 3788-3794, 2016. doi:10.1039/C6LC00903D

O. Araromi, **A. Poulin**, M. Imoboden, S. Rosset, and H. Shea, Optimization of thin-film highly-compliant elastomer sensors for contractility measurement of muscle cells, in Extreme Mechanics Letters, (in press), 2016. doi:10.1016/j.eml.2016.03.017

A. Poulin, S. Rosset, and H. Shea, Printing low-voltage dielectric elastomer actuators, in Applied Physics Letters, vol. 107, num. 24, p. 244101-3794, 2015. doi:10.1063/1.4937735

A. Poulin, R. St-Gelais, A.L. Eichenberger, L. Thévenaz, Y.A. Peter, MEMS Tunable Asymmetric Fabry-Perot Cavity for High-Precision Weighing of Macro Samples, in Journal of Microelectromechanical Systems, vol. 22, num. 4, p. 884-891, 2013.

R. St-Gelais, **A. Poulin**, Y.A. Peter, Advances in modeling, design, and fabrication of deep-etched multilayer resonators, in Journal Journal of Lightwave Technology, vol. 30, num. 12, p. 1900-1908, 2012.

Papers in conference proceedings

A. Poulin, S. Rosset, and H. Shea, Fully printed 3 microns thick dielectric elastomer actuator, In Proceedings of the Electroative Polymer Actuators and Devices conference, Las Vegas, USA, 2016.

A. Poulin, L. Maffli, S. Rosset, and H. Shea, Interfacing dielectric elastomer actuators with liquids. Electroactive Polymer Actuators and Devices, In Proceedings of the Electroative Polymer Actuators and Devices conference, San Diego, USA, 2015.

A. Poulin, S. Rosset, and H. Shea, Toward compression of small cell population: Harnessing stress in passive regions of dielectric elastomer actuators, In Proceedings of the Electroative Polymer Actuators and Devices conference, San Diego, USA, 2014.

A. Poulin, R. St-Gelais, and Y.A. Peter, Coupled electro-mechanical transducers for vertical to horizontal motion translation, Solid-State Sensors, In Proceedings of the Design, Test, Integration and Packaging of MEMS/MOEMS conference, Cannes, France, 2012.

A. Poulin, R. St-Gelais, N. Goulamhoussen, G. Zhu, C. Boudoux, and Y.A. Peter, In-plane MEMS-based Fabry-Pérot filter for high-speed wavelength-swept semiconductor laser, In Proceedings of the Solid-State Sensors, Actuators and Microsystems conference, Hilton Head Island, 2012.

Teaching assistant for courses

- Static and Dynamic (2012-2016)
  In charge of the practical exercises sessions.
  First year bachelor course
- Microfabrication (2009-2012)
  In charge of practical sessions in clean room.
  Graduate course open to undergraduate students
- Microsystems (2009-2012)
  In charge of semester projects on the design and simulation of MEMS devices.
  Graduate course open to undergraduate students

Awards and distinctions

- Best Student Presentation Award at the SPIE Smart Structures NDE conference (2016)
- International research internship award from the Fonds québécois de la recherche sur la nature et les technologies (2011)
  Competition, criteria: academic excellence and research potential.
- Natural Sciences and Engineering Research Council of Canada undergraduate research award (2006, 2007, 2009)
  Competition, criteria: GPA superior to 3.3/4
- Ministère de l'Éducation of Quebec student mobility scholarship (2007)
  Competition, criteria: GPA over 2.75/4.